ISAS - INTERNATIONAL SCHOOL
FOR ADVANCED STUDIES

Density-Functional Theory without orbitals: a path towards very large scale electronic structure calculations

Thesis submitted for the degree of

"Doctor Philosophiæ"

CANDIDATE

Alberto Franceschetti

SUPERVISOR

Prof. Stefano Baroni

October 1993

SISSA - SCUOLA
INTERNAZIONALE
SUPERIORE
DI STUDI AVANZATI
TRIESTE
Strada Costiera 11

TRIESTE

SISSA ISAS

SCUOLA INTERNAZIONALE SUPERIORE DI STUDI AVANZATI
INTERNATIONAL SCHOOL FOR ADVANCED STUDIES

Density-Functional Theory without orbitals: a path towards very large scale electronic structure calculations

Thesis submitted for the degree of

"Doctor Philosophiæ"

CANDIDATE

Alberto Franceschetti

SUPERVISOR

Prof. Stefano Baroni

October 1993

Index

Introduction

In the last few years, Density-Functional Theory (DFT) has become the most widespread method for ab-initio calculations of electronic and structural properties of molecules and solids. The success of DFT relies upon the existence of simple approximations for the exchange-correlation energy functional, which provide surprisingly accurate results for many systems of interest. Due to the continuous refinement of methods and algorithms over recent years, and to the availability of increasingly powerful computers, systems as large as several tens of atoms per unit cell can be presently tackled on workstations, and ab-initio calculations involving a few hundred atoms have been recently performed on parallel supercomputers.

However, the rush towards increasingly complex systems is seriously hindered by the so-called "$O(N^3)$ bottleneck": the computational cost of any conventional ab-initio calculations scales ultimately as the third power of the number of atoms of the system. This is by no means an intrinsic feature of Density-Functional Theory; actually, within DFT the total energy is a functional of the charge density alone, and the charge density at a given point is a local quantity, which can be calculated, in principle, with a computational workload which does not depend on the size of the system. The $O(N^3)$ bottleneck is a consequence of the fact that conventional approaches to DFT are formulated in terms of orthogonal Kohn-Sham orbitals. Large-

scale electronic-structure calculations are rapidly approaching the point where this N^3 scaling becomes the time-limiting factor; therefore, only a slight increase of the size of the systems which are tractable with conventional methods can be expected in the next few years. On the other hand, there are several interesting examples in nature of systems with thousands atoms, such as organic macromolecules, amorphous systems, extended defects and so on, which are completely out of reach for conventional schemes. In order for first-principle calculations to become feasible for such systems, new algorithms with more favourable scaling laws are called for.

Very recently, some methods have been proposed whose computational cost scales only linearly with the size of the system, thus opening the way to first-principles calculations for very large systems. There are basically two different philosophies behind these so-called "$O(N)$ methods": in one case [1-4], the Kohn-Sham orbitals are forced to be localized in real space, thereby reducing the computational cost of orthogonalization; in the second approach [5,6], the calculation of Kohn-Sham orbitals is by-passed, and the total energy is obtained in terms of the real-space density matrix.

In this work, we present a method [7] for the self-consistent calculation of ground-state properties which is based on the computation of selected elements of the real-space Green's function; taking advantage of the localized nature of the Green's function, $O(N)$ scaling is achieved for large systems. The basic ingredients of our method are:

(i) the real-space representation of the Kohn-Sham hamiltonian on a discrete mesh, and

(ii) the use of the recursion method (or the equation-of-motion method) for computing the diagonal elements of the real-space Green's function.

Basically, just two parameters are involved in the calculation of the electronic charge density: the grid-spacing h, which controls the accuracy of the real-space representation, and the number of recursion steps (or time steps) n. The method becomes exact as $h \to 0$ and $n \to \infty$. No use is made of Kohn-Sham orbitals: both the charge density and the total energy are obtained in terms of the diagonal elements of the real-space Green's function.

The present work is organized as follows. In Chapter 1, we discuss the conventional approach to Kohn-Sham theory and introduce the new Green's function approach. In Chapter 2, the application of the recursion method to the calculation of the charge density is discussed. The convergence of the charge density with respect to the number of recursion steps is examined in detail, and some possible solutions to the problem of reducing the number of steps without sacrificing the accuracy of the charge density are proposed. In Chapter 3, this scheme is applied to the self-consistent calculation of the charge density; the accuracy of total energy and atomic forces is also discussed. Finally, in Chapter 4 we propose an alternative approach to the calculation of the charge density based on the equation-of-motion method. Although the recursion method seems to have the edge on timing, some appealing features of the equation-of-motion method are outlined.

Chapter 1

Density-Functional Theory

Conventional schemes for the implementation of Density-Functional Theory suffer from unfavourable scaling with the size of the system. In the present chapter, an alternative approach to DFT is proposed whose computational cost scales only linearly with the size of the system. Both the charge density and the total energy are obtained in terms of the diagonal elements of the real-space Green's function; each diagonal element of the Green's function – being a local quantity – can be calculated with a computational workload which is independent of the size of the system. To this end, the real-space representation of the Kohn-Sham hamiltonian on a discrete mesh plays an important role.

1.1 Conventional approach to Density-Functional Theory

Density-Functional Theory (DFT) relies on two fundamental theorems [8,9] stating that:

(i) The ground-state energy E_{GS} of an interacting electron gas in a local external potential $V_{ext}(\mathbf{r})$ is determined by the ground-state charge density alone.

(ii) The ground-state charge density minimizes the energy functional

$$E[n] = F[n] + \int V_{ext}(\mathbf{r})\, n(\mathbf{r})\, d\mathbf{r}\,, \tag{1.1}$$

where F[n] is a universal functional of the density, subject to the constraint that the total number of electrons N remains constant: $E_{GS} \equiv E[n_{GS}] \leq E[n]$, for any n such that $\int n(\mathbf{r})\, d\mathbf{r} = N$.

In order to develop a computationally useful scheme out of these statements, an explicit expression for the functional $F[n]$ is required. In the Kohn-Sham approach to DFT [10], the existence of a non-interacting electron gas in an external effective potential having $n(\mathbf{r})$ as its ground-state charge density is assumed, and the functional $F[n]$ is cast in the following form:

$$F[n] = T_0[n] + E_H[n] + E_{xc}[n]\,, \tag{1.2}$$

where:

- $T_0[n]$ is the kinetic energy of the non-interacting system with density $n(\mathbf{r})$;
- $E_H[n]$ is the classical electrostatic energy (Hartree energy):

$$E_H[n] = \frac{e^2}{2} \int\int \frac{n(\mathbf{r})\, n(\mathbf{r}')}{|\mathbf{r} - \mathbf{r}'|}\, d\mathbf{r}\, d\mathbf{r}'\,; \tag{1.3}$$

- $E_{xc}[n]$ is the quantum-mechanical exchange-correlation energy, which accounts for the remaining contributions to the energy functional $E[n]$.

In principle, the functional forms of the kinetic energy $T_0[n]$ and of the exchange-correlation energy $E_{xc}[n]$ are unknown; however:

(i) the kinetic energy of the non-interacting system can be written *exactly* in terms of the so-called Kohn-Sham orbitals $\{\psi_\alpha(\mathbf{r})\}$:

$$T_0 = -\frac{\hbar^2}{2m} \sum_{\alpha=1}^{N} \int \psi_\alpha^*(\mathbf{r})\, \nabla^2 \psi_\alpha(\mathbf{r})\, d\mathbf{r}\,. \tag{1.4}$$

The Kohn-Sham orbitals are the solutions of a Schrödinger-like equation for the non-interacting system; the sum in Eq. (1.4) runs over the N lowest-energy orbitals. Although some approximate expressions for the kinetic-energy functional $T_0[n]$ have been proposed recently [11], which improve considerably over the Thomas-Fermi approximation [12], their accuracy is still too poor to allow realistic calculations of electronic and structural properties of solids.

(ii) Various approximations for the exchange-correlation energy functional $E_{xc}[n]$ are available in the literature; the most simple of them, and the most widely used, is the local-density approximation (LDA):

$$E_{xc}^{LDA}[n] = \int \varepsilon_{xc}(n(\mathbf{r}))\, n(\mathbf{r})\, d\mathbf{r}\,, \tag{1.5}$$

where $\varepsilon_{xc}(n)$ is the exchange-correlation energy per particle of a homogenous electron gas with density n [10]. Despite its simplicity, the LDA has been surprisingly successful in predicting ground-state properties of molecules and solids [13].

In terms of the Kohn-Sham orbitals $\{\psi_\alpha(\mathbf{r})\}$ the charge density reads:

$$n(\mathbf{r}) = \sum_{\alpha=1}^{N} |\psi_\alpha(\mathbf{r})|^2 \,, \tag{1.6}$$

where the sum runs over the N lowest-lying orbitals. Using Eq. (1.4) for the kinetic energy of the non-interacting system, we obtain the Kohn-Sham energy functional:

$$\begin{aligned} E_{KS}\,[\{\psi_\alpha\}] = -\frac{\hbar^2}{2m} \sum_{\alpha=1}^{N} \int \psi_\alpha^*(\mathbf{r})\, \nabla^2 \psi_\alpha(\mathbf{r})\, d\mathbf{r} \\ + \frac{e^2}{2} \int\int \frac{n(\mathbf{r})\, n(\mathbf{r}')}{|\mathbf{r}-\mathbf{r}'|}\, d\mathbf{r}\, d\mathbf{r}' + E_{xc}[n] + \int V_{ext}(\mathbf{r})\, n(\mathbf{r})\, d\mathbf{r} \,, \end{aligned} \tag{1.7}$$

which provides the total energy corresponding to the charge density given by Eq. (1.6). There are basically two conventional approaches to the calculation of ground-state properties within the Kohn-Sham scheme.

In the *global minimization* method, the energy functional (1.7) is directly minimized with respect to the Kohn-Sham orbitals $\{\psi_\alpha\}$, subject to the constraint that the orbitals remain normalized and orthogonal to each other:

$$\int \psi_\alpha^*(\mathbf{r})\, \psi_\beta(\mathbf{r})\, d\mathbf{r} = \delta_{\alpha,\beta} \,. \tag{1.8}$$

The ground-state charge density is then recovered from Eq. (1.6). This strategy was first proposed by Car and Parrinello [14], and is usually implemented using the Steepest-Descent method [14,15] or the Conjugate-Gradients method [16,17].

In the *self-consistent* method, the ground-state energy is obtained indirectly from the self-consistent solution of the Kohn-Sham equation. To

derive this equation, let us impose the Kohn-Sham energy functional (1.7) be stationary with respect to a variation of the orbital $\psi^*_\alpha(\mathbf{r})$, subject to the orthonormality condition (1.8); we obtain the following equation for the orbital $\psi_\alpha(\mathbf{r})$:

$$\left(-\frac{\hbar^2}{2m}\nabla^2 + V_H[n\,;\mathbf{r}] + V_{xc}[n\,;\mathbf{r}] + V_{ext}(\mathbf{r})\right)\psi_\alpha(\mathbf{r}) = \sum\nolimits_\beta \Lambda_{\alpha,\beta}\,\psi_\beta(\mathbf{r})\;, \quad (1.9)$$

where $\Lambda_{\alpha,\beta}$ are Lagrange multipliers, $V_H[n\,;\mathbf{r}]$ is the classical electrostatic potential:

$$V_H[n\,;\mathbf{r}] = \frac{\delta E_H[n]}{\delta n(\mathbf{r})} = e^2\int\frac{n(\mathbf{r}')}{|\mathbf{r}-\mathbf{r}'|}\,d\mathbf{r}\;, \quad (1.10)$$

and $V_{xc}[n\,;\mathbf{r}]$ is the quantum-mechanical exchange-correlation potential:

$$V_{xc}[n\,;\mathbf{r}] = \frac{\delta E_{xc}[n]}{\delta n(\mathbf{r})}\;. \quad (1.11)$$

Therefore, the Kohn-Sham orbitals can be viewed as the normalized solutions of a one-electron, Schrödinger-like equation for the *non-interacting* electron system:

$$\left(-\frac{\hbar^2}{2m}\nabla^2 + V_{KS}[n\,;\mathbf{r}]\right)\psi_\alpha(\mathbf{r}) = \varepsilon_\alpha\,\psi_\alpha(\mathbf{r})\;, \quad (1.12)$$

where $V_{KS}[n\,;\mathbf{r}]$ is the so-called Kohn-Sham potential:

$$V_{KS}[n\,;\mathbf{r}] = V_{ext}(\mathbf{r}) + V_H[n\,;\mathbf{r}] + V_{xc}[n\,;\mathbf{r}]\;. \quad (1.13)$$

The single-particle Kohn-Sham hamiltonian $H_{KS} = -(\hbar^2/2m)\,\nabla^2 + V_{KS}[n\,;\mathbf{r}]$ plays the role of an effective hamiltonian for the non-interacting electron gas with density n. Since the Kohn-Sham potential depends on the charge density $n(\mathbf{r})$, and ultimately on the orbitals $\{\psi_\alpha(\mathbf{r})\}$, the Kohn-Sham equation (1.12) has to be solved self-consistently in order to obtain the ground-state charge density of the system.

The two approaches described above are equivalent, in the sense that they produce the same ground-state charge density and the same total energy. We address now the issue of the computational cost of these conventional schemes for the calculation of the charge density; we are concerned here with the cost of either a single step of the global minimization method or a single iteration of the self-consistent method. Basically, the computational workload is affected by two factors:

(i) the number N of occupied orbitals, and

(ii) the dimension M of the basis set chosen for representing the Kohn-Sham orbitals and the Kohn-Sham hamiltonian.

Both these quantities are proportional to the number of atoms of the system.

In traditional band-structure calculations, the Kohn-Sham equation was solved by direct diagonalization of the Kohn-Sham hamiltonian; this is necessarily an $O(M^3)$ procedure. In the last few years, however, powerful iterative techniques have been developed both for the global minimization of the Kohn-Sham energy functional [16,17], and for the self-consistent solution of the Kohn-Sham equation [18]; these techniques are much more efficient than conventional diagonalization algorithms, particularly when the dimension of the basis set is considerably larger than the number of occupied states. From a computational point of view, the two basic steps required by any iterative method are: (i) the matrix-by vector product $H\psi_\alpha$, where ψ_α is a trial orbital, and (ii) the orthogonalization of the Kohn-Sham orbitals.

Due to the fact that the Kohn-Sham orbitals of an extended system are normally extended, the computational cost of each matrix-by-vector product $H\psi_\alpha$ is $O(M)$ if the hamiltonian is sparse, and $O(M^2)$ if the hamiltonian is dense. Therefore, the total computational cost ranges between $O(NM)$ and

$O(NM^2)$. Since the kinetic-energy operator is diagonal in reciprocal space, and the Kohn-Sham potential is diagonal in direct space, the matrix-by vector product $H\psi_\alpha$ can be conveniently split into two parts: the kinetic-energy contribution is calculated in reciprocal space, while the potential-energy term is computed in real space. In this case, the computational workload is dominated by the cost of Fast-Fourier-Transforms, and scales as $NM \log M$.

The computational cost of the orthogonalization of the Kohn-Sham orbitals is $O(N^2M)$; in fact, each occupied orbital ψ_α must be orthogonalized to the remaining $(N-1)$ occupied orbitals ψ_β, and the cost of the scalar product $\langle\psi_\alpha|\psi_\beta\rangle$ is $O(M)$, for the Kohn-Sham orbitals are extended.

We can conclude that, at least for large systems, the computational workload is dominated by the orthogonalization procedure, and scales as the third power of the number of atoms. The charge density at a given point, however, is a local quantity, which is weakly affected by the more distant environments; therefore, it should be possible to calculate the charge density at a given point with a computational cost which does not depend on the system size. The unfavourable scaling law of conventional approaches is due to the fact that the charge density is expressed in terms of Kohn-Sham orbitals, which are *not* local quantities. In the next sections, we will show how the charge density and the total energy can be obtained directly from the diagonal elements of the real-space Green's function, thus opening the way to an $O(N)$ algorithm.

1.2 Green's function approach to the calculation of the charge density

The one-electron Green's function operator associated to the Kohn-Sham single-particle hamiltonian $\hat{H}_{KS}$ is formally given by:

$$\hat{G}(z) = \left(z - \hat{H}_{KS}\right)^{-1} = \sum\nolimits_{\alpha} \frac{|\psi_\alpha\rangle \langle\psi_\alpha|}{z - \varepsilon_\alpha} , \tag{1.14}$$

where $|\psi_\alpha\rangle$ is the α-th eigenstate of the Kohn-Sham hamiltonian and ε_α is the corresponding eigenvalue: $\hat{H}_{KS}\,|\psi_\alpha\rangle = \varepsilon_\alpha\,|\psi_\alpha\rangle$. As a function of the complex variable z, the Green's function has simple poles on the real axis in correspondence to the eigenvalues of the Kohn-Sham hamiltonian; the residue at each pole is the projector upon the corresponding eigenstates. In the coordinate representation, the Green's function reads:

$$G(\mathbf{r},\mathbf{r}';z) \equiv \langle\mathbf{r}|\,(z - \hat{H}_{KS})^{-1}\,|\mathbf{r}'\rangle = \sum\nolimits_{\alpha} \frac{\psi_\alpha(\mathbf{r})\,\psi_\alpha^*(\mathbf{r}')}{z - \varepsilon_\alpha} . \tag{1.15}$$

As we will see, the diagonal elements $G(\mathbf{r},\mathbf{r};z)$ of the real-space Green's function contain all the information needed to calculate the electronic charge density of the system, without resorting to the explicit diagonalization of the Kohn-Sham hamiltonian.

In order to achieve this goal, we need a link between the Green's function and the one-particle density matrix operator, defined as the projector upon the occupied Kohn-Sham eigenstates:

$$\hat{\rho} = \sum\nolimits_{\alpha} |\psi_\alpha\rangle\langle\psi_\alpha|\;\theta(\varepsilon_F - \varepsilon_\alpha) . \tag{1.16}$$

The Fermi energy ε_F is fixed by the charge neutrality condition:

$$\mathrm{tr}\,\hat{\rho} = N , \tag{1.17}$$

where N is the total number of electrons of the system and $\mathrm{tr}\,\hat{\rho}$ is the trace of the density-matrix operator. In the real-space representation, the density matrix reads:

$$\rho(\mathbf{r},\mathbf{r}') = \sum\nolimits_{\alpha} \psi_{\alpha}(\mathbf{r})\,\psi_{\alpha}^{*}(\mathbf{r}')\;\theta(\varepsilon_F - \varepsilon_{\alpha})\;; \tag{1.18}$$

the diagonal elements of the real-space density matrix yield the electronic charge density:

$$n(\mathbf{r}) = \rho(\mathbf{r},\mathbf{r})\;. \tag{1.19}$$

According to the residue theorem, the density matrix is related to the real-space Green's function by the following integral representation:

$$\rho(\mathbf{r},\mathbf{r}') = \frac{1}{2\pi i}\oint_{C_F} G(\mathbf{r},\mathbf{r}';z)\,dz\;, \tag{1.20}$$

where C_F is an integration contour in the complex energy plane enclosing all and only the poles of the Green's function up to the Fermi energy ε_F (see Fig. 1.1). We are now able to write the electronic charge density in terms of the real-space Green's function:

$$n(\mathbf{r}) = \frac{1}{2\pi i}\oint_{C_F} G(\mathbf{r},\mathbf{r};z)\,dz\;. \tag{1.21}$$

With respect to the conventional approach, based on the diagonalization of the Kohn-Sham hamiltonian, this equation provides an alternative scheme for the calculation of the charge density, which does not require, in principle, the knowledge of Kohn-Sham eigenvalues and eigenfunctions. From this point of view, the Green's function approach shows a number of appealing features.

- First of all, only the diagonal elements of the real-space Green's function enter the calculation of the charge density. This has to be contrasted

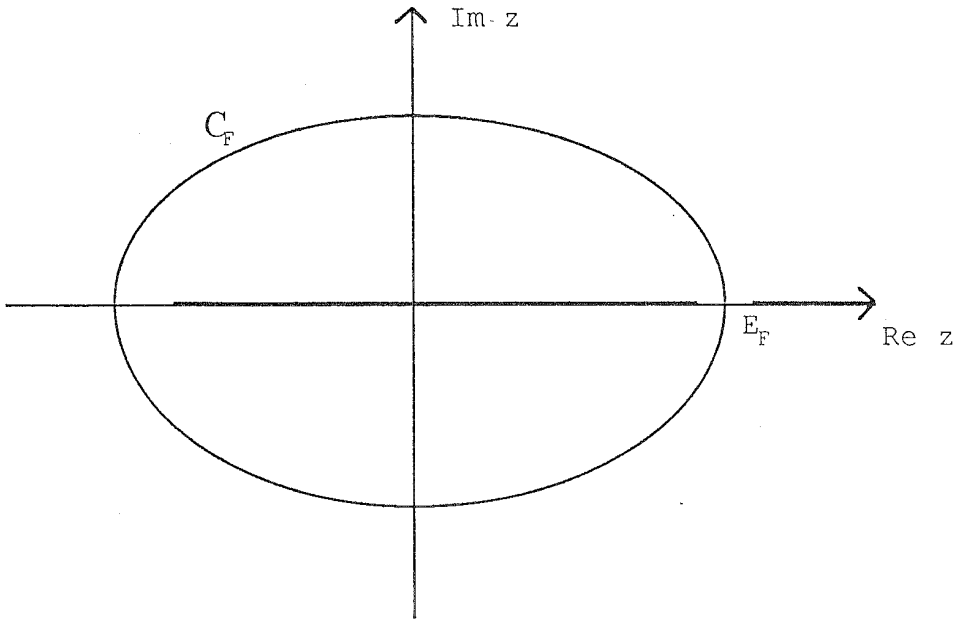

Figure 1.1 – *Integration path in the complex energy plane. The thick line sketches the spectrum of the hamiltonian; E_F is the Fermi energy.*

with conventional approaches, where the Kohn-Sham orbitals provide the entire real-space density matrix via Eq. (1.18). In a sense, the Kohn-Sham orbitals contain much more information than needed for the calculation of the charge density.

- Second, the Green's function diagonal element $G(\mathbf{r},\mathbf{r};z)$ is a local quantity, which is stable with respect to a variation of the boundary conditions far away from the point $\mathbf{r}$ [19]. Therefore, each diagonal element of the real-space Green's function can be obtained, in principle, with a computational workload which does not depend on the size of the system, at least for large systems.
- Third, the number of sampling points along the integration contour $\mathcal{C}_F$,

at which the Green's function has to be evaluated in order to calculate the integral numerically to a given accuracy, does not depend on the size of the system. Actually, the number of sampling points depends on (i) the length of the integration contour, and (ii) the smoothness of the Green's function along the contour. The length of the integration contour is related to the valence band-width, which is an intensive quantity, independent of the size of the system. The smoothness of the Green's function along the integration contour depends, basically, on the distance between the contour itself and the poles of the Green's function, which lie on the real axis; for non-metallic systems, this distance can be always kept finite. Therefore, the smoothness of the Green's function depends on the choice of the integration contour, but not on the system size.

We can conclude that the overall computational cost for the calculation of the charge density within the Green's function approach scales only linearly with the size of the system, provided the local nature of the Green's function diagonal elements is properly taken into account. In the next chapters, we will discuss two different methods which exploit the local nature of the charge density to achieve linear scaling.

1.3 Total energy and expectation values

Within the Kohn-Sham approach to DFT the interacting electron system is mapped onto a non-interacting electron gas with the same charge density $n(\mathrm{r})$. The ground-state expectation value of any single-particle operator $\hat{A}$ in the non-interacting system can be directly expressed in terms of the eigenstates

$|\psi_\alpha\rangle$ and eigenvalues ε_α of the Kohn-Sham hamiltonian:

$$\langle \hat{A} \rangle = \sum\nolimits_\alpha \langle \psi_\alpha | \, \hat{A} \, | \psi_\alpha \rangle \;\; \theta(\varepsilon_F - \varepsilon_\alpha) \, . \tag{1.22}$$

From the definition of the density-matrix operator, Eq. (1.16), it follows that:

$$\langle \hat{A} \rangle = \mathrm{tr} \, (\, \hat{\rho} \, \hat{A} \,) \, . \tag{1.23}$$

Therefore, using the integral representation of the density-matrix operator, we obtain the ground-state expectation value of the operator $\hat{A}$ in terms of the self-consistent Green's function $\hat{G}(z)$:

$$\langle \hat{A} \rangle = \frac{1}{2\pi i} \oint_{C_F} \mathrm{tr} \left[\, \hat{G}(z) \, \hat{A} \, \right] dz \, . \tag{1.24}$$

In general, both the diagonal and the off-diagonal elements of the real-space Green's function $G(\mathbf{r}, \mathbf{r}' \, ; z)$ are involved in the calculation of the trace, whereas only the diagonal elements are required for the self-consistent calculation of the charge density. Therefore, the evaluation of ground-state expectation values may be much more time consuming than the full calculation of the charge density. However, when either the operator $\hat{A}$ is a function of the Kohn-Sham hamiltonian, or it is diagonal in the coordinate representation, only the diagonal elements of the Green's function enter the calculation of the trace (see Appendix A), and no additional effort is required to obtain the ground-state expectation value of the operator $\hat{A}$.

Let us consider first the kinetic energy of the non-interacting electron system:

$$T_0 = -\frac{\hbar^2}{2m} \sum\nolimits_\alpha \langle \psi_\alpha | \, \nabla^2 \, | \psi_\alpha \rangle \;\; \theta(\varepsilon_F - \varepsilon_\alpha) \, . \tag{1.25}$$

Using the coordinate representation for the calculation of the trace, we obtain from Eq. (1.24):

$$T_0 = \frac{1}{2\pi i} \int d\mathbf{r} \lim_{\mathbf{r}' \to \mathbf{r}} \oint_{C_F} -\frac{\hbar^2}{2m} \nabla^2_{\mathbf{r}'} G(\mathbf{r}, \mathbf{r}'; z)\, dz \,. \tag{1.26}$$

Unfortunately, this approach turns out to be rather cumbersome, since some of the off-diagonal elements of the real-space Green's function are needed. Therefore, we prefer to adopt an indirect approach to the calculation of the kinetic energy.

Let E_{bs} denote the so-called *band-structure energy*, corresponding to the sum of occupied eigenvalues in conventional schemes:

$$E_{bs} = \sum\nolimits_{\alpha} \langle \psi_\alpha | \, \hat{H}_{KS} \, | \psi_\alpha \rangle \;\; \theta(\varepsilon_F - \varepsilon_\alpha) = \sum\nolimits_{\alpha} \varepsilon_\alpha \, \theta(\varepsilon_F - \varepsilon_\alpha) \,. \tag{1.27}$$

Since $\hat{H}_{KS} = -(\hbar^2/2m)\,\nabla^2 + \hat{V}_{KS}$, the kinetic energy of the non-interacting system reads:

$$T_0 = E_{bs} - \int V_{KS}(\mathbf{r})\, n(\mathbf{r})\, d\mathbf{r} \,. \tag{1.28}$$

In the Green's function formalism, the band-structure energy becomes:

$$E_{bs} = \frac{1}{2\pi i} \int d\mathbf{r} \oint_{C_F} z\, G(\mathbf{r}, \mathbf{r}; z)\, dz \,. \tag{1.29}$$

Therefore, the kinetic energy can be written in terms of the diagonal elements of the real-space Green's function as:

$$T_0 = \frac{1}{2\pi i} \int d\mathbf{r} \oint_{C_F} \left[z - V_{KS}(\mathbf{r}) \right] G(\mathbf{r}, \mathbf{r}; z)\, dz \,. \tag{1.30}$$

Once the kinetic energy of the non-interacting system has been obtained, the ground-state energy E can be easily calculated:

$$E = T_0 + \frac{1}{2} \int V_H(\mathbf{r})\, n(\mathbf{r})\; d\mathbf{r} + E_{xc} + \int V_{ext}(\mathbf{r})\, n(\mathbf{r})\; d\mathbf{r} \,, \tag{1.31}$$

where $V_H(\mathbf{r})$ is the Hartree electrostatic potential, E_{xc} is the exchange-correlation energy, and $V_{ext}(\mathbf{r})$ is the local external potential. Substituting Eq. (1.30) and (1.21) into Eq. (1.31), one arrives at the following expression of the energy in terms of the diagonal elements of the real-space Green's function:

$$E = \frac{1}{2\pi i} \int d\mathbf{r} \oint_{\mathcal{C}_F} \left[z - V_{KS}(\mathbf{r}) + \frac{1}{2} V_H(\mathbf{r}) + V_{ext}(\mathbf{r}) \right] G(\mathbf{r}, \mathbf{r}\,; z)\, dz + E_{xc}\,. \tag{1.32}$$

Since the Green's function diagonal elements are local quantities, the overall computational workload for the calculation of the total energy scales linearly with the size of the system.

1.4 Real-space discretization of the Kohn-Sham hamiltonian

The Green's function approach to the calculation of the charge density leads naturally to an $O(N)$ algorithm, provided each diagonal element of the real-space Green's function can be obtained with a computational workload which does not depend on the size of the system. To this end, the real-space representation of the Kohn-Sham hamiltonian plays an essential role.

In fact, the hamiltonian matrix is strictly sparse in this representation, in the sense that the number of non-vanishing matrix elements scales linearly with the size of the system. This is due to the fact that *both* the kinetic-energy operator and the Kohn-Sham potential are short-range operators in real space. Therefore, for any localized state ψ, the computational cost of the matrix-by-vector product $H\psi$ is independent of the size of the system,

because the state $H\psi$ is also localized; as we will see, this property is essential to any $O(N)$ method.

Furthermore, the real-space representation of the Kohn-Sham hamiltonian leads directly to the Green's functional diagonal elements $G(\mathbf{r},\mathbf{r}\,;z)$; if a different basis set $\{\phi_i\}$ were used, the real-space Green's function would be given by:

$$G(\mathbf{r},\mathbf{r}\,;z) = \sum\nolimits_{i,j} \phi_i(\mathbf{r})\, \phi_j^*(\mathbf{r})\, G_{i,j}(z)\,, \tag{1.33}$$

and the off-diagonal matrix elements $G_{i,j}(z) = \langle\phi_i|\,\hat{G}(z)\,|\phi_j\rangle$ should be calculated in order to get the charge density all over the system. From a computational point of view, the latter approach turns out to be rather demanding within the recursion method, if compared with the direct real-space-representation approach.

The real-space representation of the Kohn-Sham hamiltonian is achieved by discretizing the hamiltonian on a finite grid. The physical system is enclosed into a " computational box " Ω of appropriate size and shape; then, the computational domain is filled with a real-space mesh $\mathcal{M} = \{\mathbf{r}_i,\, i = 1,\cdots,M\}$; the number of grid-points and their positions depend, basically, on the smoothness of the Kohn-Sham potential. In the simple case of a cubic box of side L filled with a uniform real-space mesh, the building blocks are small cubes of edge $h = L/m$, where m is the number of grid-points along each direction. Therefore, the total number of grid-points is $M = m^3$, and the coordinates of the points are: $\mathbf{r}_{i,j,k} = (i-1)\,h,\ (j-1)\,h,\ (k-1)\,h$, with $i,\, j,\, k = 1,\cdots,m$.

An orthonormal basis set $\{\,|\,\mathbf{r}_i\rangle\,\}$ can be readily drawn out of the real-space grid $\mathcal{M}$, each basis vector $|\,\mathbf{r}_i\rangle$ being localized at the corresponding

grid-point. Any non-singular function $\phi(\mathbf{r})$, defined over the computational domain Ω, can be represented on the basis set $\{ |\mathbf{r}_i\rangle \}$ by taking the values of the function at the nodes of the real-space grid. When using periodic boundary conditions, the discretization of a function $\phi(\mathbf{r})$ on a uniform mesh with grid-spacing h turns out to be equivalent, by means of the sampling theorem [20], to a plane-wave expansion retaining all the Fourier components corresponding to the reciprocal lattice vectors $\mathbf{G}$ enclosed in a cubic box with edge $G_{max} = 2\pi/h$. However, the real-space representation is more flexible than a conventional plane-wave expansion, because (i) it allows different boundary conditions to be implemented in a convenient fashion, and (ii) the real-space grid can be locally refined to deal with a more oscillatory behaviour of the function.

The discretization of the Kohn-Sham potential over a real-space grid is straightforward, provided the external potential is local. However, even if non-local pseudopotentials are used to deal with electron-ion interactions, the Kohn-Sham potential can still be represented on a real-space mesh. Since the range of the non-local part of the pseudopotential is determined by the core radius (~ 1 a.u.), the Kohn-Sham potential is still a short-range, sparse operator in real-space.

The discretization of the kinetic-energy operator on a real-space grid is slightly more complicate. Given an analytic function $\phi(\mathbf{r})$, defined over the computational box Ω, the laplacian of ϕ at the point $\mathbf{r}_i$, $\nabla^2\phi_i$, can be derived using a finite-differences scheme. First, the laplacian is formally expanded as:

$$\nabla^2\phi_i \simeq \sum_{k=1}^{M} c_{i,k}\,\phi_k \ , \tag{1.34}$$

where ϕ_k is the value of the function $\phi(\mathbf{r})$ at the point $\mathbf{r}_k$, and k runs over

the M nodes of the real-space mesh $\mathcal{M}$. Since the laplacian is a local operator in real-space, it is sensible to retain in expansion (1.34) just a few coefficients $c_{i,k}$, corresponding to m_s grid-points localized around the point $\mathbf{r}_i$; this set of m_s points fixes the so-called *stencil*. Then, for each point $\mathbf{r}_k$ of the stencil, the function ϕ_k is Taylor-expanded around the point $\mathbf{r}_i$:

$$\phi_k = \sum_{n=0}^{\infty} \frac{1}{n!} \left(h_{k,x} \frac{\partial}{\partial x} + h_{k,y} \frac{\partial}{\partial y} + h_{k,z} \frac{\partial}{\partial z} \right)^n \phi \Big|_{\mathbf{r}=\mathbf{r}_i} , \tag{1.35}$$

where $\mathbf{h}_k = \mathbf{r}_k - \mathbf{r}_i$; substituting this Taylor expansion into Eq. (1.34), and equating the coefficients of the derivatives $\partial^2\phi/\partial x^2$, $\partial^2\phi/\partial y^2$ and $\partial^2\phi/\partial z^2$ to 1, and the coefficients of the remaining derivatives to 0, one arrives at a set of linear equations for the coefficients $c_{i,1}$, $\cdots$, c_{i,m_s}. In general, this linear system cannot be solved unless the derivatives of order $n > n_{max}$ are neglected, where n_{max} depends on the choice of the stencil. In other words, the higher is the order of the derivatives retained – and therefore the accuracy of the Taylor expansion (1.35) – the larger must be the extension of the real-space stencil.

As an example, let us consider a uniform mesh with grid-spacing h and periodic boundary conditions; the simplest discretization of the laplacian leading to an $O(h^2)$ error is provided by a 7-point stencil:

$$\nabla^2\phi_i = \frac{1}{h^2} \left(\sum\nolimits'_{\alpha} \phi_\alpha - 6\,\phi_i \right) + O(h^2) , \tag{1.36}$$

where α runs over the 6 nearest neighbours of the point $\mathbf{r}_i$. Similarly, the simplest discretization of the laplacian leading to an $O(h^4)$ error requires a 13-point stencil:

$$\nabla^2\phi_i = \frac{1}{12\,h^2} \left(16 \sum\nolimits'_{\alpha} \phi_\alpha - \sum\nolimits''_{\beta} \phi_\beta - 90\,\phi_i \right) + O(h^4) , \tag{1.37}$$

where α and β run over the 6 first nearest-neighbours and the 6 fourth nearest-neighbours of the point $\mathbf{r}_i$, respectively.

The Kohn-Sham hamiltonian in the real-space representation has the general form:

$$H_{KS} = \sum_{i,j} h_{i,j} \, |\mathbf{r}_i\rangle\langle\mathbf{r}_j| \, , \tag{1.38}$$

where $h_{i,j} = 0$ for $|\mathbf{r}_i - \mathbf{r}_j| > R_H$. The range of the hamiltonian R_H is the maximum between the core radius (0 in the case of a local potential) and the extension of the real-space stencil. In the simple case of a uniform mesh with grid-spacing h, a local Kohn-Sham potential $V_{KS}(\mathbf{r})$, and a first-nearest-neighbour discretization of the kinetic energy, the matrix elements of the hamiltonian are (in atomic units):

$$h_{i,j} = \begin{cases} 3/h^2 + V_{KS}(\mathbf{r}_i) & \text{if } i = j \\ -1/2h^2 & \text{if } i \text{ and } j \text{ are nearest neighbours} \\ 0 & \text{otherwise} \end{cases} \tag{1.39}$$

To test the validity of the real-space discretization of the Kohn-Sham hamiltonian, we have calculated the charge density of a simple system using different grids and stencils. The trial system consists of 8 Silicon atoms, slightly displaced at random from their bulk equilibrium positions. In order to mimic an infinite system, the Silicon atoms are arranged in a cubic unit cell with periodic boundary conditions; the lattice parameter is fixed at the experimental value: $a_0 = 10.26$ a.u. The Kohn-Sham potential is approximated using the Appelbaum-Hamann ionic pseudopotential [21] screened by the Thomas-Fermi diagonal dielectric function; this approximation will be used throughout this work for every non-selfconsistent calculation. The hamiltonian has been represented on a real-space grid, and diagonalized to yield the

charge density at the grid-points:

$$n(\mathbf{r}_i) = \sum\nolimits_{\alpha} |\psi_\alpha(\mathbf{r}_i)|^2 \;\; \theta(\varepsilon_F - \varepsilon_\alpha) \; . \tag{1.40}$$

For comparison, the "exact" charge density has been obtained by a conventional plane-wave calculation at $\mathbf{k} = 0$, corresponding to periodic boundary conditions on the unit cell; a kinetic-energy cutoff of 20 Rydbergs has been used for the plane-wave expansion.

The solid lines in Fig. 1.2 show the exact, plane-wave charge density along the diagonal of the unit cell; the dots and the circles show, instead, the charge density obtained using the real-space discretization of the Kohn-Sham hamiltonian. In the case of Fig. 1.2 (a), the hamiltonian has been represented on a uniform $24 \times 24 \times 24$ real-space grid, using a 7-point stencil (closed circles) and a 13-point stencil (open circles) for the discretization of the kinetic-energy operator. As we can see, the 13-point stencil produces a very accurate charge density, but the 7-point stencil result is also acceptable. In the case of Fig. 1.2 (b), a coarser $16 \times 16 \times 16$ grid has been used; whereas the 13-point stencil (closed circles) still does reproduce the charge density closely, the 7-point stencil (open circles) fails. We can conclude that the $16 \times 16 \times 16$ real-space grid is fine enough to provide an accurate description of the potential in this case, but requires an $O(h^4)$ discretization of the kinetic energy to yield the charge density correctly.

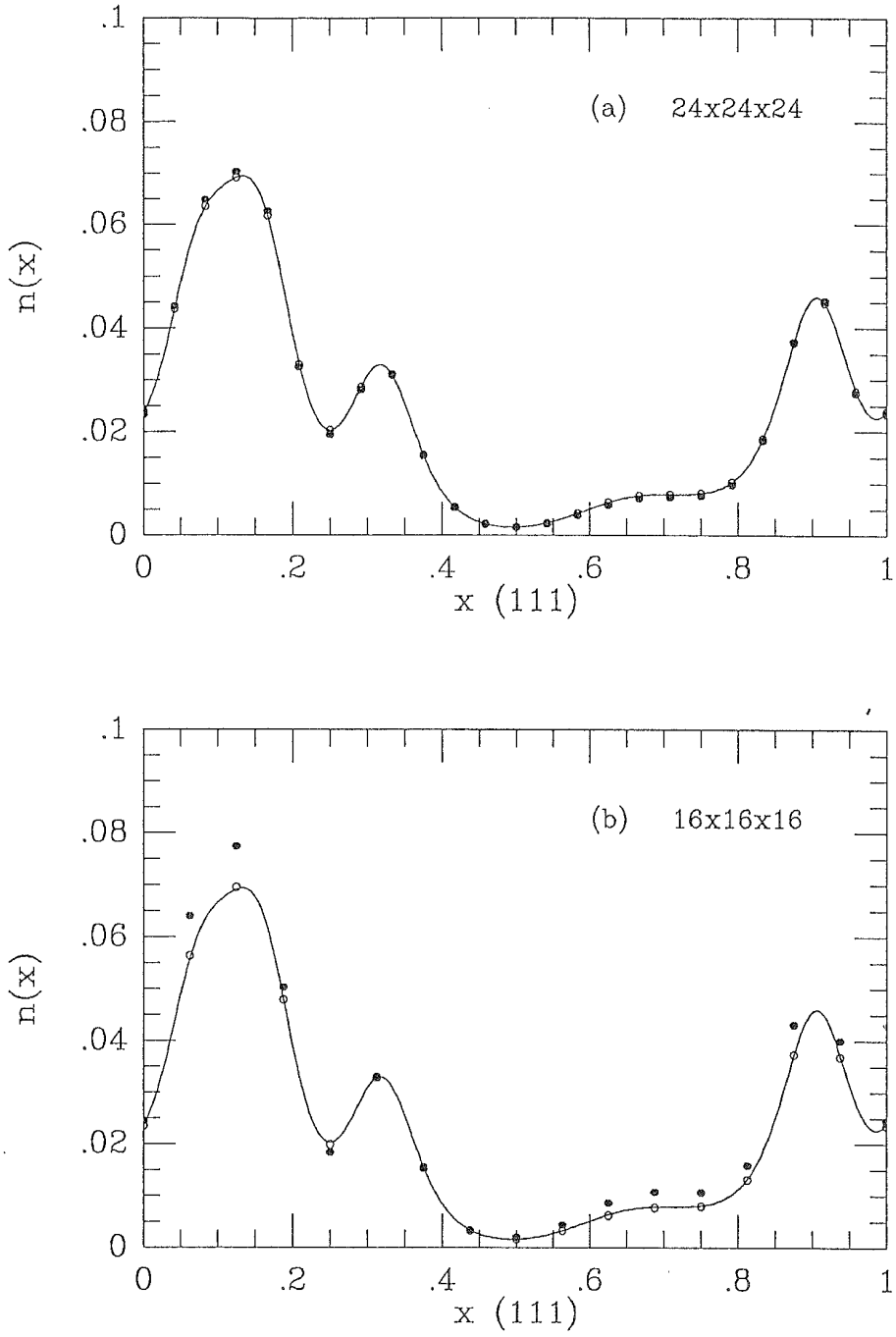

Figure 1.2 – *Charge density along the (111) direction obtained from a conventional plane-wave expansion (solid lines) and from the real-space representation of the Kohn-Sham hamiltonian (circles). Different grids and stencils have been used. (a):* $24 \times 24 \times 24$ *real-space grid; (b):* $16 \times 16 \times 16$ *real-space grid; closed circles: 7-point stencil; open circles: 13-point stencil.*

Chapter 2

Recursion Method

The recursion method [22] provides a simple and efficient scheme for calculating each diagonal element of the real-space Green's function with a computational workload which does not depend, in principle, on the size of the system; this goal is achieved by fully taking into account the local nature of the real-space Green's function. Therefore, the recursion method opens the way to the formulation of an $O(N)$ algorithm for the self-consistent calculation of electronic and structural properties of large systems, in the framework of Density-Functional Theory. The recursion-method formalism is presented in detail in Appendix A; in this chapter we discuss its application to the calculation of the electronic charge density.

2.1 Calculation of the charge density

Our starting point is the real-space representation of the Kohn-Sham hamiltonian on a discrete mesh $\mathcal{M} = \{\mathbf{r}_i, i = 1, \cdots, M\}$. At every point of the real-space grid $\mathcal{M}$, the charge density is calculated using the integral representation of the density matrix; according to Eq. (1.21), we have:

$$n(\mathbf{r}_i) = \frac{1}{2\pi i} \oint_{C_F} G(\mathbf{r}_i, \mathbf{r}_i\,; z)\, dz \ . \tag{2.1}$$

The recursion method (RM) provides a simple and powerful algorithm for computing the diagonal elements $G(\mathbf{r}_i, \mathbf{r}_i\,; z)$ of the real-space Green's function. For each point $\mathbf{r}_i$ of the real-space grid, an independent chain transformation (see Appendix A) is performed starting from an initial state $|\,0\,\rangle$ localized at the point $\mathbf{r}_i$: $\langle \mathbf{r}_j | 0 \rangle = \delta_{i,j}$, for any point $\mathbf{r}_j \in \mathcal{M}$. The Kohn-Sham hamiltonian, discretized over the real-space grid, is repeatedly applied to generate a set of orthonormal states $\{\,|\,n\,\rangle\,\}$ via the three-term recurrence relation:

$$\hat{H}_{KS}\,|\,n\,\rangle = a_n\,|\,n\,\rangle + b_{n+1}\,|\,n+1\,\rangle + b_n\,|\,n-1\,\rangle\ , \tag{2.2}$$

where $|\,-1\,\rangle$ is the null state, and the chain parameters a_n's and b_n's are chosen to ensure the orthonormality of the recursion states:

$$\begin{aligned} a_n &= \langle\, n\,|\,\hat{H}_{KS}\,|\,n\,\rangle \\ b_{n+1} &= \|\,(\hat{H}_{KS} - a_n)\,|\,n\,\rangle\, - b_n\,|\,n-1\,\rangle\,\| \ . \end{aligned} \tag{2.3}$$

Clearly, the chain parameters $\{a_n, b_n\}$ and the recursion states $\{\,|\,n\,\rangle\,\}$ depend on the starting point $\mathbf{r}_i$. Since both the kinetic energy and the Kohn-Sham potential are short-range operators in real-space, the n-th state of the recursion chain is localized within a region of size R_n proportional to

n around the starting point $\mathbf{r}_i$. As an example, let us consider the simple case of a uniform cubic mesh with a first-nearest-neighbour (7-point stencil) discretization of the laplacian. Provided the boundary of the real-space grid has not been reached, the n-th state of the recursion chain is localized within a regular octahedron centered at the point $\mathbf{r}_i$, whose diagonal is given by $R_n = 2nh$. Similarly, in the case of a fourth-nearest-neighbour (13-point stencil) discretization of the laplacian, the diagonal of the octahedron is $R_n = 4nh$.

In principle, the chain transformation (2.2) can be carried on until the state $|\, n_s \,\rangle$ is generated, $n_s + 1$ being the dimension of the Hilbert subspace spanned by the vectors $\{H_{KS}^n \,|\, 0\,\rangle,\ n = 0, \cdots, \infty\}$. In disordered systems $n_s + 1$ coincides with the dimension M of the real-space grid; only if symmetries are present it may happen that $n_s + 1 < M$. The Kohn-Sham hamiltonian turns out to be tridiagonal in the representation of the recursion states $\{\, |\, n\,\rangle,\ n = 0, \cdots, n_s\,\}$, so that it can be easily inverted to yield the Green's function diagonal element $G(\mathbf{r}_i, \mathbf{r}_i\,; z) \equiv \langle\, 0\,|\,\hat{G}(z)\,|\,0\,\rangle$:

$$G(\mathbf{r}_i, \mathbf{r}_i\,; z) = \cfrac{1}{z - a_0(\mathbf{r}_i) - \cfrac{b_1^2(\mathbf{r}_i)}{z - a_1(\mathbf{r}_i) - \cdots - \cfrac{b_{n_s}^2(\mathbf{r}_i)}{z - a_{n_s}(\mathbf{r}_i)}}}\ , \tag{2.4}$$

where the dependence of the chain parameters on the starting point $\mathbf{r}_i$ has been made explicit. Once the recursion coefficients $\{a_n(\mathbf{r}_i),\, b_n(\mathbf{r}_i)\}$ have been computed, the charge density at the point $\mathbf{r}_i$ can be readily obtained by contour integration; substituting Eq. (2.4) into Eq. (2.1), we obtain:

$$n(\mathbf{r}_i) = \frac{1}{2\pi i} \oint_{C_F} \frac{1}{z - a_0(\mathbf{r}_i) - \cdots}\ dz\ . \tag{2.5}$$

The integration contour C_F is somewhat arbitrary, provided it encloses all the poles of the Green's function $G(\mathbf{r}_i, \mathbf{r}_i; z)$ up to the Fermi energy ε_F; in general, however, an optimum choice exists that minimizes the number of sampling points at which the Green's function has to be calculated in order to evaluate the integral numerically to a given accuracy. We choose a rectangular path in the complex energy plane (see Fig. 2.1) crossing the real axis at $\mathrm{Re}\, z = \varepsilon_F$ and $\mathrm{Re}\, z = \varepsilon_L$, where ε_L is any lower bound for the spectrum of the Kohn-Sham hamiltonian; provided the Kohn-Sham potential is bounded from below, a safe choice for ε_L is given by the minimum of the potential itself. The integration path is symmetrical with respect to the real axis, and crosses the imaginary axis at $\mathrm{Im}\, z = \pm 0.2$ Ryd; the integral is evaluated numerically, using an adaptive Simpson's rule.

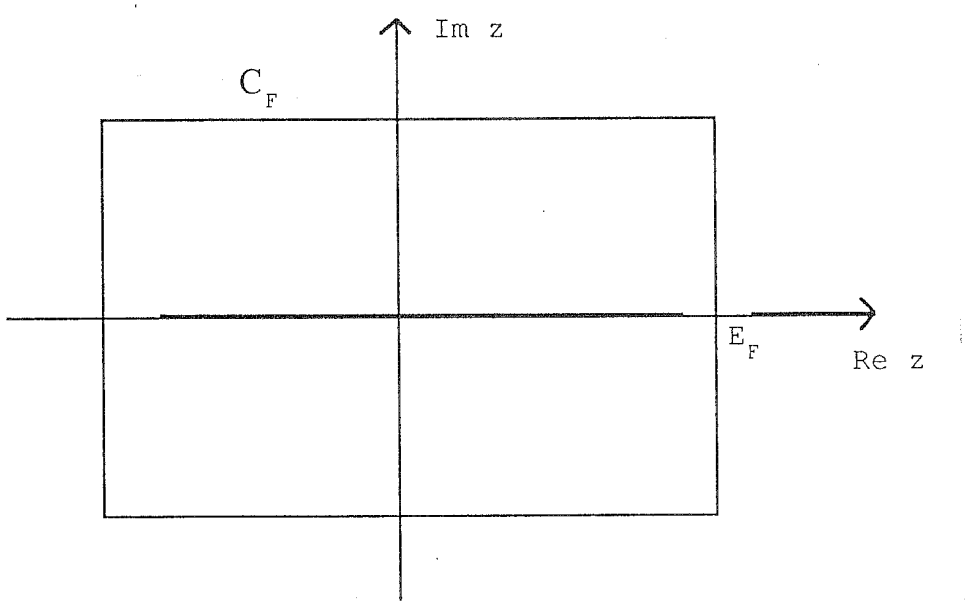

Figure 2.1 – *Integration contour in the complex energy plane for the calculation of the charge density; E_F is the Fermi energy.*

In the calculation of the charge density, the continued-fraction expansion (2.4) can be truncated after a relatively small number of steps $n \ll n_s$; in the next section, we will discuss in detail the convergence of the charge density with respect to the number of recursion steps. In order to check the validity of the recursion-method approach to the calculation of the charge density, we have performed a trial calculation on the same sample system described in the previous section. The valence charge density along the (111) direction is plotted in Fig. 2.2.

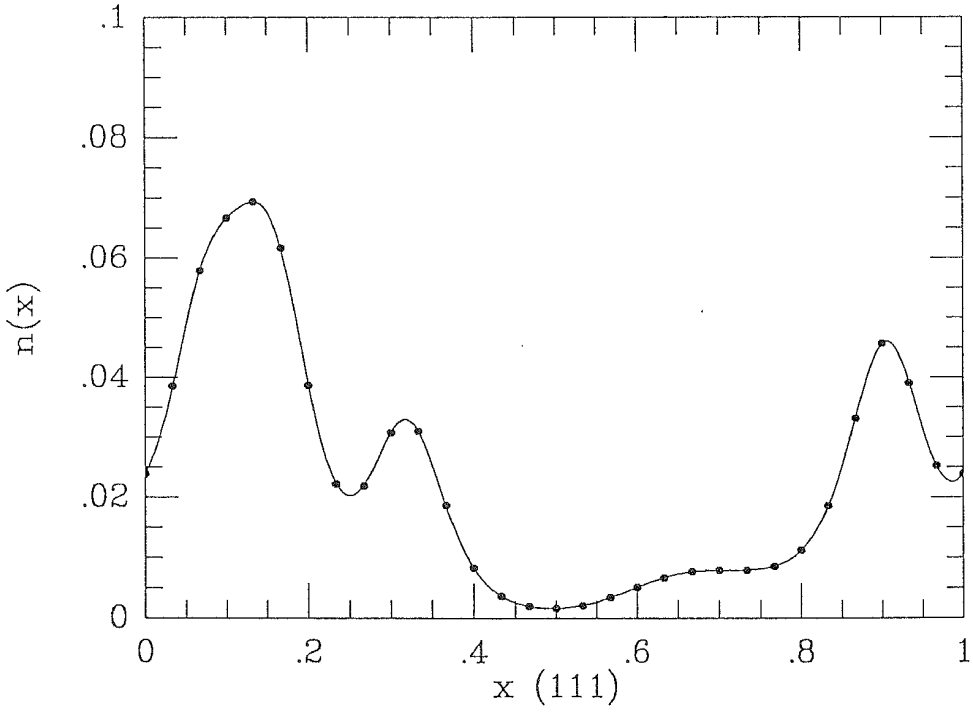

Figure 2.2 – *Charge density along the diagonal of the cubic cell, as obtained from a conventional plane-wave calculation (solid line) and from the recursion-method approach (dots).*

The solid line is the "exact" charge density, obtained from a well-converged plane-wave calculation, as discussed in the previous section. The dots show

the charge density calculated with the present approach. The hamiltonian has been represented on a uniform $30 \times 30 \times 30$ real-space grid, using a 13-point stencil for the discretization of the kinetic-energy operator, and the chain transformation has been carried on until the charge density has converged within machine precision (500 steps). As we can see, the agreement is nearly perfect.

2.2 Convergence of the recursion chain

The basic feature of the recursion method, which makes it an efficient tool for the calculation of local properties, is the fast convergence of any local energy-integrated quantity with respect to the number of recursion steps. Within the present approach, the first state of the recursion chain is localized at a given point of the real-space grid, and the successive states explore the surrounding regions, expanding outwards at a rate which is linear in the number of recursion steps. Therefore, the convergence of the charge density with the number of chain steps reflects the physical intuition that the charge density at a given point is affected progressively less by the more distant environments.

In practice, one finds that for insulating systems the charge density converges exponentially with the number of recursion steps, whereas the rate of convergence is only a power law for metallic systems at zero temperature. For finite systems, the spectrum of the Kohn-Sham hamiltonian is always discrete, and the rate of convergence of the charge density depends basically on the width of the gap between the highest occupied state and the lowest

unoccupied state.

We give now a formal argument to explain the convergence of the charge density with the number of recursion steps. Let us truncate the continued-fraction expansion of the Green's function after n steps:

$$G^{(n)}(\mathbf{r}_i, \mathbf{r}_i\,; z) = \cfrac{1}{z - a_0(\mathbf{r}_i) - \cfrac{b_1^2(\mathbf{r}_i)}{z - a_1(\mathbf{r}_i) - \cdots - \cfrac{b_n^2(\mathbf{r}_i)}{z - a_n(\mathbf{r}_i)}}} \,. \tag{2.6}$$

The truncated Green's function $G^{(n)}(\mathbf{r}_i, \mathbf{r}_i\,; z)$ has $n+1$ distinct poles on the real axis, and its spectral decomposition reads:

$$G^{(n)}(\mathbf{r}_i, \mathbf{r}_i\,; z) = \sum_{\alpha=0}^{n} \frac{\omega_\alpha(\mathbf{r}_i)}{z - \varepsilon_\alpha(\mathbf{r}_i)} \,, \tag{2.7}$$

where $\varepsilon_\alpha(\mathbf{r}_i)$ is th α-th eigenvalue of the recursion chain started at point $\mathbf{r}_i$, and $\omega_\alpha(\mathbf{r}_i)$ is the corresponding weight. Substituting the spectral decomposition (2.7) into the equation for the charge density (2.1), we obtain:

$$n^{(n)}(\mathbf{r}_i) = \sum_{\alpha=0}^{n} \omega_\alpha(\mathbf{r}_i)\, \theta\left(\varepsilon_F - \varepsilon_\alpha(\mathbf{r}_i)\right) \,. \tag{2.8}$$

One can show that this is precisely the n-th order Gaussian quadrature formula for the integral

$$n(\mathbf{r}_i) = \int_{-\infty}^{\infty} \rho(\mathbf{r}_i\,; \varepsilon)\, \theta(\varepsilon_F - \varepsilon)\, d\varepsilon \,, \tag{2.9}$$

where $\rho(\mathbf{r}_i\,; \varepsilon)$ is the *exact* local density of states calculated at the point $\mathbf{r}_i$. In an insulating system, the step-like function $\theta(\varepsilon_F - \varepsilon)$ can be replaced with a relatively smooth, well-behaved function $f(\varepsilon_F - \varepsilon)$, for the local density of states vanishes inside the gap. Since the Gaussian integration formula converges exponentially with the number of nodes and weights for

any non-singular function [23], it follows that the "truncated" charge density $n^{(n)}(\mathbf{r}_i)$ converges with an exponential rate to the exact charge density $n(\mathbf{r}_i)$; furthermore, the larger is the gap, the faster is the convergence. In a metallic system at zero temperature, the step-like character of the θ-function must be retained, and the convergence of the Gaussian quadrature formula is only polynomial-like.

The typical behaviour of the charge density as a function of the number of recursion steps n is shown in Fig. 2.3. The system considered here is a cubic supercell containing 216 Silicon atoms in their bulk equilibrium geometry. The hamiltonian has been discretized on a uniform $48 \times 48 \times 48$ grid with periodic boundary conditions, and the charge density has been calculated at a grid-point corresponding to the position of a Silicon atom. As a function of the number of recursion steps, the point-wise charge density shows a characteristic damped oscillatory behaviour; each oscillation corresponds to a pole of the truncated Green's function dropping below the Fermi level. Since the poles are nearly uniformly distributed over the spectrum of the hamiltonian, the period of the oscillations is given by to the ratio between the total band-width and the valence band-width. The total band-width W depends, basically, on the grid-spacing h: $W \propto 1/h^2$; therefore, the finer is the real-space grid, the larger is the period of the oscillations. As Fig. 2.3 clearly demonstrates, the charge density converges well before the number of poles below the Fermi energy equals the number of valence states (432 in this case); in other words, the number of recursion steps needed to achieve convergence is much smaller than the dimension of the basis set ($\sim 10^5$).

Let us consider now in more detail the link between the rate of convergence and the grid-spacing, h. According to our previous discussion,

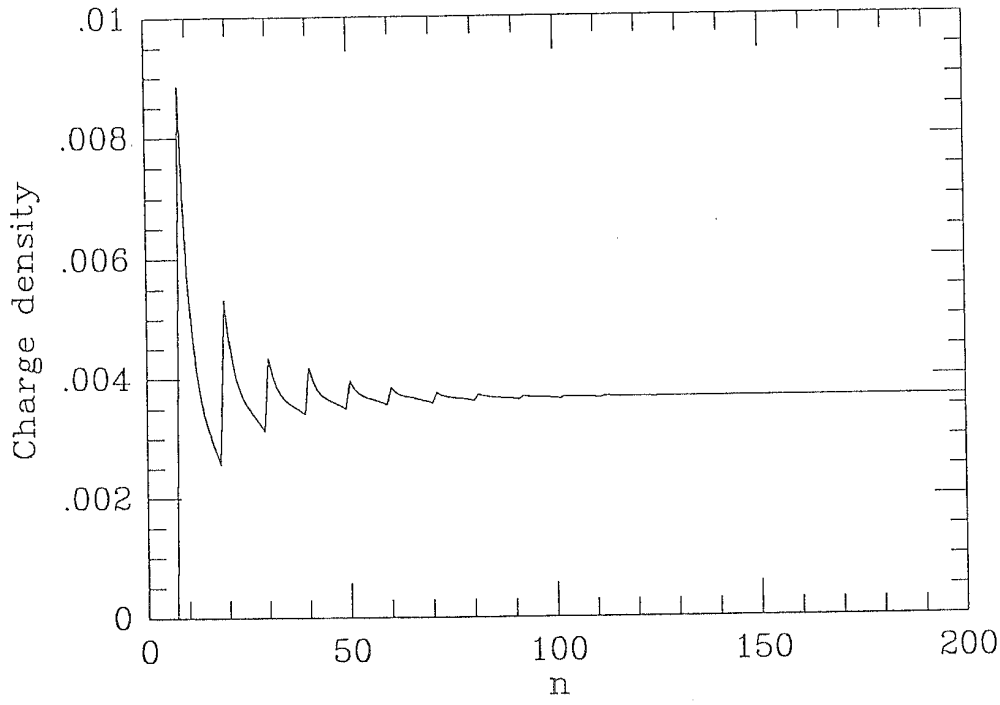

Figure 2.3 – *Convergence of the point-wise charge density with the number n of recursion steps.*

the number of poles below the Fermi energy scales as $n\,h^2$, where n is the number of recursion steps; however, this is not the only factor affecting the convergence of the charge density. To clarify this point, we have calculated the charge density of a simple trial system using different grids. The system considered here is a cubic cell containing 8 Silicon atoms arranged in their equilibrium positions, at the experimental lattice constant $a_0 = 10.26$ a.u.; for each real-space grid, the charge density has been calculated at a grid-point corresponding to the bond-center between two Silicon atoms. The open circles in Fig. 2.4 show the charge density ρ_h as a function of the number of divisions N_h along each direction: $N_h = a_0/h$. For $N_h \geq 24$, the charge density remains nearly constant. The black circles in Fig. 2.4 show, for

every value of N_h, the number of recursion steps $n_{\rm conv}$ which are required to reproduce the exact charge density ρ_h within 0.5%; evidently, $n_{\rm conv}$ is well approximated by a straight line, so that $n_{\rm conv}\ h \sim$ constant. We can conclude that the rate of convergence of the charge density scales linearly with the grid spacing h. For very large systems, this matches the physical intuition that the convergence of the recursion chain is determined essentially by the spatial extension of the region explored by the states of the chain.

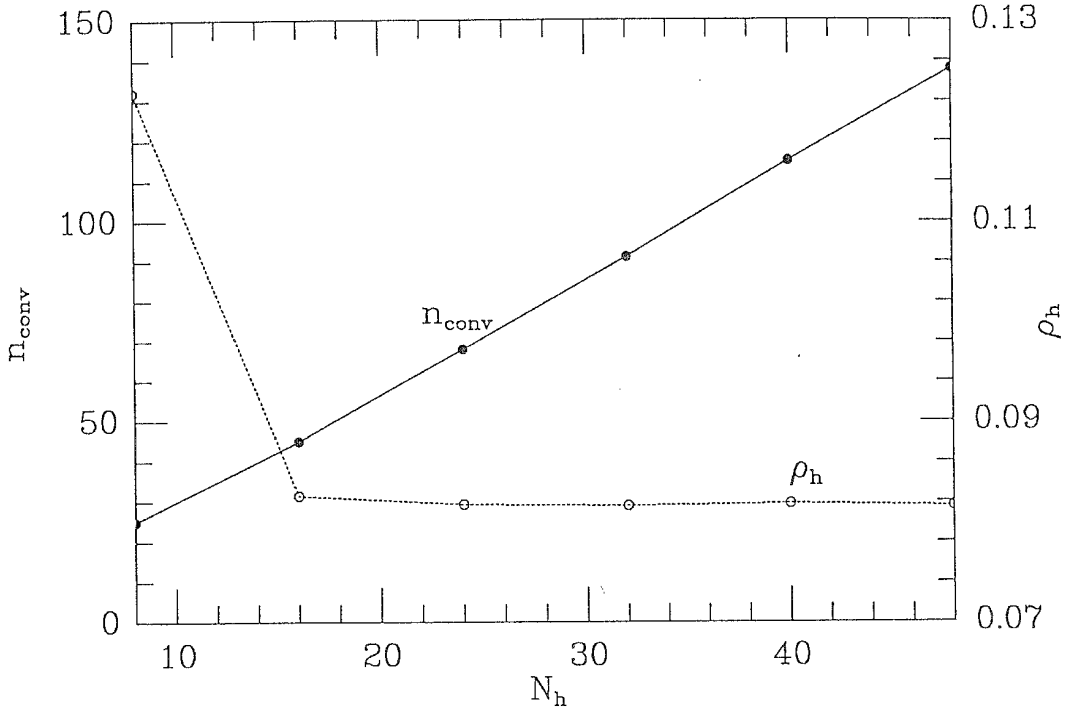

Figure 2.4 – *Charge density ρ_h as a function of the number of grid-points N_h along each direction of the unit cell. For each value of N_h, $n_{\rm conv}$ gives the number of recursion steps which are needed to obtain ρ_h within 0.5%.*

We address now the crucial issue of the relation between the convergence of the charge density and the size of the system. In order for the computational

cost to scale linearly with the number of atoms, the rate of convergence of the charge density with the number of recursion steps must not depend on the system size. To shed light on this matter, we have calculated the charge density as a function of the number of chain steps for a set of Silicon supercells of different size. Within each supercell, the Silicon atoms are arranged in their bulk equilibrium positions, and periodic boundary conditions are assumed. The Kohn-Sham hamiltonian has been discretized on a uniform real-space mesh, adopting the same grid-spacing $h = 0.855$ a.u. for all the calculations.

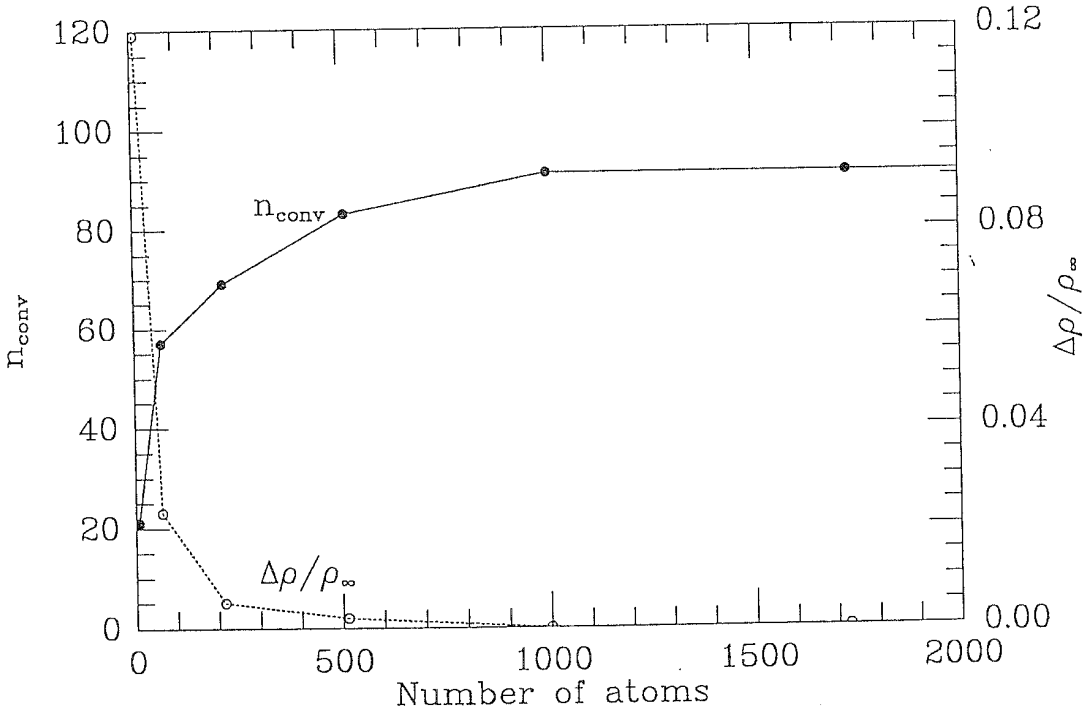

Figure 2.5 – *Rate of convergence of the point-wise charge density as a function of the number of atoms of the system. For each supercell s (see text), the black circles show the ratio $\Delta\rho_s/\rho_\infty$, and the open circles show the number of recursion steps $n_{\rm conv}$ required to obtain the exact charge density ρ_s within* 0.5%.

For every supercell s, the valence charge density ρ_s has been calculated at a point of the real-space grid corresponding to the position of a Silicon atom. The open circles in Fig. 2.5 show the ratio $\Delta\rho_s/\rho_\infty$, where ρ_∞ is the charge density at the given point for the largest supercell considered here (2744 atoms), and $\Delta\rho_s = \rho_s - \rho_\infty$ is the difference between the exact charge density of the supercell s and that of the "infinite" system. The black circles in Fig. 2.5 show, for each supercell s, the number of recursion steps which are needed to reproduce the exact charge density ρ_s within 0.5%. As the size of the system grows large ($N_{atoms} \geq 1000$), the ratio $\Delta\rho_s/\rho_\infty$ vanishes, reflecting the physically intuitive fact that the charge density at a given point is weakly affected by the more distant regions of space. At the same time, the rate of convergence of the charge density stabilizes, becoming independent of the number of atoms. We can conclude from this set of calculations that, at least for large systems, the number of recursion steps to obtain the point-wise charge density to a given accuracy does not depend on the size of the system.

As a final test of the convergence of the charge density with the number of recursion steps, we have considered a very large system, consisting of 2744 Silicon atoms arranged in a cubic supercell, and we have calculated the charge density along the (111) direction. The Silicon atoms are slightly displaced at random from their equilibrium positions, to simulate some degree of disorder. The Kohn-Sham hamiltonian has been represented on a uniform $110 \times 110 \times 110$ real-space grid, using a 13-point stencil for the discretization of the laplacian. The solid line in Fig. 2.6 is the exact charge density along the first part of the diagonal of the cubic supercell, as obtained from a well-converged continued-fraction expansion of the Green's function. The dotted line and the dashed line show the charge density obtained by truncating the

continued-fraction expansion of the Green's function after 20 levels (dotted line) and 80 levels (dashed line).

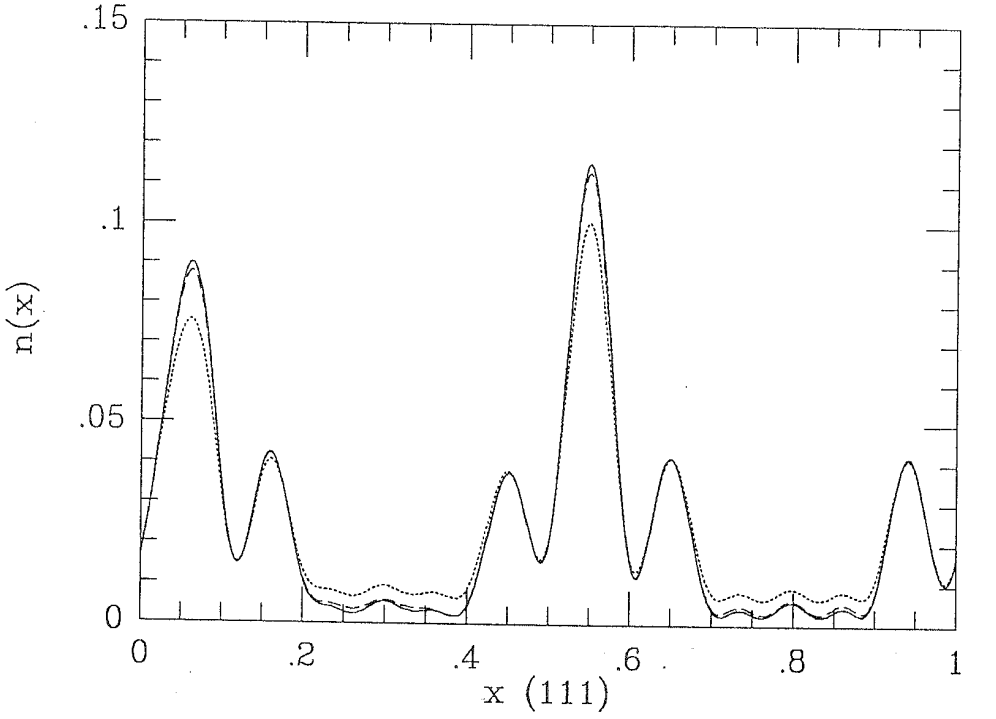

Figure 2.6 – *Charge density along the (111) direction obtained from a 20-step truncated chain (dotted lines) and from a 80-step truncated chain (dashed line). For comparison, the exact charge density is also shown (solid line).*

As this example demonstrates, in a realistic calculation a number of recursion steps of the order of 100 is required to obtain the charge density within a reasonable accuracy; also, the number of chain steps may be different for different points of the real-space grid.

2.3 Computational cost

Let us summarize now how linear scaling is achieved within the present approach.

- First, the discretization of the Kohn-Sham hamiltonian on a real-space grid produces a sparse representation, in the sense that the number of non-vanishing matrix elements scales linearly with the system size.
- Second, for each point of the real-space grid the number of recursion steps required to achieve a given accuracy in the charge density is independent of the number of atoms.
- Third, the states of the chain generated by the three-term recurrence relation (2.2) are localized around the starting point, so that the computational cost of the matrix-by-vector product $H_{KS}\,|\,n\,\rangle$ does not depend on the size of the system.

For large systems, these conditions are satisfied, and the overall computational workload scales linearly with the size of the system.

In the linear regime, the number of floating-point operations for the computation of the charge density scales as:

$$N_{flops} = (\alpha\, n^4 + \beta\, n)\, M\ , \tag{2.10}$$

where M is the dimension of the real-space grid, proportional to the number of atoms of the system, and n is the the number of recursion steps, which we assume to be the same for every grid-point.

The first term in parenthesis accounts for the calculation of the chain parameters $a_0(\mathbf{r}_i), \cdots, a_n(\mathbf{r}_i)$ and $b_1(\mathbf{r}_i), \cdots, b_n(\mathbf{r}_i)$, which are generated by application of the three-term recurrence relation (2.2) to a starting state

localized at the point $\mathbf{r}_i$. The fourth-order power law arises from the fact that each matrix-by-vector product $\hat{H}_{KS}|\,m\,\rangle$, with $0 \leq m \leq n$, involves $O(m^3)$ floating-point operations, because the state $|\,m\,\rangle$, being localized in region of volume proportional to $(mh)^3$ around the point $\mathbf{r}_i$, has $O(m^3)$ non-vanishing elements; therefore, the computational cost for the calculation of the first n recursion coefficients scales as $\sum_{m=0}^{n} m^3$, which is $O(n^4)$. The prefactor α depends basically on the choice of the stencil for the discretization of the kinetic-energy operator; if a simple nearest-neighbour stencil is adopted, the value of α is roughly 10.

The second term in parenthesis in Eq. (2.10) accounts for the computation of the Green's function diagonal element $G(\mathbf{r}_i, \mathbf{r}_i\,; z)$ via the continued-fraction expansion (2.6) and for the integration of the Green's function along the contour C_F in the complex energy plane. The prefactor β depends basically on the number of sampling points at which the Green's function has to be calculated in order to evaluate the integral to a given accuracy.

Although in general $\beta \gg \alpha$, for most systems the $O(n^4)$ contribution to the total computational time is by far the dominant one. Therefore, it is vital to keep the number of recursion steps as low as possible; for example, the calculation of the charge density of a 1000-atom system with a 50-step truncated chain would require about 10 hours of CPU time on a single 1-Gflops processor. Unfortunately, it is apparent from the previous examples (see in particular Fig. 2.6) that quite a large number of steps, of the order of 100 or more, is required to achieve a satisfactory convergence of the charge density. In the next section, we will discuss some possible solutions to the problem of reducing the number of chain steps without compromising the accuracy on the charge density.

2.4 Approximate terminators

Assuming that the first n states of the chain model for the point $\mathbf{r}_i$ have been calculated exactly, the continued-fraction expansion of the Green's function diagonal element $G(\mathbf{r}_i, \mathbf{r}_i\,; z)$ can be cast in the form:

$$G(\mathbf{r}_i, \mathbf{r}_i\,; z) = \cfrac{1}{z - a_0(\mathbf{r}_i) - \cfrac{b_1^2(\mathbf{r}_i)}{z - a_1(\mathbf{r}_i) - \cdots - t_n(\mathbf{r}_i\,; z)}}\,, \tag{2.11}$$

where $t_n(\mathbf{r}_i\,; z)$, the so-called n-th order *terminator*, accounts for the missing part of the chain:

$$t_n(\mathbf{r}_i\,; z) = \cfrac{b_{n+1}^2(\mathbf{r}_i)}{z - a_{n+1}(\mathbf{r}_i) - \cfrac{b_{n+2}^2(\mathbf{r}_i)}{z - a_{n+2}(\mathbf{r}_i) - \cdots}}\,. \tag{2.12}$$

All the information coming from the recursion states which follow $|\,n\,\rangle$ in the chain model is incorporated into the n-th order terminator $t_n(\mathbf{r}_i\,; z)$. Since the state $|\,n\,\rangle$ is localized within a region of size $R_n \propto n$ around the starting point $\mathbf{r}_i$, the regions of the system which are more distant than R_n from the point $\mathbf{r}_i$ contribute to the Green's function $G(\mathbf{r}_i, \mathbf{r}_i\,; z)$ exclusively through the terminator $t_n(\mathbf{r}_i\,; z)$.

The charge density at a given point, being a local quantity, is scarcely affected by the more distant environments; therefore, it is physically sensible to replace the exact terminator $t_n(\mathbf{r}_i\,; z)$ with an approximate terminator $\tilde{t}_n(\mathbf{r}_i\,; z)$, which takes into account the smaller contribution of the more distant regions to the charge density at the point $\mathbf{r}_i$. From a computational point of view, the aim of an approximate terminator is to reduce as much as possible the number of chain parameters which have to be calculated exactly to obtain the charge density to a given accuracy.

The truncated continued-fraction expansion

$$G^{(n)}(\mathbf{r}_i, \mathbf{r}_i\,; z) = \cfrac{1}{z - a_0(\mathbf{r}_i) - \cfrac{b_1^2(\mathbf{r}_i)}{z - a_1(\mathbf{r}_i) - \cdots - \cfrac{b_n^2(\mathbf{r}_i)}{z - a_n(\mathbf{r}_i)}}} \tag{2.13}$$

corresponds to the choice of a vanishing terminator: $t_n(\mathbf{r}_i\,; z) = 0$. In a sense, this is the most simple and cheap approximation for the terminator, though a very crude one: the surroundings of the point $\mathbf{r}_i$ are fully taken into account in the calculation of the charge density, whereas the more distant environments are completely neglected. Therefore, the convergence of the charge density with the number of recursion steps is determined by the extension of the cluster explored by the states of the chain: when the charge density becomes stable with respect to a variation of the size of the cluster, the continued-fraction expansion converges. This the basic reason why quite a large number of chain steps is required to achieve a reasonable accuracy in the charge density, as the previous examples demonstrate.

Indeed, this is not the only unpleasant feature of the vanishing-terminator scheme. First, the different regions of space which are actually included in the calculation of the charge density at a given point are treated on an equal footing, irrespective of their relative importance and weight. The same real-space grid, in fact, is used all over the system, whatever the distance from the selected point is. Second, and related, no use is made of the property that the recursion chains started at neighbouring points contain nearly the same amount of physical information.

In order to overcome these difficulties, we have explored a number of possibilities in search of an accurate and reliable approximate terminator.

(a) Free-particle terminator

Let us consider first the "free-particle" terminator t_n^0; this is the terminator for a free electron moving in a constant potential corresponding to the average potential of the system. The same real-space grid and the same boundary conditions as in the real system are employed for the calculation of the free-particle terminator; in the usual case of a uniform grid with periodic boundary conditions, the free-particle terminator does not depend on the grid-point, and is a function of the complex energy z alone: $t_n^0 = t_n^0(z)$.

The recipe for the calculation of the free-particle terminator is extremely simple: given the real-space representation of the Kohn-Sham hamiltonian on a discrete grid, the average value $\bar{V}_{KS}$ of the Kohn-Sham potential is calculated, and the free-particle chain parameters $\{a_n^0, b_n^0\}$, corresponding to the hamiltonian $\bar{H}_{KS} = -1/2\,\nabla^2 + \bar{V}_{KS}$, are generated; the free-particle terminator is then recovered from a converged continued-fraction expansion:

$$t_n^0(z) = \cfrac{(b_{n+1}^0)^2}{z - a_{n+1}^0 - \cfrac{(b_{n+2}^0)^2}{z - a_{n+2}^0 - \cdots}} \,. \tag{2.14}$$

The free-particle approximation consists in replacing the exact n-th order terminator with the corresponding free-particle terminator: $t_n(\mathbf{r}_i\,; z) \rightarrow t_n^0(z)$. This is a sort of mean-field approximation for the terminator: the cluster of points explored by the first n states of the recursion chain is embedded in a uniform, featureless background. However, it should be kept in mind that this is not the same thing as setting the potential to a constant average value outside the cluster spanned by the first n states of the chain and calculating the charge density for this new system by means of a converged continued-fraction expansion of the Green's function; the n-th order terminator, indeed,

is affected by the potential inside the cluster, and differs from the free-particle one. Actually, a calculation performed on a very large system has shown that the free-particle terminator can do nearly the same job, at a much lower cost.

The effect of the free-particle terminator on the convergence of the charge density is demonstrated in Fig. 2.7. As in the case of Fig. 2.3, the system considered here is a cubic supercell containing 216 Silicon atoms in their experimental equilibrium geometry; the charge density has been calculated at a point of the real-space grid corresponding to the position of a Silicon atom. The solid line shows the charge density as a function of the number of levels in the truncated continued-fraction expansion of the Green's function; in other words, a vanishing terminator is assumed in this case. The dashed line in Fig. 2.7 shows the charge density obtained by replacing the exact n-th order terminator $t_n(\mathbf{r}_i\,;z)$ with the corresponding free-particle terminator $t_n^0(z)$; a well-converged 300-step chain has been used for the calculation of the free-particle terminator. The most striking feature of the free-particle approximation is the lack of periodic oscillations in the charge density; this is due to the fact that, for any value of n, the number of poles of the Green's function coincides with the number of free-particle chain steps (300 in the present case). Therefore, the number of poles below the Fermi level is nearly independent of n; adding a new step to the chain just changes the relative position of the poles and the corresponding residues.

To test the accuracy of the free-particle approximation, we have performed some trial calculations on large Silicon supercells. The first system considered here is a cubic cell containing 64 Silicon atoms, slightly displaced at random from their equilibrium positions to simulate some degree of disorder. The Kohn-Sham hamiltonian has been represented on a uniform $32 \times 32 \times 32$

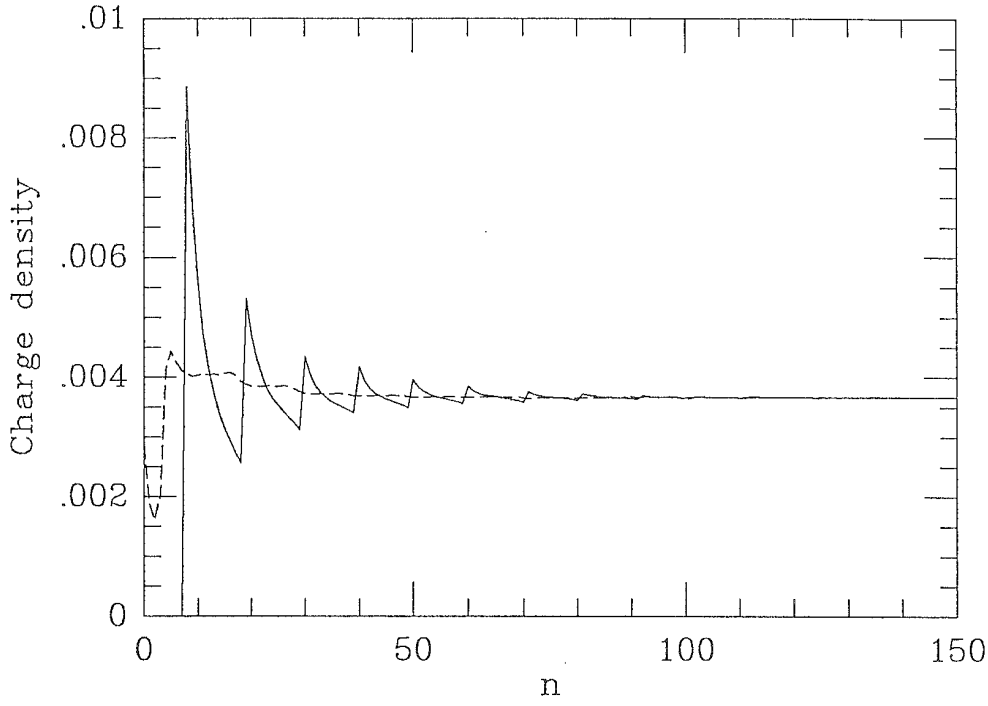

Figure 2.7 – *Convergence of the point-wise charge density with the number of recursion steps n. The solid line corresponds to the vanishing terminator* $t_n(\mathbf{r}_i\,;z) = 0$*; the dashed line has been obtained using the free-particle terminator:* $t_n(\mathbf{r}_i\,;z) \rightarrow t_n^0(z)$.

grid with periodic boundary conditions. The Fermi energy was taken from an exact, conventional orbital calculation involving the diagonalization of the real-space hamiltonian. The charge density calculated at the grid-points located along the diagonal of the cubic cell has been Fourier-interpolated to yield the continuous lines plotted in Fig. 2.8.

The solid line in Fig. 2.8 (a) shows the exact charge density, resulting from a well-converged continued-fraction expansion of the Green's function. The dotted and the dashed lines have been obtained by calculating just the first 20 steps of the recursion chain exactly: in the first case (dotted line) the continued-fraction expansion is *truncated* after 20 levels, assuming a vanishing

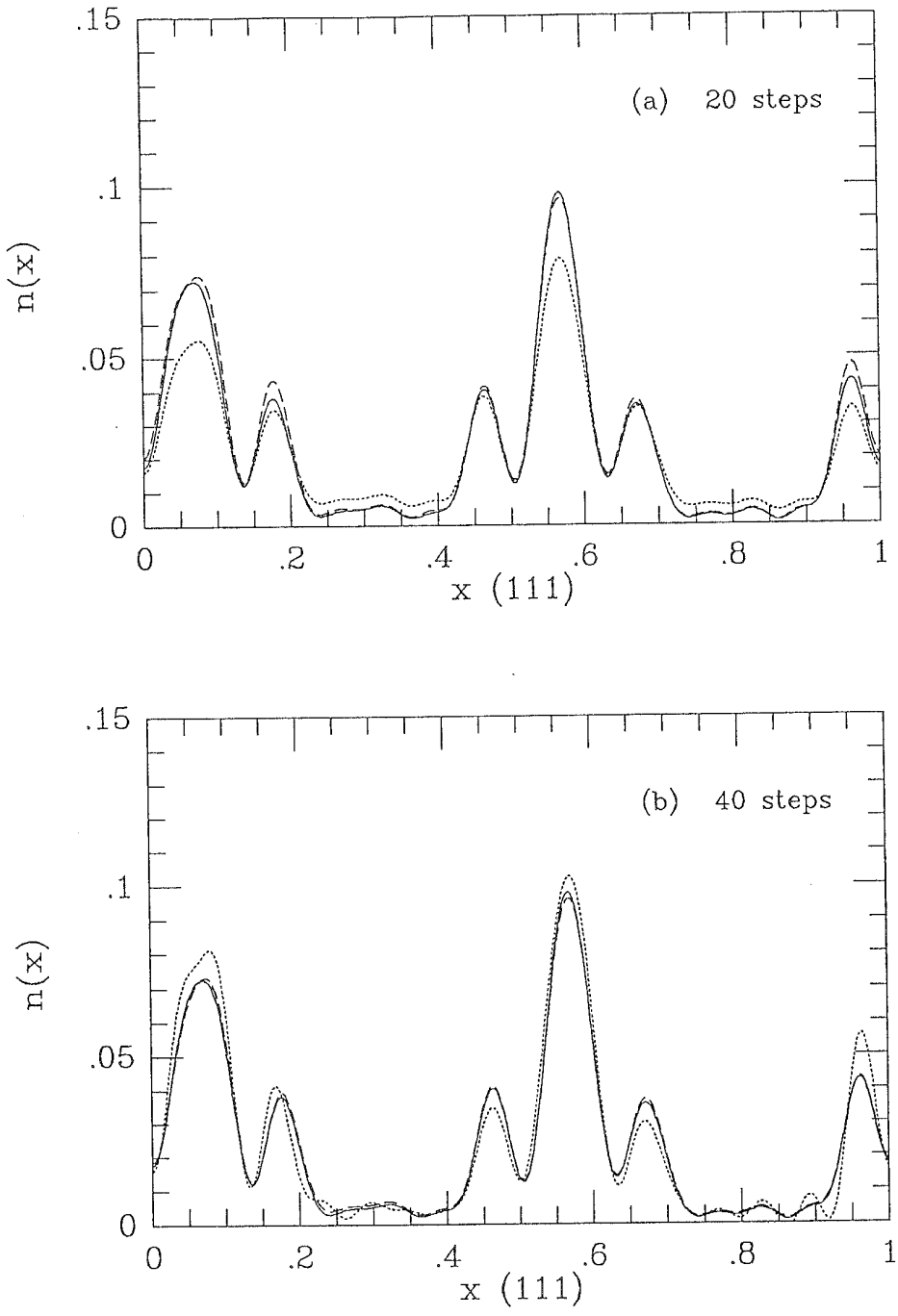

Figure 2.8 – *(a) Charge density along the (111) direction obtained from a 20-step truncated chain (dotted line) and a free-particle terminated 20-step chain (dashed line). (b) Charge density obtained from a 40-step truncated chain (dotted line) and a free-particle terminated 40-step chain (dashed line). For comparison, the solid lines show the exact charge density.*

terminator; in the second case (dashed line) the free-particle terminator $t_{20}^{0}(z)$ is appended to the continued fraction. The convergence of the charge density with respect to the number of free-particle chain steps has been checked carefully, and a 500-step free-particle chain has been used for the calculation of the free-particle terminator. The corresponding results for a 40-step chain are shown in Fig. 2.8 (b).

As a second example, let us consider again the large Silicon supercell described in the previous section (see Fig. 2.6). The charge density along the (111) direction is plotted in Figs. 2.9 (a) and 2.9 (b); the solid lines show the exact charge density. The dotted and the dashed lines in Fig. 2.9 (a) correspond to a truncated 20-step chain and to a free-particle-terminated chain, respectively. A well-converged 1000-step free-particle chain has been used for the calculation of the free-particle terminator. The corresponding results for a 30-step chain are shown in Fig. 2.9 (b).

As these calculations demonstrate, the accuracy of the charge density for a given number of recursion steps is remarkably enhanced by the use of the free-particle terminator. Actually, a comparison with Fig. 2.6 shows that the charge density obtained using the free-particle-terminated 20-step chain is nearly as accurate as the 80-step truncated chain result. We can conclude that the free-particle terminator provides a working approximation for the exact terminator in the calculation of the charge density. Furthermore, this approximation is extremely cost-effective: due to the point-independence of the free-particle terminator, its computational cost is independent of the size of the system, at least for very large systems.

Since the free-particle terminator does not depend on the point position, one could argue that more sophisticated mean-field approaches to the

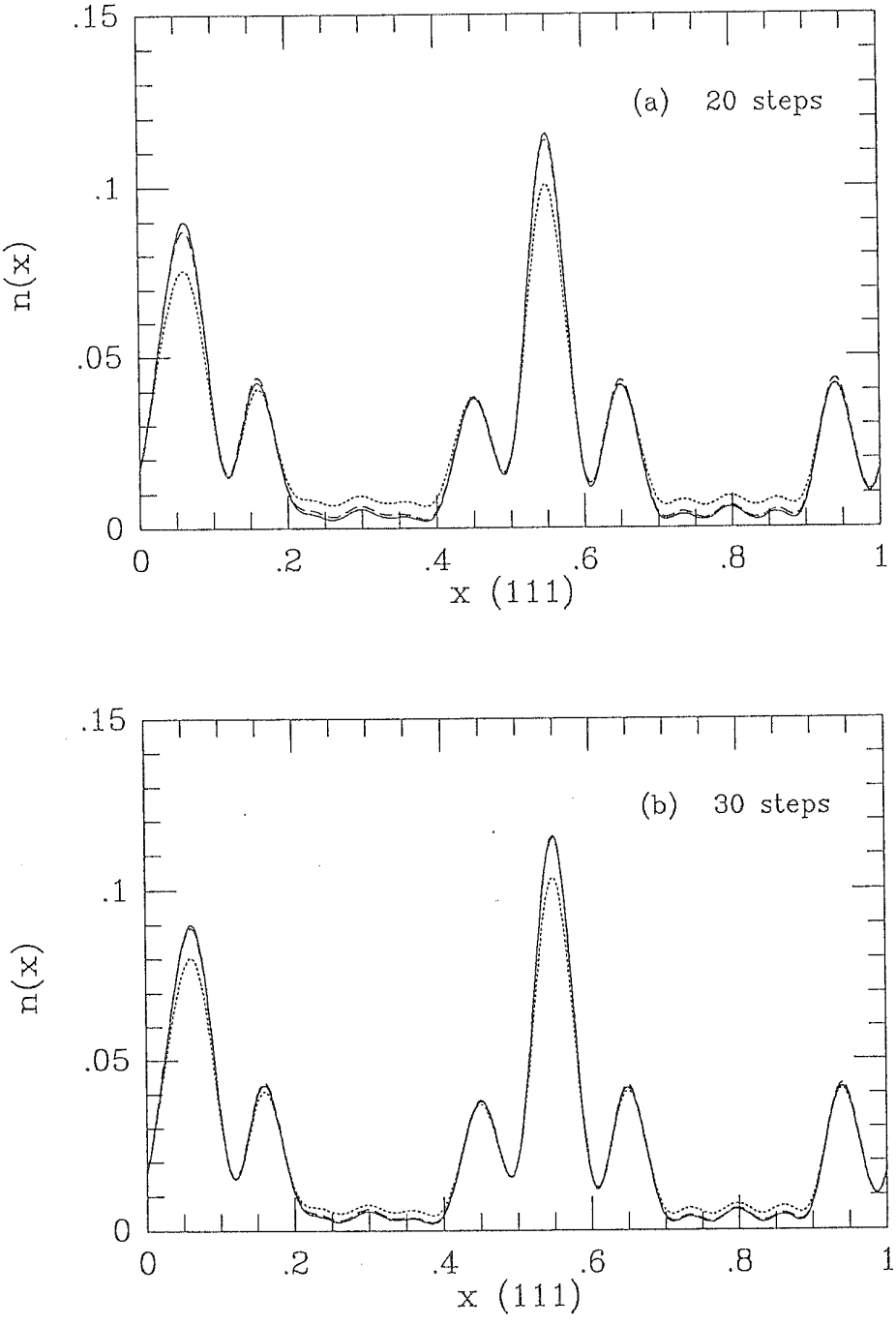

Figure 2.9 – *(a) Charge density along the (111) direction obtained from a 20-step truncated chain (dotted line) and a free-particle terminated 20-step chain (dashed line). (b) Charge density obtained from a 30-step truncated chain (dotted line) and a free-particle terminated 30-step chain (dashed line). For comparison, the solid lines show the exact charge density.*

calculation of the terminator should improve the accuracy of the charge density. In order to test this hypothesis, we have performed a simple calculation on the same trial system considered in the previous example (see Fig. 2.8). Let us replace the exact n-th order terminator $t_n(\mathbf{r}_i\,;z)$ with a complex constant γ_n; the parameter γ_n can be fitted in order to reproduce the exact charge density at the point $\mathbf{r}_i$. However, if the same value of γ_n is used for a large number of grid-points, the accuracy of the charge density cannot be expected to be so high. Given the exact charge density along the (111) direction, we have tried to fit the parameter γ_n in order to minimize the mean square deviation σ_n between the exact and the approximate charge density:

$$\sigma_n = \left\{ \frac{1}{N} \sum_{i=1}^{N} \left[n^{exact}(\mathbf{r}_i) - n(\mathbf{r}_i\,;\gamma_n) \right]^2 \right\}^{1/2} , \qquad (2.15)$$

where $n(\mathbf{r}_i\,;\gamma_n)$ is the charge density at the point $\mathbf{r}_i$ obtained by replacing the exact terminator $t_n(\mathbf{r}_i\,;z)$ with the parameter γ_n, and N is the number of sampling points (32 in this case). The complex constant γ_n^{fit} which minimizes the mean-square deviation σ_n provides an approximate charge density, as shown in Fig. 2.10.

The solid line is the exact charge density along the diagonal of the cubic cell, whereas the dotted line has been obtained by replacing the terminator $t_{20}(\mathbf{r}_i\,;z)$ with the fitted parameter γ_{20}^{fit}. As we can see, the overall agreement between the two curves is rather good; however, only a slight improvement is achieved with respect to the free-particle approximation (see Fig. 2.8). The approximate terminator γ_{20}^{fit} has been determined by fitting the exact charge density at a small number of selected grid-points, and we believe it provides nearly an upper bound to the precision any point-independent approximation for the terminator can aim to achieve. Therefore, we argue that one has to

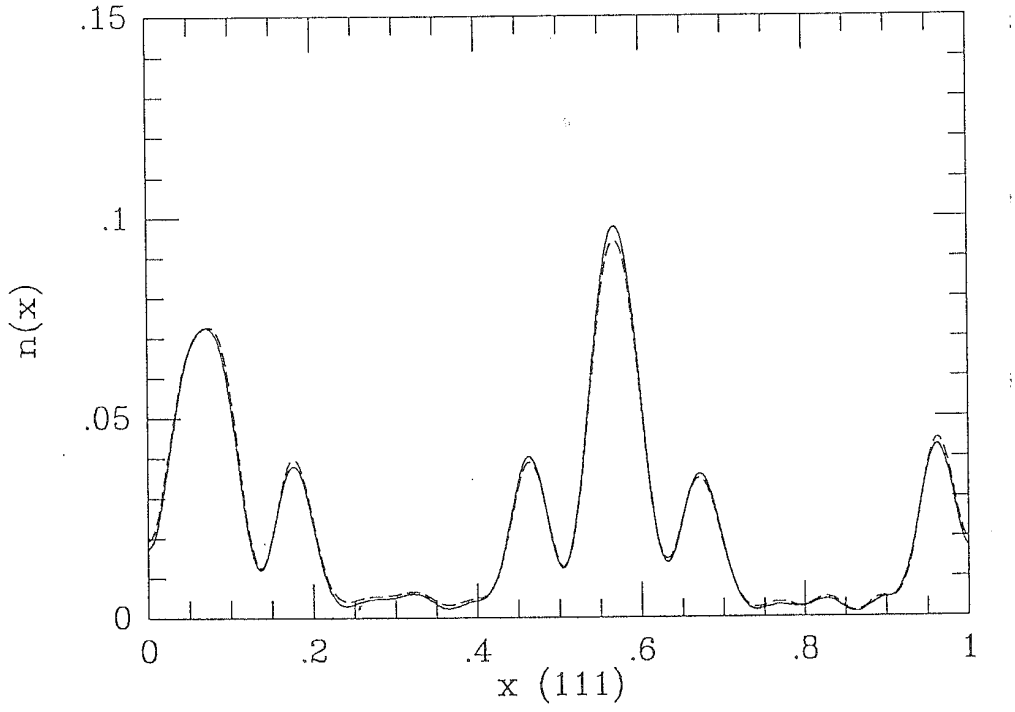

Figure 2.10 – *Charge density along the (111) direction, as obtained by replacing the exact terminator $t_{20}(\mathbf{r}_i\,;z)$ with the fitted constant γ_{20}^{fit} (dashed line); for comparison, the exact charge density (solid line) is also shown.*

go beyond the mean-field scheme to improve the accuracy of the free-particle approximation consistently.

Before discussing different approaches to the calculation of the terminator, it is interesting to compare the free-particle terminator with the "Thomas-Fermi" terminator. The Thomas-Fermi terminator at the point $\mathbf{r}_i$ is defined as the free-particle terminator for a particle in a constant potential corresponding to the Kohn-Sham potential calculated at the point $\mathbf{r}_i$: $t_n^{TF}(\mathbf{r}_i\,;z) = t_n^0[V = V_{KS}(\mathbf{r}_i)\,;z]$. Both the free-particle and the Thomas-Fermi terminator are exact in the limit of a constant potential; however, while the free-particle terminator may be viewed as a mean-field approximation, the Thomas-Fermi terminator

accounts for local effects. Although the computation of the Thomas-Fermi terminator is nearly as simple as that of the free-particle terminator, the accuracy in the resulting charge density is considerably lower. This is not surprising, since the states of the recursion chain, due to the orthonormality constraint, develop a hole in the middle, and become less and less sensitive to the behaviour of the potential in the neighbourhood of the starting point. In particular, all the states of the chain, except the first one, vanish at the starting point; hence, the true terminator $t_n(\mathbf{r}_i\,;z)$ does not depend on the value of the potential at the point $\mathbf{r}_i$.

(b) Coarse-grid terminator

The basic idea behind the coarse-grid terminator is that the contribution of the more distant regions of space to the charge density at a given point can be accounted for in an approximate way using a coarser grid in these regions. Since the terminator is mostly affected by the more distant environments, this goal can be achieved by a grid-coarsening approach to the calculation of the terminator.

Assuming that the first n states of the chain have been generated on a fine real-space grid $\mathcal{M}^h = \{\mathbf{r}_i,\, i = 1, \cdots, M^h\}$, we want to evaluate the n-th order terminator $t_n(\mathbf{r}_i\,;z)$ using a coarser grid $\mathcal{M}^H = \{\mathbf{r}_i,\, i = 1, \cdots, M^H\}$, with $M^H < M^h$. The simple idea of replacing the fine-grid terminator $t_n^h(\mathbf{r}_i\,;z)$ with the corresponding coarse-grid terminator $t_n^H(\mathbf{r}_i\,;z)$, however, has little justification in this case, because (i) it can be applied only to those points $\mathbf{r}_i$ which are shared by the fine and the coarse grid, and (ii) the regions of space spanned by the first n recursion states generated on different grids do not match. Therefore, we have explored two different techniques for the

calculation of the coarse-grid terminator.

(i) In the first approach, the last two states of the fine-grid chain, $|n-1\rangle$ and $|n\rangle$, are projected onto the coarse grid, and the recursion chain is carried on in the new representation by discretizing the Kohn-Sham hamiltonian on the coarse grid. The n-th order terminator $t_n(\mathbf{r}_i\,;z)$ is then obtained from its definition, Eq. (2.12).

(ii) In the second approach, just the last state of the fine-grid chain, $|n\rangle$, is projected onto the coarse-grid; a new chain is then generated on the coarse-grid starting from the projected state $|n\rangle$ to obtain the Green's function diagonal element $G_{n,n}(\mathbf{r}_i\,;z) \equiv \langle n\,|\,\hat{G}(z)\,|\,n\rangle$. Finally, the n-th order terminator is then recovered from the following equation (see Appendix A, Eq. A.25):

$$t_n(\mathbf{r}_i\,;z) = \frac{P_{n+1}(\mathbf{r}_i\,;z)}{P_n(\mathbf{r}_i\,;z)} - \frac{1}{G_{n,n}(\mathbf{r}_i\,;z)}\,, \tag{2.16}$$

where $P_n(\mathbf{r}_i\,;z)$ and $P_{n+1}(\mathbf{r}_i\,;z)$ are the monic polynomials for the first chain.

To test the accuracy of these methods, we have performed some trial calculations on the same sample system described in the case of Fig. 2.8. The first n states of the chain are generated on a fine $32 \times 32 \times 32$ uniform grid; a coarser $16 \times 16 \times 16$ grid is used for the calculation of the terminator. The same stencil has been used in both cases for the discretization of the kinetic-energy operator. The charge density along the (111) direction is plotted in Fig. 2.11. The solid lines in Figs. 2.11 (a) and 2.11 (b) show the exact charge density, the dotted lines show the 20-step truncated-chain charge density, and the dashed lines have been obtained using a coarse-grid terminator. In the first case, Fig. 2.11 (a), the last two states of the first chain were projected

onto the coarse grid and orthonormalized before going on with the new chain. In the second case, Fig. 2.11 (b), only the last state of the first chain was projected onto the new basis set, and the coarse-grid approximation for the terminator was obtained from Eq. (2.16).

Although a slight improvement is achieved in both cases with respect to the truncated-chain result, the accuracy of the charge density is still too poor. We believe that the failure of the coarse-grid terminator is related to the lack of orthonormality between the states of the fine-grid chain and those of the coarse-grid chain. Since the latter are not prevented by orthogonality constraints from propagating towards the interior of the region of space spanned by the states of the fine-grid chain, the terminator contains a large amount of spurious information originating from the surroundings of the starting point, which are poorly described by the coarse grid.

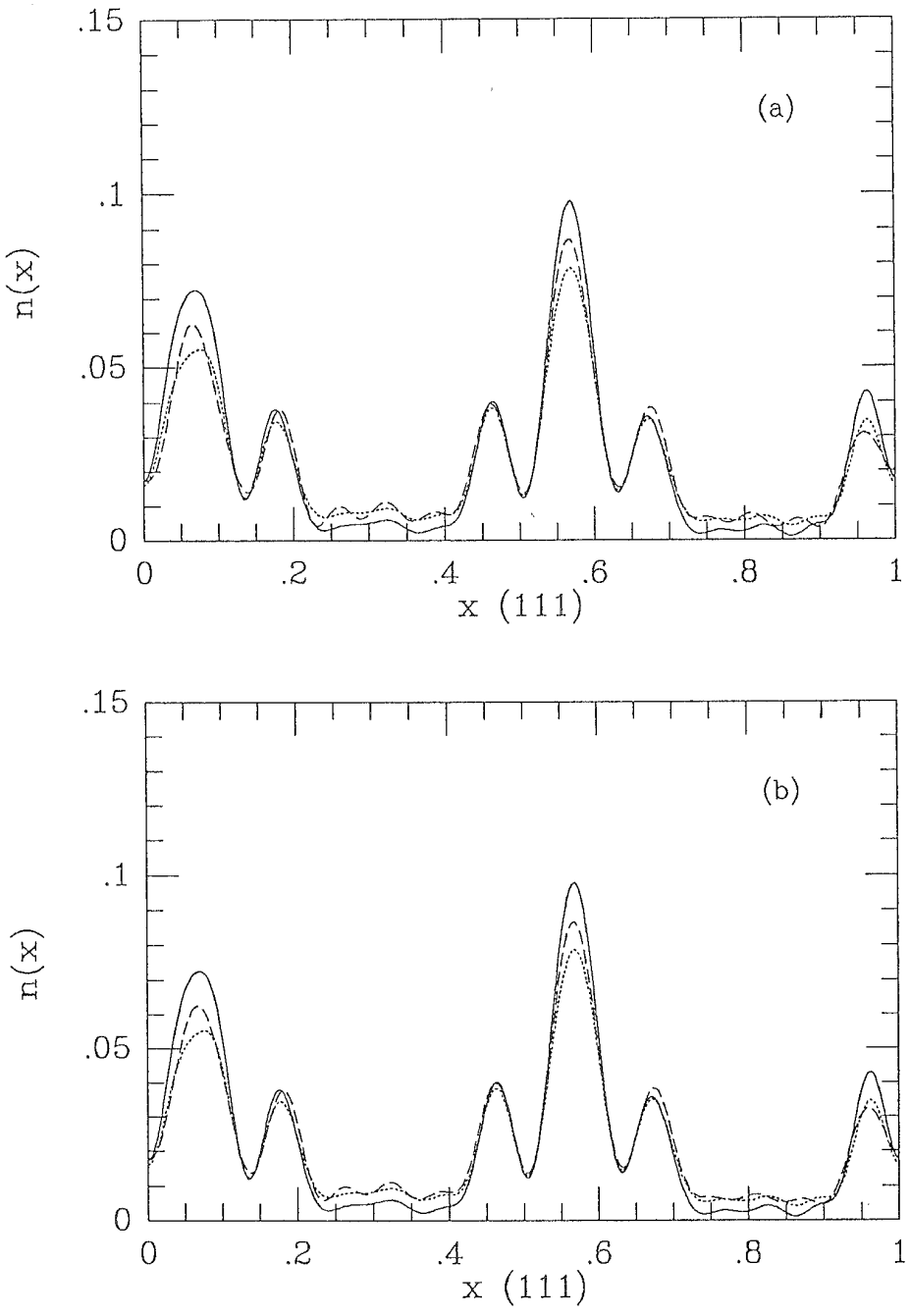

Figure 2.11 – *Charge density along the (111) direction obtained from a 20-step chain with a coarse-grid terminator (dashed lines). In (a) the last two states of the fine-grid chain have been projected onto the coarse grid, and the chain has been carried on in the coarse-grid representation; in (b) just the last state of the chain has been projected onto the new basis set. For comparison, the 20-step truncated-chain charge density (dotted line), and the exact charge density (solid line) are also shown.*

Chapter 3

Self-Consistent Calculations

The Kohn-Sham potential $V_{KS}[n\,;\mathbf{r}]$ depends on the electronic charge density $n(\mathbf{r})$ through the classical electrostatic potential and the quantum-mechanical exchange-correlation potential; therefore, the charge density has to be determined self-consistently in order to evaluate the ground-state properties of the system. In the present chapter, we describe the practical implementation of the self-consistent procedure in the context of the Green's Function – Recursion Method approach to DFT, and discuss the accuracy of total energies and atomic forces. Finally, we present some test results for very large Silicon supercells.

3.1 Self-consistent calculation of the charge density

Given the atomic positions, the first step is the construction of the ionic potential $V_{ion}(\mathbf{r})$, which accounts for electron-ion interactions. In periodic systems, the ionic potential is most simply calculated in reciprocal space:

$$V_{ion}(\mathbf{r}) = \frac{1}{\Omega_c} \sum_{\mathbf{G}} \sum_{\alpha} V_\alpha(\mathbf{G})\, S_\alpha(\mathbf{G})\, e^{i\mathbf{G}\cdot\mathbf{r}} \,, \tag{3.1}$$

where Ω_c is the volume of the unit cell, $V_\alpha(\mathbf{G})$ is the Fourier transform of the ionic potential for atoms of type α, and $S_\alpha(\mathbf{G})$ is the corresponding structure factor:

$$S_\alpha(\mathbf{G}) = \sum_{j_\alpha} e^{-i\mathbf{G}\cdot\mathbf{R}_{j_\alpha}} \,, \tag{3.2}$$

where j_α runs over the atoms of type α in the unit cell.

A trial Kohn-Sham potential $V_{KS}(\mathbf{r})$ can be obtained by screening the ionic potential with a model dielectric function, such as the Thomas-Fermi one. The Kohn-Sham hamiltonian $H_{KS} = (-1/2)\ \nabla^2 + V_{KS}(\mathbf{r})$ is then discretized on a real-space grid $\mathcal{M} = \{\mathbf{r}_i, i = 1, \cdots, M\}$, according to the prescriptions discussed in the previous chapters. For each point $\mathbf{r}_i$ of the grid, a set of chain parameters $\{a_l(\mathbf{r}_i),\ b_l(\mathbf{r}_i),\ l = 0, \cdots, n\}$ is generated by the recursion method. The initial state $(l = 0)$ is localized at the point $\mathbf{r}_i$, and the number of recursion steps n determines the accuracy of the charge density at the point $\mathbf{r}_i$. In principle, the number of recursion steps might be different for different points of the grid; a simple and reliable method exists [24] which provides an upper and a lower bound to the exact charge density given the first n coefficients of the recursion chain. In practice, however, it seems rather difficult to extrapolate the "right" number of recursion steps from the knowledge of these bounds; therefore, in our calculations we always

use the same number of chain parameters for every point of the real-space grid. The $2(n+1) \times M$ recursion coefficients are then stored; neither the Green's function nor the approximate terminator are required at this stage.

The next step is the determination of the Fermi energy ε_F, which is the solution of the implicit equation

$$N(\varepsilon_F) = N_{el} \,, \tag{3.3}$$

$N(\varepsilon)$ being the number of electrons with energy lower than ε. Using the integral representation of the density-matrix operator, we obtain:

$$N(\varepsilon) = \mathrm{tr}\,\hat{\rho}(\varepsilon) = \frac{1}{2\pi i} \oint_{\mathcal{C}_\varepsilon} \mathrm{tr}\,\hat{G}(z)\, dz \,, \tag{3.4}$$

where $\mathcal{C}_\varepsilon$ is an integration contour in the complex energy plane enclosing all the poles of the trace of the Green's function up to the trial energy ε. The trace of the Green's function is most simply calculated in real space:

$$\mathrm{tr}\,\hat{G}(z) = \sum_{i=1}^{M} G(\mathbf{r}_i, \mathbf{r}_i\,; z) \,, \tag{3.5}$$

where the index i runs over the M points of the real-space mesh $\mathcal{M}$. The Green's function diagonal elements $G(\mathbf{r}_i, \mathbf{r}_i\,; z)$ are obtained from the chain parameters $\{a_l(\mathbf{r}_i),\, b_l(\mathbf{r}_i),\, l = 0, \cdots, n\}$ using a terminated continued-fraction expansion; if the free-particle approximation (see Section 2.4) is assumed, the calculation of the trace is particularly simple, due to the point-independence of the free-particle terminator. In principle, the contour integration in Eq. (3.4) could be even performed analytically, upon spectral decomposition of the Green's function diagonal elements:

$$N(\varepsilon) = \sum_{i=1}^{M} \sum\nolimits_{\alpha} \omega_\alpha(\mathbf{r}_i)\; \theta(\varepsilon_F - \varepsilon_\alpha(\mathbf{r}_i)) \,, \tag{3.6}$$

where $\varepsilon_\alpha(\mathbf{r}_i)$ is the α-th eigenvalue of the chain and $\omega_\alpha(\mathbf{r}_i)$ is the corresponding residue. From a computational point of view, however, this approach turns out to be rather expensive, particularly when a non-vanishing terminator is assumed.

The choice of the integration contour $\mathcal{C}_\varepsilon$ for the evaluation of the electron number $N(\varepsilon)$ is to some extent arbitrary; we have used a rectangular path in the complex energy plane crossing the real axis at $\mathrm{Re}\, z = \varepsilon$, as shown in Fig. 3.1. The integral can be readily evaluated numerically, by sampling the trace of the Green's function at a number of points along the contour $\mathcal{C}_\varepsilon$. The Fermi energy ε_F is obtained by varying the trial energy ε and calculating the corresponding electron number $N(\varepsilon)$, until Eq. (3.3) is satisfied within a given precision. In practice, we find that using a simplified version of Brent's algorithm [25], a few steps are enough to get the Fermi energy within 10^{-5} Ryd/atom.

Once the Fermi energy has been determined, the charge density is calculated at every point of the real-space grid:

$$n(\mathbf{r}_i) = \frac{1}{2\pi i} \oint_{\mathcal{C}_F} G(\mathbf{r}_i, \mathbf{r}_i\,; z)\, dz \ . \tag{3.7}$$

The integration contour $\mathcal{C}_F$ is closed at the Fermi energy ε_F; the same integration contour is used for all the grid-points.

The knowledge of the electronic charge density $n(\mathbf{r}_i)$ over the real-space grid $\mathcal{M}$ allows the calculation of a new Kohn-Sham potential:

$$V_{KS}[n\,;\mathbf{r}_i] = V_{ion}(\mathbf{r}_i) + V_H[n\,;\mathbf{r}_i] + V_{xc}[n\,;\mathbf{r}_i] \ , \tag{3.8}$$

where $V_H[n\,;\mathbf{r}_i]$ is the classical electrostatic potential (Hartree potential), and $V_{xc}[n\,;\mathbf{r}_i]$ is the exchange-correlation potential. The Hartree potential is the

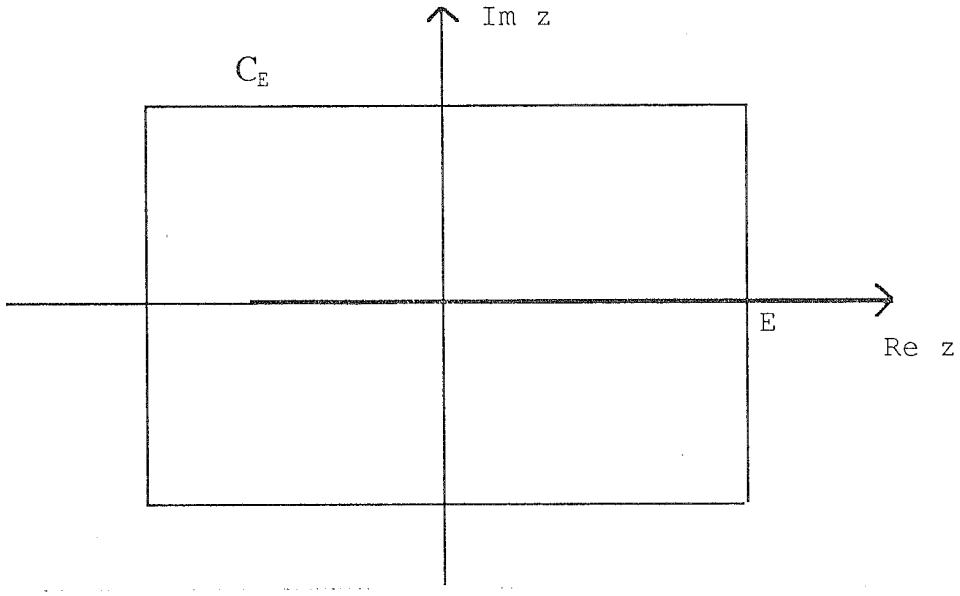

Figure 3.1 – *Integration contour in the complex energy plane for the calculation of the electron number* $N(\varepsilon)$.

solution of the Poisson equation:

$$\nabla^2 V_H[n\,;\mathbf{r}_i] = -4\pi e^2\, n(\mathbf{r}_i)\;, \tag{3.9}$$

which satisfies the appropriate boundary conditions. The Poisson equation can be readily mapped onto the real-space grid $\mathcal{M}$ by discretizing the laplacian operator; the same real-space stencil used for the discretization of the kinetic-energy operator is adopted here for the laplacian. The Poisson equation reduces to a system of linear equations which can be solved iteratively to get the Hartree potential; if multigrid techniques [26] are used , the computational workload scales linearly with the dimension M of the real-space mesh. In the common case of a uniform grid with periodic boundary conditions,

however, the Poisson equation is most simply solved in reciprocal space. The computational cost of the required Fourier transforms scales as $M \log M$; however, this is only a very small fraction of the total computational time. The exchange-correlation potential in the local-density approximation has the simple expression:

$$V_{xc}^{LDA}[n\,;\mathbf{r}_i] = n(\mathbf{r}_i)\,\frac{d\varepsilon_{xc}}{dn}\bigg|_{n=n(\mathbf{r}_i)} + \varepsilon_{xc}(n(\mathbf{r}_i))\,, \tag{3.10}$$

where $\varepsilon_{xc}(n)$ is the exchange-correlation energy per particle of a homogeneous electron gas with density n. The parametrized form of $\varepsilon_{xc}(n)$ proposed in [27] has been adopted.

Adding the Hartree potential and the exchange-correlation potential to the bare ionic potential, a new Kohn-Sham potential is generated. The input potential for the next iteration of the self-consistent procedure is then prepared according to the Anderson's underrelaxation/extrapolation scheme [28], and the whole procedure is repeated until input and output potentials agree to within a given threshold.

Whenever a full-converged continued-fraction expansion is used for the calculation of the Green's function, this self-consistent scheme turns out to be relatively safe, provided a finite gap exists between the highest occupied state and the lowest unoccupied one. If, due to symmetry reasons, two or more degenerate states fall exactly at the Fermi level, and only a few of them are occupied, the algorithm fails, because all the states at the Fermi level are either included in the calculation of the charge density, or completely neglected, thereby violating the charge neutrality condition.

In most cases, however, one has to resort to some approximate terminator to deal with the calculation of diagonal elements of the Green's function.

This may give rise to a number of technical problems in the self-consistent procedure:

(i) Although each diagonal element of the real-space Green's function has a discrete number of well-separated poles along the real axis ($n+1$ in the case of a truncated chain), the position of these poles is different for different points of the real-space grid. Therefore, the *trace* of the Green's function has nearly a continuum of poles on the real axis, even inside the physical gap, if the number of recursion steps is low. Due to the presence of a dense set of poles on the real axis, the trace of the Green's function may have a rather oscillatory behaviour along the integration contour $\mathcal{C}_\varepsilon$; hence, the numerical evaluation of the integral may require a rather large number of sampling points to achieve a reasonable accuracy.

(ii) A similar problem occurs in the calculation of the charge density. In correspondence to some points of the real-space grid, the local Green's function may happen to have a pole close to the computed Fermi energy; in this case, a large number of sampling points along the integration contour $\mathcal{C}_F$ may be necessary to obtain the charge density within a given precision.

(iii) Finally, a major difficulty may arise in the context of the self-consistent procedure, due to the fact that a small variation in the Kohn-Sham potential may cause a pole of the Green's function to jump across the Fermi level, leading to a sharp discontinuity in the charge density (see for example Fig. 2.3). On turn, the Kohn-Sham potential globally responds to this local variation of the charge density, determining an instability which can seriously hinder the achievement of self-consistency.

In order to cope with these problems, we have used a finite-temperature

approach to deal with the calculation of the charge density and other energy-integrated quantities. Within the RM, the finite-temperature charge density at the point $\mathbf{r}_i$ of the real-space grid reads:

$$n(\mathbf{r}_i, T) = \sum\nolimits_{\alpha} \frac{\omega_\alpha(\mathbf{r}_i)}{1 + e^{[\varepsilon_\alpha(\mathbf{r}_i) - \varepsilon_F]/K_B T}} , \tag{3.11}$$

where $\varepsilon_\alpha(\mathbf{r}_i)$ is the α-th eigenvalue of the *terminated* recursion chain started at the point $\mathbf{r}_i$, and $\omega_\alpha(\mathbf{r}_i)$ is the corresponding residue (see Appendix A). The temperature-dependent Fermi energy ε_F is the solution of the implicit equation:

$$N(\varepsilon_F, T) = N_{el} , \tag{3.12}$$

$N(\varepsilon, T)$ being the number of electrons with energy lower than ε at temperature T:

$$N(\varepsilon, T) = \sum_{i=1}^{M} \sum\nolimits_{\alpha} \frac{\omega_\alpha(\mathbf{r}_i)}{1 + e^{[\varepsilon_\alpha(\mathbf{r}_i) - \varepsilon]/K_B T}} . \tag{3.13}$$

Of course, the finite-temperature charge density slightly differs from the exact one. However, provided the temperature is much lower than the average spacing $\delta\varepsilon$ among the eigenvalues, $K_B T \ll \delta\varepsilon$, (i) only those points of the real-space grid which happen to have a pole close to the Fermi energy are affected by the finite temperature, and (ii) for most of these points, the difference in the charge density is negligible. Therefore, for $K_B T \ll \delta\varepsilon$ the finite-temperature Fermi energy nearly coincides with the zero-temperature Fermi energy.

In principle, the calculation of the finite-temperature charge density would require, for every point of the real-space grid, the highly time-consuming computation of all the eigenvalues of the corresponding recursion chain. However, since we are concerned here with temperatures which are low

compared to the average spacing of the eigenvalues, we can focus on a small energy interval Δ around the Fermi energy ε_F, and consider the "depurated" Green's function:

$$\tilde{G}(\mathbf{r}_i, \mathbf{r}_i\,; z) = G(\mathbf{r}_i, \mathbf{r}_i\,; z) - {\sum_{\alpha}}' \frac{\omega_\alpha(\mathbf{r}_i)}{z - \varepsilon_\alpha(\mathbf{r}_i)}\,, \tag{3.14}$$

where the prime indicates that the sum is restricted to the poles included in the energy interval Δ. Clearly, the modified Green's function $\tilde{G}(\mathbf{r}_i, \mathbf{r}_i\,; z)$ has no poles close to the Fermi energy. Provided the energy interval Δ satisfies the requirement $\exp\left[-\Delta/K_BT\right] \ll 1$, the finite-temperature charge density can be written as:

$$n(\mathbf{r}_i\,, T) = \frac{1}{2\pi i} \oint_{\mathcal{C}_F} \tilde{G}(\mathbf{r}_i, \mathbf{r}_i\,; z)\, dz + {\sum_{\alpha}}' \frac{\omega_\alpha(\mathbf{r}_i)}{1 + e^{[\varepsilon_\alpha(\mathbf{r}_i) - \varepsilon_F]/K_BT}}\,. \tag{3.15}$$

Only the chain-eigenvalues within an interval Δ around the Fermi energy ε_F have to be calculated explicitly.

Similarly, the total number of electrons with energy lower than ε is given by:

$$N(\varepsilon, T) = \frac{1}{2\pi i} \oint_{\mathcal{C}_\varepsilon} \mathrm{tr}\, \tilde{G}(z)\, dz + \sum_{i=1}^{M} {\sum_{\alpha}}' \frac{\omega_\alpha(\mathbf{r}_i)}{1 + e^{[\varepsilon_\alpha(\mathbf{r}_i) - \varepsilon]/K_BT}}\,, \tag{3.16}$$

where the primed sum involves the chain-eigenvalues $\varepsilon_\alpha(\mathbf{r}_i)$ within an energy interval Δ around the trial energy ε.

The finite-temperature approach has a number of advantages. From a computational point of view, the numerical evaluation of any integral involving the modified Green's function $\tilde{G}(z)$ is greatly simplified, because of the enhanced smoothness of $\tilde{G}(z)$ along the integration contour. Furthermore, since the chain-eigenvalues close to the Fermi energy are assigned a weight

which depends smoothly on their energy, the poles of the Green's function are prevented from jumping across the Fermi level in a discontinuous fashion; therefore, the self-consistent procedure is stabilized, and the convergence is faster and safer.

3.2 Total energy

Within Density-Functional Theory, the ground-state total energy is a functional of the self-consistent charge density n:

$$E_{tot}[n] = T_0[n] + E_H[n] + E_{xc}[n] + E_{ext}[n] \,, \tag{3.17}$$

where:

(i) $T_0[n]$ is the kinetic energy of a non-interacting electron gas with density $n(\mathbf{r})$;

(ii) $E_H[n]$ is the classical electrostatic energy, due to electron-electron interactions:

$$E_H[n] = \frac{1}{2} \int V_H[n\,;\mathbf{r}]\, n(\mathbf{r})\, d\mathbf{r} \,, \tag{3.18}$$

where $V_H[n\,;\mathbf{r}]$ is the Hartree electrostatic potential;

(iii) $E_{xc}[n]$ is the exchange-correlation energy; in the local-density approximation, it reads:

$$E_{xc}^{LDA}[n] = \int \varepsilon_{xc}(n(\mathbf{r}))\, n(\mathbf{r})\, d\mathbf{r} \,, \tag{3.19}$$

where $\varepsilon_{xc}(n)$ is the exchange-correlation energy of a homogeneous electron gas with density n.

(iv) $E_{ext}[n]$ is the external energy due to electron-ion and ion-ion interactions:

$$E_{ext}[n] = \int V_{ion}(\mathbf{r})\, n(\mathbf{r})\, d\mathbf{r} + E_{ion-ion} \,. \tag{3.20}$$

The integrals occurring in the last three contributions to the total energy extend over the volume of the system, and can be easily calculated on a real-space grid with a computational workload which scales linearly with the size of the system.

Let us consider now the kinetic-energy term $T_0[n]$; according to the discussion of section 1.3, in the context of the recursion method the kinetic energy is most simply calculated following an indirect way:

$$T_0[n] = E_{bs} - \int V_{KS}[n\,;\mathbf{r}]\, n(\mathbf{r})\, d\mathbf{r} \,, \tag{3.21}$$

where the band-structure energy E_{bs} is the ground-state expectation value of the self-consistent Kohn-Sham hamiltonian $H_{KS} = (-1/2)\,\nabla^2 + V_{KS}[n\,;\mathbf{r}]$. Using the integral representation of the density matrix, we obtain:

$$E_{bs} = \mathrm{tr}\,(\hat{\rho}\,\hat{H}_{KS}) = \frac{1}{2\pi i} \oint_{C_F} z\ \mathrm{tr}\,\hat{G}(z)\, dz \,; \tag{3.22}$$

the trace of the self-consistent Green's function $\hat{G}(z)$ is calculated in real-space, using the same chain parameters and the same approximate terminator as in the calculation of the self-consistent charge density.

However, it is by no means obvious that an approximate terminator which reproduces the charge density to a given precision would work equally well in the case of the band-structure energy. To check this point let us write the band-structure energy as:

$$E_{bs} = \int e_{bs}(\mathbf{r})\, d\mathbf{r} \,, \tag{3.23}$$

where $e_{bs}(\mathbf{r})$ plays the role of a band-structure energy density:

$$e_{bs}(\mathbf{r}) = \frac{1}{2\pi i} \oint_{C_F} z\, G(\mathbf{r}, \mathbf{r}; z)\, dz \,. \tag{3.24}$$

We have tested a number of approximate terminators in the calculation of the band-structure energy-density; in particular, the effect of the free-particle terminator is shown in Fig. 3.2. The system considered here is the same Silicon supercell described in the case of Fig. (2.6); the band-structure energy-density is plotted along the (111) direction. The solid lines in Fig. 3.2 (a) and Fig. 3.2 (b) show the exact band-structure energy-density, obtained from a well-converged continued-fraction expansion of the Green's function. The dotted line in Fig. 3.2 (a) has been obtained by truncating the continued-fraction expansion after 20 steps, whereas the free-particle terminator $t^0_{20}(z)$ has been used in the case of the dashed line. The corresponding results for a truncated 30-step chain (dotted line) and for a free-particle terminated 30-step chain (dashed line) are shown in Fig. 3.2 (b).

We can conclude from these calculations that, as in the case of the charge density, the accuracy of the band-structure energy-density is improved by the free-particle terminator. Furthermore, the computational cost for the calculation of the band-structure energy scales only linearly with the size of the system, for the same reasons discussed in the case of the charge density.

Let us consider now the accuracy of the ground-state total energy. A number of self-consistent calculations have been performed on a simple trial system, consisting of a cubic unit cell containing 8 Silicon atoms, slightly displaced at random from their equilibrium positions; the average value of the displacement is $\Delta R = 0.1$ a.u. The Kohn-Sham hamiltonian has been discretized on a uniform $14 \times 14 \times 14$ grid, using a 13-point stencil for the

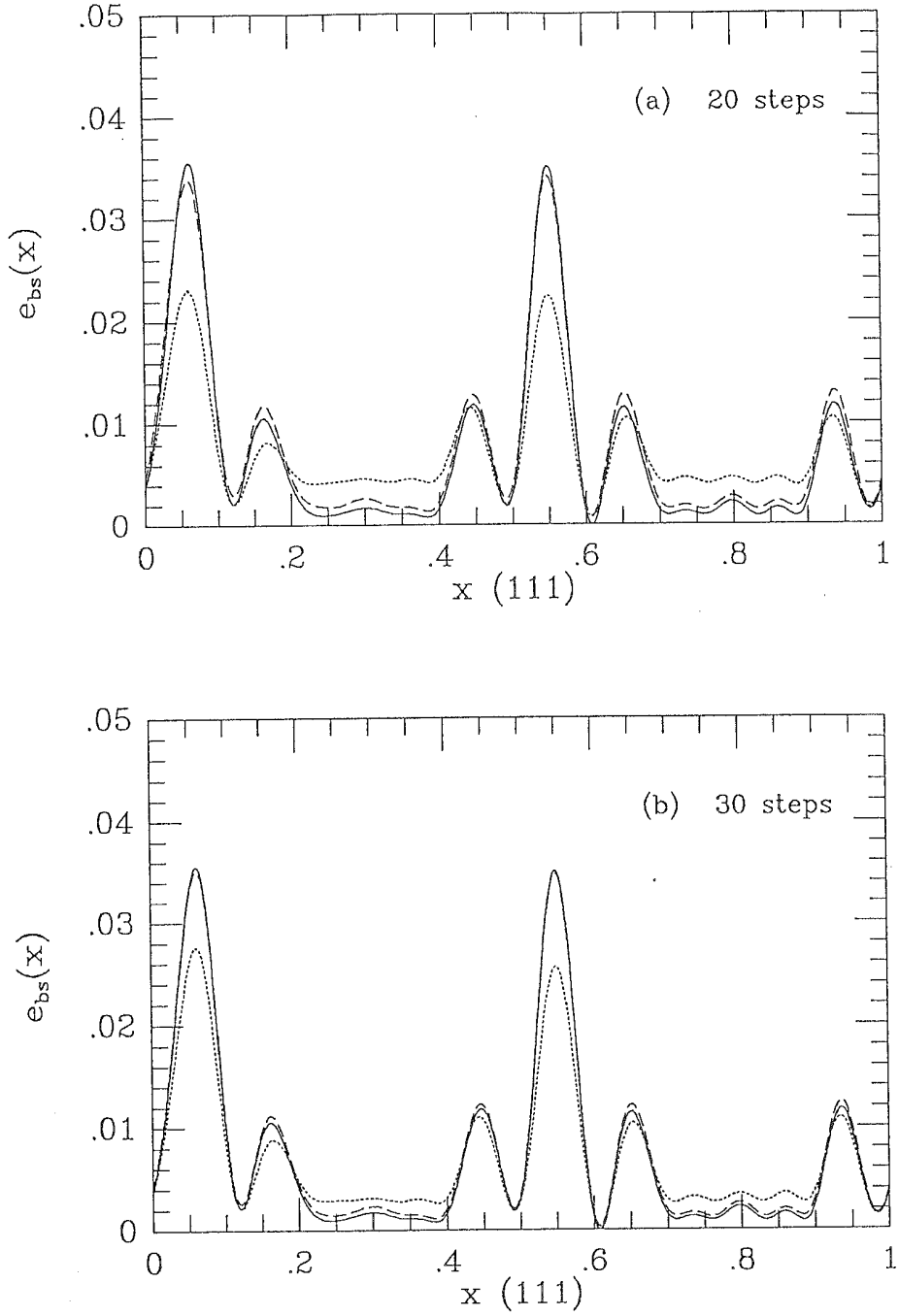

Figure 3.2 – *Band-structure energy density (in Ryd/a.u.) along the first part of the diagonal of the cubic cell. The solid lines show the exact energy density. (a) Energy density obtained from a 20-step truncated chain (dotted line) and from a free-particle-terminated 20-step chain (dashed line). (b) Energy density obtained from a 30-step truncated chain (dotted line) and a free-particle-terminated 30-step chain (dashed line).*

discretization of the kinetic energy. The self-consistent procedure described in the previous section has been carried on until input and output potentials agree to within 10^{-4} Ryd . The results are shown in Tab. 3.1 for different lengths of the recursion chain and different terminators.

# steps	TC	FP
20	-8.4489	-8.4161
30	-8.4836	-8.4079
40	-8.4438	-8.4216
Exact	-8.4236	

Table 3.1 – *Total energy (in Ryd/atom) as a function of the number of recursion steps. TC: truncated chain; FP: free-particle-terminated chain. The "exact" total energy has been obtained from a well-converged 350-step chain.*

An exact self-consistent calculation at zero-temperature has been performed using a well-converged 350-step chain to deal with the calculation of the Green's function. The resulting ground-state total energy is shown in the last row of Tab. 3.1. The remaining entries have been obtained using a truncated chain (TC) or a free-particle-terminated chain (FP); a finite temperature $K_BT = 0.002$ Ryd, corresponding to room-temperature, has been adopted in all cases for the calculation of both the self-consistent charge density and the band-structure energy.

Some conclusions can be drawn from Tab. 3.1:

(i) The free-particle terminator works consistently better than the vanishing terminator: the error in the total energy is typically 3-4 times smaller.

(ii) Increasing the number of recursion steps improves the accuracy of the total energy; however, the error does not decrease monotonically with the number of recursion steps. For example, the 30-step result is worse than the 20-step one. Unfortunately, this is true even when the free-particle terminator is used.

(iii) Finite-temperature effects are relatively small compared to the error introduced by the terminator. For example, a calculation performed with a 20-step chain at $K_BT = 0.0002$ Ryd yields $E_{tot} = -8.4483$ Ryd/atom for the truncated chain and $E_{tot} = -8.4138$ Ryd/atom for the free-particle-terminated chain.

3.3 Forces

Within Density-Functional Theory, the calculation of forces acting on atoms relies upon the Hellmann-Feynman theorem. This is a very general theorem, indeed, stating that whenever the local external potential $V_{ext}(\mathbf{r})$ depends on a parameter λ, the derivative of the ground-state total energy with respect to λ is:

$$\frac{dE_\lambda}{d\lambda} = \int \frac{\partial V_{ext}(\mathbf{r}\,;\lambda)}{\partial\lambda}\; n_\lambda(\mathbf{r})\; d\mathbf{r}\,, \tag{3.25}$$

where $n_\lambda(\mathbf{r})$ is the ground-state charge density corresponding to the external potential $V_{ext}(\mathbf{r}\,;\lambda)$. The validity of the Hellmann-Feynman theorem is based

on the property that the contributions to the derivative of the total energy originating from the λ-dependence of the charge density vanish:

$$\int \frac{\delta E_\lambda}{\delta n_\lambda(\mathbf{r})} \frac{\partial n_\lambda(\mathbf{r})}{\partial \lambda} \, d\mathbf{r} = 0 \, . \tag{3.26}$$

This is a consequence of the variational nature of the total energy within DFT. The functional derivative of the energy with respect to the charge density $n_\lambda(\mathbf{r})$, in fact, is the chemical potential μ_λ appropriate to the external potential $V_{ext}(\mathbf{r}\,;\lambda)$; hence, Eq. (3.26) follows from the charge neutrality condition. In the conventional Kohn-Sham approach to DFT, the ground-state charge density $n_\lambda(\mathbf{r})$ is expressed in terms of the Kohn-Sham orbitals $\{\psi_\alpha(\mathbf{r}\,;\lambda)\}$ which minimize the energy functional $E_\lambda = E_\lambda[\{\psi_\alpha\}]$. Therefore, the implicit contribution to the derivative of the total energy reads:

$$\begin{aligned} &\sum\nolimits_\alpha \int \frac{\delta E_\lambda}{\delta \psi_\alpha(\mathbf{r}\,;\lambda)} \frac{\partial \psi_\alpha(\mathbf{r}\,;\lambda)}{\partial \lambda} \, d\mathbf{r} + \text{c.c.} = \\ &= \sum\nolimits_\alpha \varepsilon_\alpha \frac{\partial}{\partial \lambda} \int |\psi_\alpha(\mathbf{r}\,;\lambda)|^2 \, d\mathbf{r} = 0 \, , \end{aligned} \tag{3.27}$$

due to the normalization of the Kohn-Sham orbitals.

The force acting on atom i is the derivative of the total energy with respect to a displacement $\mathbf{u}_i$ of the atom:

$$\mathbf{F}_i = - \left. \frac{dE_{tot}}{d\mathbf{u}_i} \right|_{\mathbf{u}_i = 0} \, . \tag{3.28}$$

According to the Hellmann-Feynman theorem, we have:

$$\mathbf{F}_i = - \int \left. \frac{\partial V_{ion}(\mathbf{r})}{\partial \mathbf{u}_i} \right|_{\mathbf{u}_i = 0} n_0(\mathbf{r}) \, d\mathbf{r} - \left. \frac{\partial E_{ion-ion}}{\partial \mathbf{u}_i} \right|_{\mathbf{u}_i = 0} , \tag{3.29}$$

where V_{ion} is the ionic potential, $E_{ion-ion}$ is the electrostatic energy of the ions, and $n_0(\mathbf{r})$ is the ground-state charge density calculated at $\mathbf{u}_i = 0$.

Within the RM approach to DFT, the numerical implementation of the Hellmann-Feynman scheme for the calculation of energy derivatives is straightforward. When an approximate terminator is used for the evaluation of the Green's function, however, the variational character of the total energy is lost, and, strictly speaking, the Hellmann-Feynman theorem does not apply. Therefore, the contribution originating from the λ-dependence of the charge density should be taken properly into account in the calculation of the derivative of the energy with respect to the parameter λ:

$$\frac{dE_\lambda}{d\lambda} = \left.\frac{\partial E_\lambda}{\partial \lambda}\right|_{\text{H.F.}} + \int \frac{\delta E_\lambda}{\delta n_\lambda(\mathbf{r})} \frac{\partial n_\lambda(\mathbf{r})}{\partial \lambda} \, d\mathbf{r} \, . \tag{3.30}$$

We address now the question of the validity of the Hellmann-Feynman theorem in the context of the calculation of atomic forces. To this end, we have considered a system of 8 Silicon atoms arranged in a cubic supercell, at the experimental lattice constant $a_0 = 10.26$ a.u. The atom originally at the equilibrium position $(0.25, 0.25, 0.25)\, a_0$ has been moved to $(0.20, 0.20, 0.20)\, a_0$. The remaining atoms have been slightly displaced at random from their equilibrium positions, the average value of the displacement being $\Delta R = 0.1$ a.u. The Kohn-Sham hamiltonian has been represented on a uniform $14 \times 14 \times 14$ grid, using a 13-point stencil for the discretization of the laplacian; the self-consistent procedure has been carried on until input and output potentials agree to within 10^{-5} Ryd. The force acting on the atom at $(0.20, 0.20, 0.20)\, a_0$ along the (111) direction has been calculated both numerically and by means of the Hellmann-Feynman theorem, according to Eq. (3.29); the results are given in Tab. 3.2 for different lengths of the recursion chain and different terminators. All the self-consistent calculations, except the last one, have been performed at finite temperature: $K_B T = 0.002$ Ryd. The column labeled $F_{\Delta E}$ provides the numerical derivative of

the total energy with respect to a displacement of the atom along the (111) direction :

$$F_{\Delta E} = \frac{E_{tot}(\mathbf{u}) - E_{tot}(-\mathbf{u})}{2\,u}\,, \tag{3.31}$$

where $\mathbf{u} = (0.001,\, 0.001,\, 0.001)\, a_0$; the linearity of the energy as a function of the displacement $\mathbf{u}$ has been checked. The last two columns in Tab. 3.2 give the Hellmann-Feynman force F_{HF} and the difference $\Delta F = F_{HF} - F_{\Delta E}$.

# steps	Terminator	$F_{\Delta E}$	F_{HF}	ΔF
20	TC	0.424	0.462	0.038
20	FP	0.460	0.535	0.075
40	TC	0.524	0.502	-0.022
40	FP	0.465	0.396	-0.069
350	TC	0.414	0.413	-0.001

Table 3.2 – *Forces acting on the atom at (0.20,0.20,0.20)a_0 along the (111) direction (in Ryd/a.u.) as a function of the number of recursion steps. TC: truncated chain; FP: free-particle-terminated chain. $F_{\Delta E}$ is the numerical derivative of the total energy with respect to a displacement of the atom in the (111) direction, F_{HF} is the Hellmann-Feynman force, and ΔF is the difference $F_{HF} - F_{\Delta E}$.*

As these calculations demonstrate, the Hellmann-Feynman theorem is obeyed in the case of the well-converged 350-step chain, so that the Hellmann-Feynman force coincides with the numerical derivative of the total energy. When a vanishing terminator or a free-particle terminator are assumed,

however, the Hellmann-Feynman theorem does not apply, the typical error being as large as a few tens of mRyd/a.u. The error is somewhat larger when the free-particle terminator is used, and decreases as the number of recursion steps increases. We have found that the effects of finite temperature on the validity of the Hellmann-Feynman theorem are negligible; therefore, we can conclude that within the present approach the Hellmann-Feynman forces provide only a qualitative estimate of the derivatives of the total energy.

Let us consider now the accuracy of the energy derivative $F_{\Delta E}$, which reflects the accuracy of the energy *difference* $\Delta E = E_{tot}(\mathbf{u}) - E_{tot}(-\mathbf{u})$. In the case of the free-particle-terminated chain, the error in $F_{\Delta E}$ is of the order of 0.05 Ryd/a.u., both for the 20-step chain and for the 40-step chain; this corresponds to an error of $\sim 2 \times 10^{-4}$ Ryd/atom in the energy difference ΔE, which should be compared with the typical error of ~ 0.01 Ryd/atom affecting the absolute value of the energy (see Tab. 3.1). The error in the energy derivative $F_{\Delta E}$ is comparable with that introduced by the use of the Hellmann-Feynman theorem.

3.4 Results

To demonstrate the feasibility of self-consistent calculations in large systems, we present some results obtained for large Silicon supercells.

(a) Silicon cluster

The system considered here is a spherical Silicon cluster containing 441 atoms; the diameter of the cluster is $d = 48.12$ a.u. The Silicon atoms are

arranged in their bulk equilibrium positions, with one atom sitting at the center of the cluster. The cluster is enclosed in a cubic unit cell of size $a = 61.56$ a.u.; periodic boundary conditions are assumed on the cubic cell. The Kohn-Sham hamiltonian has been discretized on a uniform $90 \times 90 \times 90$ real-space grid filling the cubic unit cell. A free-particle-terminated 15-step chain has been used for the calculation of the charge density at every point of the grid. The self-consistent procedure described in section 3.1 has been carried on until input and output potentials agree to within 0.001 Ryd; about 30 iterations were necessary to achieve self-consistency. The self-consistent charge density along the diameter in the (110) direction is shown in Fig. 3.3; there are 7 Silicon atoms along this line, corresponding to the dips in the charge density.

Once the self-consistent potential had been obtained, we have calculated the local density of states $n(\mathbf{r}_i; E)$ at two different points of the real-space grid. In order to achieve high energy-resolution, a 1000-step continued-fraction expansion of the Green's function has been used for the computation of the local density of states. In one case (left-panel in Fig. 3.4) the density of states has been calculated at a grid-point corresponding to the bond-center between the Silicon atom located at the center of the cluster and one of its nearest neighbours. In the other case (right-panel in Fig. 3.4) the local density of states in the middle of a dangling-bond close to the surface is shown. Whereas the local density of states near the center of the cluster resembles the density of states of bulk Silicon, a pronounced peak corresponding to a surface state appears in the local density of states close to the surface.

(b) Vacancy in Silicon

As a second example, let us consider a neutral vacancy in Silicon. The

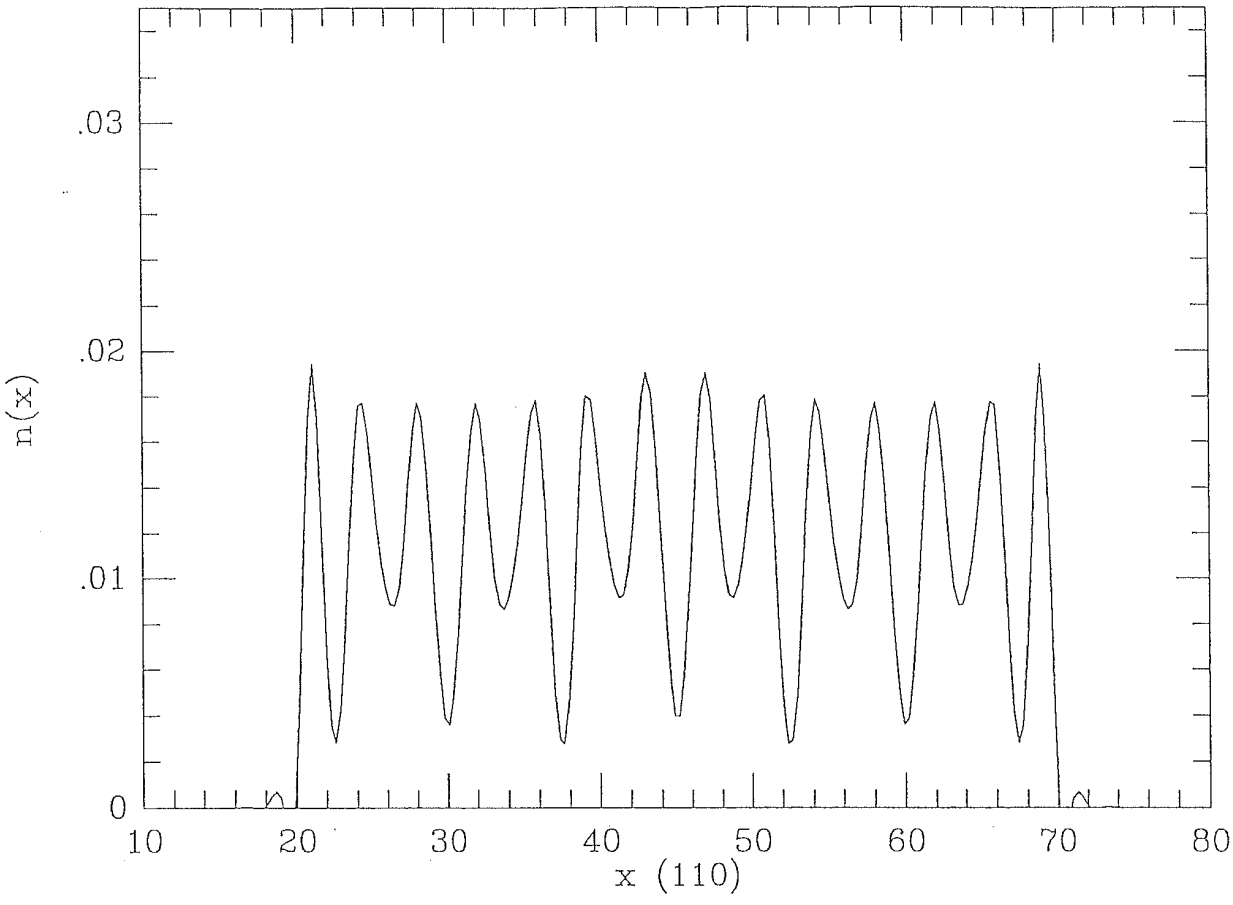

Figure 3.3 – *Self-consistent charge density along the diameter of the cluster in the (110) direction.*

presence of a point defect in a Silicon crystal has important consequences on both the electronic structure and the atomic geometry [29,30]. Due to the loss of translational invariance, however, this problem cannot be tackled within conventional schemes for band-structure calculations; various techniques – such as finite-cluster, periodic-supercell, and Green's function methods – have been recently devised to deal with the inherent difficulty of the vacancy problem. Since the perturbation induced in a Silicon crystal by removal of one atom is screened over relatively short distances, the use of a periodically

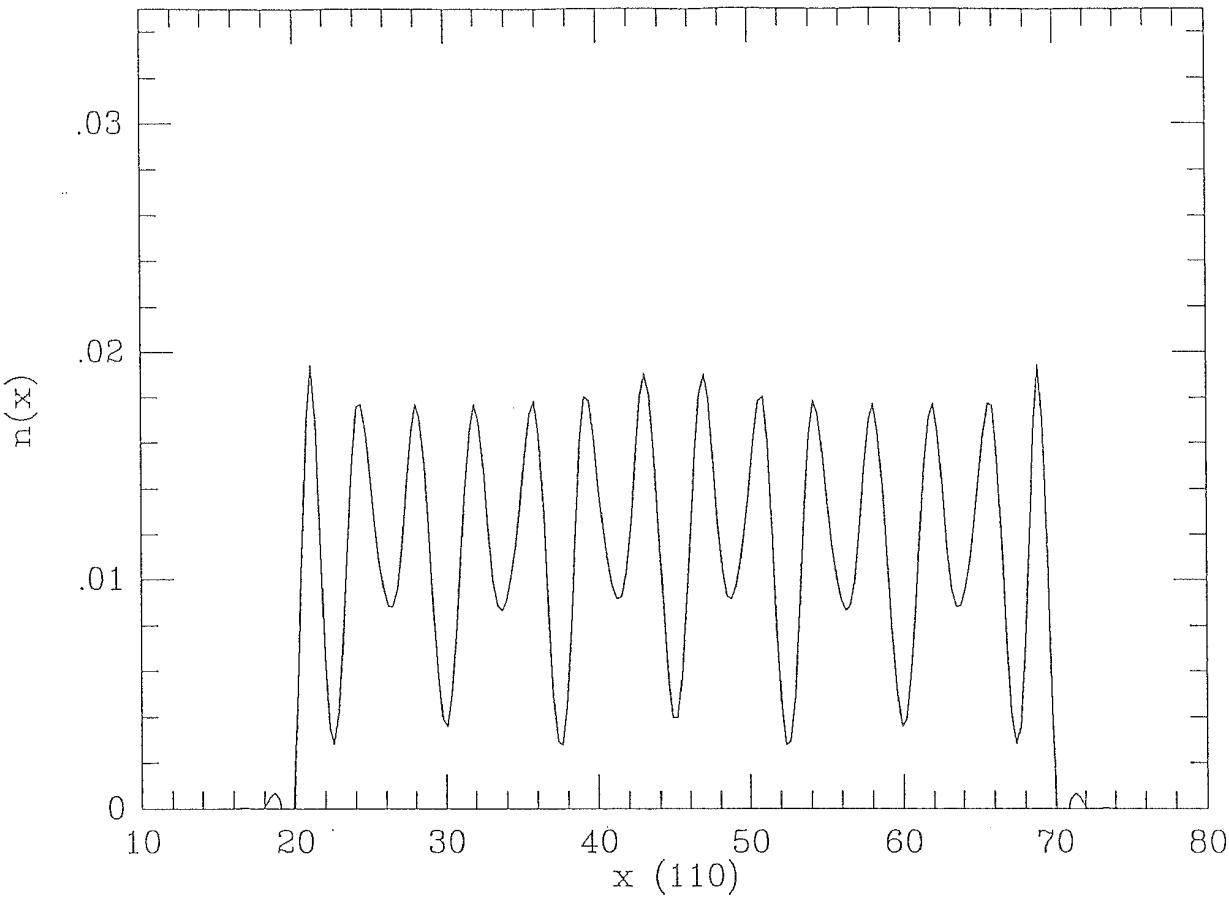

Figure 3.3 – *Self-consistent charge density along the diameter of the cluster in the (110) direction.*

presence of a point defect in a Silicon crystal has important consequences on both the electronic structure and the atomic geometry [29,30]. Due to the loss of translational invariance, however, this problem cannot be tackled within conventional schemes for band-structure calculations; various techniques – such as finite-cluster, periodic-supercell, and Green's function methods – have been recently devised to deal with the inherent difficulty of the vacancy problem. Since the perturbation induced in a Silicon crystal by removal of one atom is screened over relatively short distances, the use of a periodically

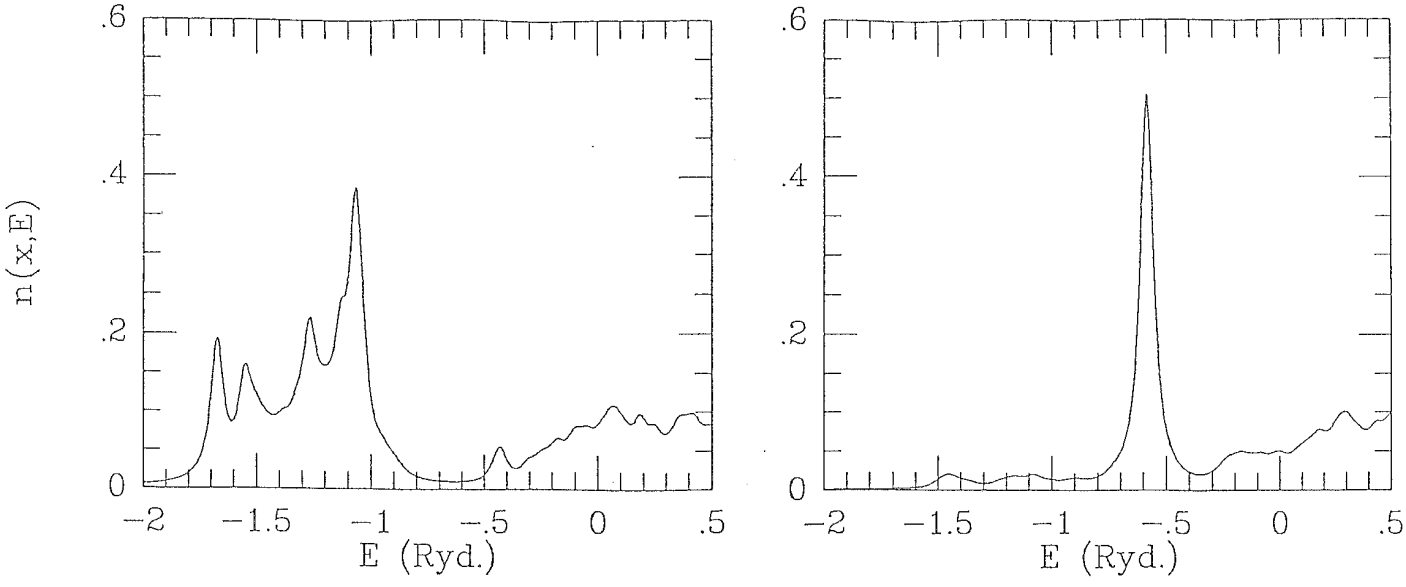

Figure 3.4 – *Local density of states at the bond-center between two Silicon atoms close to the center of the cluster (left-panel) and in the middle of a dangling bond (right-panel).*

repeated supercell makes sense provided the supercell is large enough to avoid interactions between neighbouring vacancies.

We have investigated the relaxation of the first two shells of atoms around a vacancy in a Silicon crystal using the supercell technique. A vacancy has been created in a large Silicon supercell by removing one atom out of 216; periodic boundary conditions are assumed on the supercell. The Kohn-Sham hamiltonian has been discretized on a uniform $42 \times 42 \times 42$ real-space grid. The self-consistent calculation has been carried on at finite temperature ($K_B T = 0.006$ Ryd) until input and output potentials agree to within 0.001 Ryd; about 30 iterations are required, for each atomic geometry, to achieve convergence. The relaxed geometry of the system minimizes the total energy with respect to the atomic positions. Forces acting on atoms are calculated by means of the Hellmann-Feynman theorem, Eq. 3.29; although the agreement with the derivative of the total energy is only qualitative, as

demonstrated in the previous section, nevertheless Hellmann-Feynman forces provide useful information whenever they are much larger in modulus than their typical error ($\sim 10^{-2}$ Ryd/a.u.).

In the unrelaxed geometry, the atoms surrounding the vacancy are kept fixed in their bulk experimental positions. In this configuration, we detect rather large forces acting on the four atoms belonging to the first shell of neighbours around the vacancy; for each of these atoms, we calculate a force of 0.115 Ryd/a.u. pointing outwards in the radial direction. The forces acting on the twelve atoms of the second nearest-neighbour shell are much weaker, and point inward in the direction of the missing atom. The question of the direction of the forces acting on the first shell is quite controversial; for example, Scheffler et al. [29] find an outward displacement of the nearest neighbours, whereas Kelly and Car [30] obtain an inward relaxation. Our results are in qualitative and even quantitative agreement with those of Ref. [29]. When considering the accuracy of our calculation, however, one should take into account that (i) we have used the local Appelbaum-Hamann pseudopotential to deal with electron-ion interactions, and (ii) for computational reasons, the Kohn-Sham hamiltonian has been discretized on a relatively coarse real-space grid. We believe that these are the two main sources of error in our calculation.

Moving the atoms in the direction of the forces lowers the total energy of the system. In particular, the first-shell atoms are pushed toward the interior of the tetrahedra they form with the second-shell atoms, which on turn move away from the missing atom. In the lowest-energy configuration we have found, the total energy of the system is 0.54 Ryd lower than the unrelaxed-configuration energy; the displacement of the first-shell atoms in the

radial direction is as large as 1.6 a.u., whereas the second-shell atoms move outward by 0.5 a.u. However, the Hellmann-Feynman forces do not vanish in this configuration, nor they would in the minimum-energy configuration, according to our previous discussion.

In correspondence to the lowest-energy configuration, we have calculated the local density of states at a few selected points of the real-space grid. The local density of states averaged over the Wigner-Seitz cell around the vacancy is shown in Fig. 3.5 (a); the corresponding average density of states around a Silicon atom located 17.8 a.u. far away from the vacancy is plotted in Fig. 3.5 (b). The Fermi energy is $\varepsilon_F = 0.719$ Ryd. As Fig. 3.5 demonstrates, the Fermi energy is pinned by a localized state in the gap.

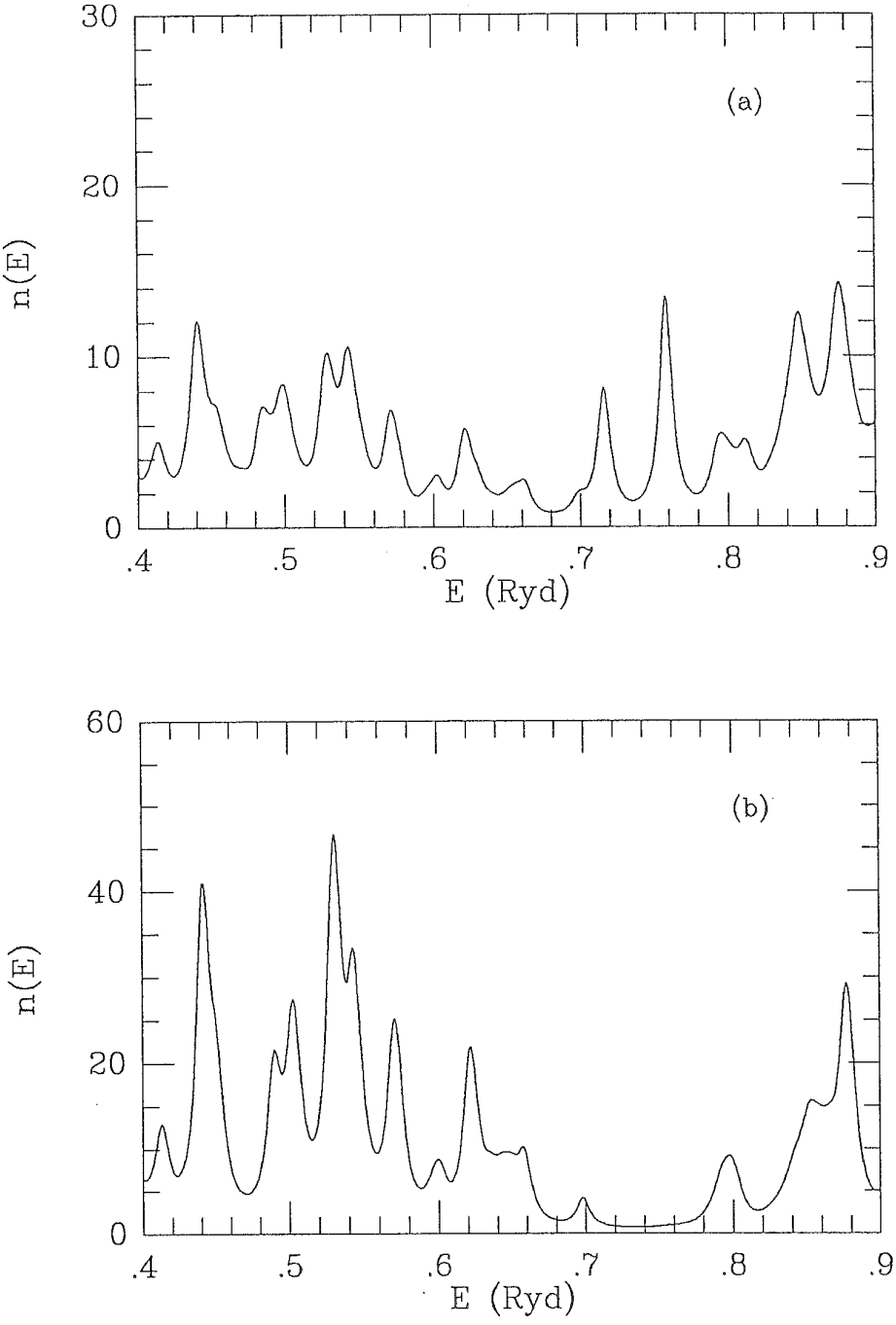

Figure 3.5 – *(a): average density of states around the vacancy; (b): average density of states around a Silicon atom far away from the vacancy.*

Chapter 4

Equation-of-Motion Method

The Equation-of-Motion (EOM) method provides an alternative approach to the calculation of the electronic charge density within the Kohn-Sham scheme. Actually, the EOM method was originally introduced to deal with the computation of the local density of states in large, disordered systems [31]; however, its extension to the calculation of energy-integrated quantities, such as the charge density, is straightforward.

4.1 Real-time propagator

The basic ingredient of the equation-of-motion method is the real-time propagator:

$$\hat{g}(t) = e^{-i\hat{H}t} \,. \tag{4.1}$$

A system in the state $\psi(0)$ at time $t = 0$ will find itself in the state $\psi(t) = \hat{g}(t)\psi(0)$ at time $t > 0$. The spectral decomposition of the real-time propagator reads:

$$\hat{g}(t) = \sum\nolimits_{\alpha} |\psi_\alpha\rangle\langle\psi_\alpha| \, e^{-i\varepsilon_\alpha t} \,, \tag{4.2}$$

where $|\psi_\alpha\rangle$ is the α-th eigenstate of the hamiltonian $\hat{H}$, and ε_α is the corresponding eigenvalue: $\hat{H}\,|\psi_\alpha\rangle = \varepsilon_\alpha\,|\psi_\alpha\rangle$.

The Green's function operator $\hat{G}(z)$ is related to the real-time propagator $\hat{g}(t)$ by a Laplace transform:

$$\hat{G}(z) = -i \int_0^\infty \hat{g}(t)\, e^{izt}\, dt \,, \qquad \text{for } \operatorname{Im} z > 0 \tag{4.3a}$$

and

$$\hat{G}(z) = i \int_0^\infty \hat{g}^\dagger(t)\, e^{-izt}\, dt \,, \qquad \text{for } \operatorname{Im} z < 0 \,. \tag{4.3b}$$

The Green's function operator defined by equations (4.3a) and (4.3b) correctly satisfies the property $\hat{G}(z^*) = \hat{G}^\dagger(z)$.

A simple, direct relation exists between the density-matrix operator and the real-time propagator. To derive this equation, let us introduce the spectral operator

$$\hat{A}(\varepsilon) = \sum\nolimits_{\alpha} |\psi_\alpha\rangle\langle\psi_\alpha| \, \delta(\varepsilon - \varepsilon_\alpha) \,, \tag{4.4}$$

which is related to the imaginary part of the Green's function:

$$\hat{A}(\varepsilon) = -\frac{1}{\pi} \lim_{\gamma \to 0+} \operatorname{Im} \hat{G}(\varepsilon + i\gamma) \,. \tag{4.5}$$

From equation (4.3a), we obtain:

$$\hat{A}(\varepsilon) = \frac{1}{\pi} \lim_{\gamma \to 0+} \mathrm{Re} \int_0^\infty \hat{g}(t)\, e^{i(\varepsilon + i\gamma)t}\, dt\ . \tag{4.6}$$

In terms of the spectral operator $\hat{A}(\varepsilon)$, the density matrix reads:

$$\hat{\rho} = \int_{\varepsilon_L}^{\varepsilon_F} \hat{A}(\varepsilon)\, d\varepsilon\ , \tag{4.7}$$

where ε_L is any lower bound for the energy-spectrum of the hamiltonian: $\varepsilon_L < \min\{\varepsilon_\alpha\}$. Provided the potential energy is bounded from below, a safe choice for ε_L is given by the minimum of the potential. Substituting equation (4.6) into (4.7), and integrating over the energy, we arrive at the following expression for the density-matrix operator:

$$\hat{\rho} = \frac{1}{\pi} \lim_{\gamma \to 0+} \mathrm{Im} \int_0^\infty \hat{g}(t)\, \frac{e^{i\varepsilon_F t} - e^{i\varepsilon_L t}}{t}\, e^{-\gamma t}\, dt\ . \tag{4.8}$$

The expectation value of the real-time propagator on a normalized state ψ_0 is the time-correlation amplitude:

$$g_0(t) \equiv \langle \psi_0 |\, \hat{g}(t)\, | \psi_0 \rangle = \langle \psi_0 |\, e^{-i\hat{H}t}\, | \psi_0 \rangle\ . \tag{4.9}$$

The corresponding diagonal element of the spectral operator provides the local density of states projected upon the state ψ_0:

$$n_0(\varepsilon) \equiv \langle \psi_0 |\, \hat{A}(\varepsilon)\, | \psi_0 \rangle = \frac{1}{\pi} \lim_{\gamma \to 0+} \mathrm{Re} \int_0^\infty g_0(t)\, e^{i(\varepsilon + i\gamma)t}\, dt\ . \tag{4.10}$$

For the integral over time to converge, the imaginary part of the energy must be finite and positive:

$$n_0(\varepsilon) = \frac{1}{\pi} \mathrm{Re} \int_0^\infty g_0(t)\, e^{i\varepsilon t}\, e^{-\gamma t}\, dt\ , \tag{4.11}$$

which corresponds to a Lorentzian broadening γ of the spectrum. However, a Gaussian broadening can also be introduced in a simple way:

$$n_0(\varepsilon) = \frac{1}{\pi} \mathrm{Re} \int_0^\infty g_0(t)\, e^{i\varepsilon t}\, e^{-\sigma^2 t^2}\, dt\,. \tag{4.12}$$

The expectation value of the density-matrix operator on the state ψ_0 reads:

$$\rho_0 \equiv \langle \psi_0 | \hat{\rho} | \psi_0 \rangle = \frac{1}{\pi} \lim_{\gamma \to 0+} \mathrm{Im} \int_0^\infty g_0(t)\, \frac{e^{i\varepsilon_F t} - e^{i\varepsilon_L t}}{t}\, e^{-\gamma t}\, dt\,. \tag{4.13}$$

In this case, the integral converges even for $\gamma = 0$, because it reduces to a sum of Sine integrals; however, a finite broadening of the spectrum may be useful to accelerate the convergence.

The numerical implementation of the EOM method involves two basic steps:

(i) the calculation of the time-correlation amplitude $g_0(t)$;

(ii) the evaluation of time-integrated quantities, such as the local density of states or the density matrix.

The calculation of the time-correlation function $g_0(t)$ is performed by propagating the initial state ψ_0 forward in time; this is equivalent to the solution of the time-dependent Schrödinger equation

$$i\dot{\psi} = \hat{H}\psi\,, \tag{4.14}$$

subject to the initial condition $\psi(t=0) = \psi_0$. A considerable literature exists concerning the numerical integration of the Schrödinger equation. Basically, the solution is evaluated at a number of consecutive time steps $t_n = n\,\delta t$, with $n = 0, 1, \cdots$. The choice of the time interval δt depends on the hamiltonian $\hat{H}$ and, also, on the integration algorithm; in order to describe

the most oscillatory component of the real-time propagator correctly, δt must be small compared to $1/\varepsilon_{max}$, where ε_{max} is the largest eigenvalue of the hamiltonian. If ψ_n is the solution of the Schrödinger equation at time $t = t_n$, the real-time propagator provides the exact solution at time $t = t_{n+1}$:

$$\psi_{n+1} = \hat{g}(\delta t)\,\psi_n \;; \tag{4.15}$$

in general, however, the real-time propagator is unknown, and one has to resort to some approximation to evaluate ψ_{n+1}.

A simple and reliable method for the numerical integration of the equation of motion is provided by the so-called *leap-frog* (LF) algorithm:

$$\psi_{n+1} = \psi_{n-1} - 2i\,\delta t\,\hat{H}\,\psi_n \;. \tag{4.16}$$

One can show by simple arguments (see for example [32]) that the numerical solution of the Schrödinger equation by means of the LF algorithm (4.16) is equivalent to the use of the real-time propagator corresponding to an approximate "leap-frog" hamiltonian $\hat{H}^{LF}$:

$$\hat{g}^{LF}(t) = e^{-i\hat{H}^{LF}t} \;, \tag{4.17}$$

where:

$$\hat{H}^{LF} = \frac{\arcsin\left(\hat{H}\,\delta t\right)}{\delta t} \;. \tag{4.18}$$

A few comments are in order here:

- Provided the LF hamiltonian $\hat{H}^{LF}$ is real, the LF propagator $\hat{g}^{LF}(t)$ is unitary, so that the norm of the wave-function is conserved in time. This requirement determines the stability condition for the leap-frog algorithm:

$$\delta t < 1/\max\{|\varepsilon_\alpha|\} \;, \tag{4.19}$$

where $\{\varepsilon_\alpha\}$ are the eigenvalues of the hamiltonian $\hat{H}$.

- The LF propagator reduces to the exact, real-time propagator in the limit $\delta t \to 0$.
- The error in the LF propagator is first-order in δt; this does not mean, however, that one has to choose an exceedingly small time interval to integrate the equation of motion properly. Quite surprisingly, in fact, any time-integrated quantity can be corrected a-posteriori to compensate for the systematic error introduced by the discrete time interval δt.

Let us consider first the Green's function operator $\hat{G}(z)$. Substituting the LF propagator into equations (4.3a) and (4.3b), we obtain the leap-frog Green's function $\hat{G}^{LF}(z)$, whose poles z_α^{LF} are shifted with respect to the eigenvalues of the hamiltonian by a finite amount: $z_\alpha^{LF} = F_{\delta t}(\varepsilon_\alpha)$, where $F_{\delta t}(z) \equiv \arcsin(z\delta t)/\delta t$. The *corrected* Green's function can be derived observing that the poles of $\hat{G}^{LF}(F_{\delta t}(z))$ coincide with the eigenvalues of the hamiltonian, but the residues are scaled by $\sqrt{1-\varepsilon_\alpha^2\,\delta t^2}$; therefore, the function

$$\tilde{G}(z) = \frac{1}{\sqrt{1-z^2\,\delta t^2}}\;\hat{G}^{LF}(F_{\delta t}(z)) \tag{4.20}$$

has the same singularities and the same residues as the exact Green's function. Notice that the extra singularities at $z = \pm 1/\delta t$ lie outside the spectrum, because of the stability condition (4.19). It is now an easy task to derive the *corrected* local density of states:

$$\tilde{n}_0(\varepsilon) = \frac{1}{\pi\sqrt{1-\varepsilon^2\,\delta t^2}}\lim_{\gamma\to 0+}\mathrm{Re}\int_0^\infty g_0^{LF}(t)\;e^{i\,[F_{\delta t}(\varepsilon)+i\gamma]\,t}\,dt\,, \tag{4.21}$$

and the *corrected* density matrix:

$$\tilde{\rho}_0 = \frac{1}{\pi}\lim_{\gamma\to 0+}\mathrm{Im}\int_0^\infty g_0^{LF}(t)\;\frac{e^{i\,F_{\delta t}(\varepsilon_F)\,t}-e^{i\,F_{\delta t}(\varepsilon_L)\,t}}{t}\;e^{-\gamma t}\,dt\,, \tag{4.22}$$

where $g_0^{LF}(t)$ is the leap-frog time-correlation amplitude.

The numerical evaluation of the integrals occurring in these equations is affected by two main sources of error: (i) the leap-frog time-correlation function $g_0^{LF}(t)$ is known at discrete time steps $t_n = n\,\delta t$, because it is obtained from the leap-frog solution of the equation of motion; (ii) a finite time-cutoff $T = N\delta t$ has to be assumed as the upper limit of the integral.

As far as the first point is concerned, a simple, first-order integration algorithm can be devised which provides, in principle, the exact density of states and, consequently, the exact density matrix. Basically, the integrals over time are replaced by infinite sums to yield:

$$\tilde{n}_0(\varepsilon) = \frac{\delta t}{\pi\sqrt{1-\varepsilon^2\,\delta t^2}} \left\{ \lim_{\gamma\to 0+} \mathrm{Re} \sum_{n=0}^{\infty} g_0^{LF}(t_n)\, e^{i\,[F_{\delta t}(\varepsilon)+i\gamma]\,t_n} - \frac{1}{2} \right\}, \tag{4.23}$$

and:

$$\tilde{\rho}_0 = \frac{\delta t}{\pi} \left\{ \lim_{\gamma\to 0+} \mathrm{Im} \sum_{n=0}^{\infty} g_0^{LF}(t_n)\, \frac{e^{i\,F_{\delta t}(\varepsilon_F)\,t_n} - e^{i\,F_{\delta t}(\varepsilon_L)\,t_n}}{t_n}\, e^{-\gamma t_n} \right. \tag{4.24}$$

$$\left. - \frac{1}{2}\left[F_{\delta t}(\varepsilon_F) - F_{\delta t}(\varepsilon_L)\right] \right\}.$$

However, the sums occurring in these equations have to be truncated after a finite number of steps N, corresponding to the time-cutoff $T = N\delta t$; according to the energy-time uncertainty relation, the peaks in the density of states are broadened by a quantity $\Delta\varepsilon \sim 2\pi/T$, even if γ vanishes.

4.2 Calculation of the charge density

In the present section we discuss the application of the EOM method to the calculation of the electronic charge density, and compare this approach with the recursion method. The real-space representation of the real-time propagator $\hat{g}(t)$ reads:

$$g(\mathbf{r}, \mathbf{r}'; t) = \langle \mathbf{r}| \, e^{-i\hat{H}t} \, |\mathbf{r}'\rangle \; ; \tag{4.25}$$

given the wave-function at time $t = 0$, the real-space propagator yields the wave-function at any time $t > 0$:

$$\psi(\mathbf{r}, t) = \int g(\mathbf{r}, \mathbf{r}'; t) \; \psi(\mathbf{r}', 0) \, d\mathbf{r}' \; . \tag{4.26}$$

The real-space propagator $g(\mathbf{r}, \mathbf{r}'; t)$ leads directly to the real-space density matrix $\rho(\mathbf{r}, \mathbf{r}')$; from equation (4.8) we obtain in fact:

$$\rho(\mathbf{r}, \mathbf{r}') = \frac{1}{\pi} \lim_{\gamma \to 0^+} \mathrm{Im} \int_0^\infty g(\mathbf{r}, \mathbf{r}'; t) \; \frac{e^{i\varepsilon_F t} - e^{i\varepsilon_L t}}{t} \; e^{-\gamma t} \, dt \; . \tag{4.27}$$

Therefore, the charge density $n(\mathbf{r}) \equiv \rho(\mathbf{r}, \mathbf{r})$ is related to the real-space time-correlation function $g(\mathbf{r}, \mathbf{r}; t)$.

The numerical implementation of the EOM method for the calculation of the charge density proceeds along the following lines:

(i) A real-space basis set $\mathcal{M} = \{\mathbf{r}_i, \, i = 1, \cdots, M\}$ is selected, and the Kohn-Sham hamiltonian $\hat{H}_{KS}$ is discretized over the real-space grid. For each grid-point $\mathbf{r}_i$, an initial state ψ_0 localized at the point $\mathbf{r}_i$ is constructed:

$$\langle \mathbf{r}_k | \psi_0 \rangle = \delta_{k,i} \; , \qquad \text{for any } \mathbf{r}_k \in \mathcal{M} \; . \tag{4.28}$$

(ii) The time-dependent Schrödinger equation $i\dot{\psi} = \hat{H}_{KS}\,\psi$, subject to the initial condition $\psi(t = 0) = \psi_0$, is solved on the real-space grid. The

wave-function $\psi(t)$ is evaluated at discrete time steps $t_n = n\,\delta t$ using the leap-frog algorithm; for the first time step t_1, a second-order expansion of the real-time propagator is employed. If a uniform real-space mesh with grid-spacing h is adopted, a safe choice for the time interval δt is $\delta t \simeq (h^2/20)$ a.u. ; this choice ensures that the stability condition (4.19) is satisfied. The equation of motion is integrated up to a finite time-cutoff $T = N\delta t$.

(iii) At each time step t_n, the LF time-correlation function $g^{LF}(\mathbf{r}_i\,,\mathbf{r}_i\,;\,t_n)$ is given by:

$$g^{LF}(\mathbf{r}_i\,,\mathbf{r}_i\,;\,t_n) = \langle\psi_0|\psi_n\rangle\;, \tag{4.29}$$

where ψ_n is the leap-frog solution of the Schrödinger equation at time $t = t_n$.

(iv) Finally, the charge density at point $\mathbf{r}_i$ is calculated as:

$$n(\mathbf{r}_i) = \frac{\delta t}{\pi}\,\mathrm{Im}\;S^{LF}(\mathbf{r}_i) \;-\frac{\delta t}{2\pi}\left[F_{\delta t}(\varepsilon_F) - F_{\delta t}(\varepsilon_L)\right]\;, \tag{4.30}$$

where $S^{LF}(\mathbf{r}_i)$ is the finite sum:

$$S^{LF}(\mathbf{r}_i) = \sum_{n=0}^{N} g^{LF}(\mathbf{r}_i\,,\mathbf{r}_i\,;\,t_n)\;\frac{e^{i\,F_{\delta t}(\varepsilon_F)\,t_n} - e^{i\,F_{\delta t}(\varepsilon_L)\,t_n}}{t_n}\;e^{-\gamma t_n}\;. \tag{4.31}$$

A finite broadening factor γ is chosen such that $\gamma T = 1$.

Since the states $\{\psi_n\}$ generated along with the numerical solution of the Schrödinger equation are localized around the starting point $\mathbf{r}_i$, the EOM method provide, in principle, an $O(N)$ algorithm for the calculation of the charge density.

The charge density obtained using the EOM method is compared in Fig. 4.1 with the result of a recursion-method calculation. The system considered

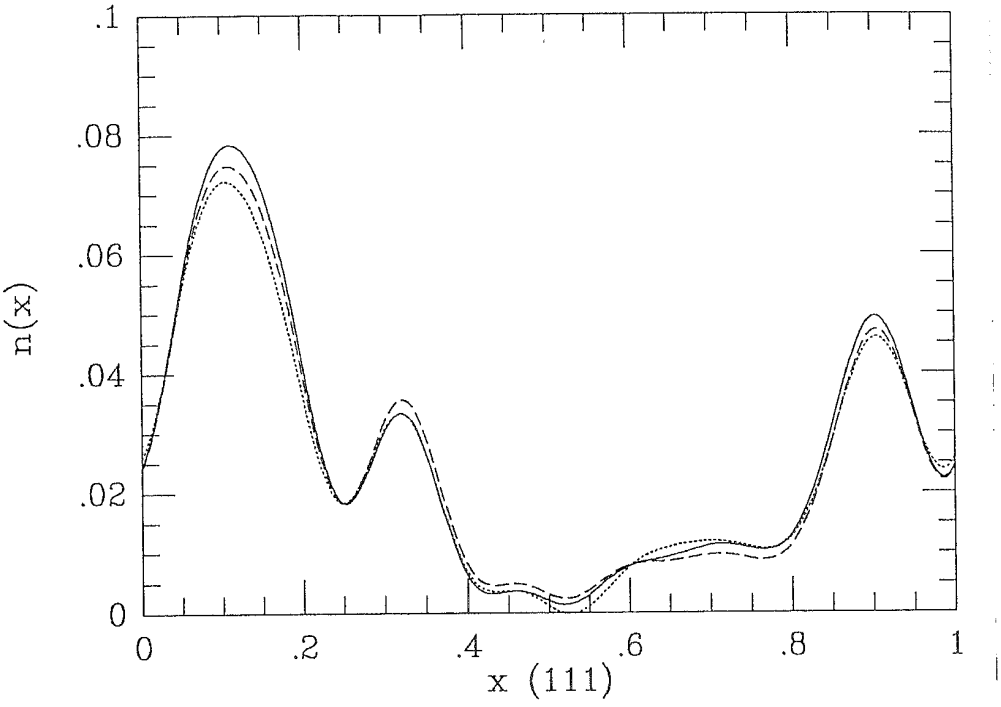

Figure 4.1 – *Charge density along the diagonal of the cubic cell; the solid line shows the exact result. The charge density obtained from a 100-step recursion chain (dotted line) is compared with the EOM charge density after 2000 time steps (dashed line).*

here is the same Silicon supercell described in the case of Fig. (2.2); the solid line in Fig 4.1 shows the exact charge density along the (111) direction.

A time interval $\delta t = 0.02$ a.u., corresponding to $\sim 2/3$ of the maximum value compatible with the stability constraint (4.19), has been used for the numerical integration of the Schrödinger equation with the leap-frog algorithm; we have checked that a longer time interval $\delta t = 0.04$ a.u. leads to instabilities in the solution of the equation of motion. The dashed line in Fig. 4.1 shows the EOM charge density after 2000 time steps, corresponding to a time-cutoff $T = 40$ a.u. The dotted line has been obtained using a 100-step truncated chain within the recursion-method approach.

As these calculations demonstrate, a much larger number of steps is required within the EOM method to achieve a similar accuracy; actually, we have found that nearly 20000 time steps are needed to reproduce the exact charge density of the system closely. Furthermore, the computational cost of each time step is roughly twice the cost of a recursion step, due to the fact that the time-dependent wave-function is complex-valued. Therefore, the timing of the EOM method is largely unfavourable. A qualitative explanation of the slow convergence of the charge density with the number of time steps is provided by the following argument. Due to the finite number of steps N, the peaks in the density of states are broadened by a quantity $\Delta\varepsilon \simeq 2\pi/N\delta t$; roughly speaking, the charge density converges when $\Delta\varepsilon < \varepsilon_G$, where ε_G is the gap-width. In the case considered here, the gap is rather small, of the order of 0.01 Ryd, so that a large number of time steps $N \sim 10^4$ is needed to achieve a reasonable convergence of the charge density. Nevertheless, a few points deserve a further comment, since they could open the way to new strategies for the implementation of the EOM method.

- From a physical point of view, the asymptotic behaviour of the time-correlation amplitude $g_0(t)$ is more meaningful then the evolution of the recursion coefficients a_n's and b_n's with the number of recursion steps. Also, the calculation of the time-correlation function from a given density of states is straightforward, compared to the tricky computation of the corresponding chain parameters within the recursion method.

- The states $\{\psi_n\}$ generated along with the numerical solution of the Schrödinger equation are not constrained to be orthogonal to each other; this can facilitate a grid-coarsening approach to the calculation of the long-time tail of the correlation function $g(\mathbf{r}_i\,,\mathbf{r}_i\,;\,t)$. Furthermore, due to

the fact that the time interval δt can be taken proportional to the square of the grid-spacing, $\delta t \propto h^2$, the computational cost of the numerical integration of the equation of motion up to a given cutoff T scales as $1/h^2$, so that much has to be gained from a grid-coarsening scheme.

- The tail of the time-correlation function contributes to the charge density just through an additive term:

$$n(\mathbf{r}_i) = n^T(\mathbf{r}_i) + \Delta n(\mathbf{r}_i) \,, \tag{4.32}$$

where $n^T(\mathbf{r}_i)$ is the charge density obtained by integrating the equation of motion up to the finite time T. This has to be contrasted with the complicate dependence of the charge density on the terminator within the recursion method.

- Finally, the off-diagonal elements of the real-time propagator in a given representation $\{\phi_i\}$ can be calculated as easily as the diagonal elements, with little extra computational cost. This opens the way to the use of smaller basis sets, namely atomic orbitals, for the calculation of the charge density, or, at least, of its long-time component $\Delta n(\mathbf{r}_i)$.

Conclusions

In this work we have presented a method for the self-consistent calculation of ground-state properties based on the computation of selected elements of the Green's function. Both the charge density and the total energy, in fact, can be expressed in terms of the diagonal elements of the real-space Green's function.

Two different approaches have been discussed which allow the calculation of the Green's function without requiring the time-consuming evaluation of Kohn-Sham orbitals. In the recursion method, the point-wise Green's function is obtained by generating a set of orthonormal states starting from an initial state localized at the given point. In the equation-of-motion method, the initial state is evolved in time to get the time-correlation function, which is the Laplace transform of the Green's function. Both these methods take advantage of the localized nature of the real-space Green's function to achieve linear scaling for large systems. However, they suffer from a relatively slow convergence with the size of the region explored by the states generated from the initial point. Some possible solutions to this problem have been discussed; in particular, we have shown that the free-particle terminator, in the framework of the recursion method, provides a working approximation to deal with the self-consistent calculation of the charge density and other ground-state properties.

Appendix A

Technicalities of the Recursion Method

A.1 Transformation to a Chain

Given a normalized state $|0\rangle$ and a hamiltonian $\hat{H}$, the recursion method (RM) aims at calculating the Green's function diagonal element

$$G_0(z) = \langle 0 | \hat{G}(z) | 0 \rangle , \tag{A.1}$$

where:

$$\hat{G}(z) = \left(z - \hat{H}\right)^{-1} . \tag{A.2}$$

This goal is achieved by generating a set of orthonormal states $\{|n\rangle\}$ starting from the initial state $|0\rangle$, through the application of the three-term recurrence relation:

$$\hat{H}|n\rangle = a_n |n\rangle + b_{n+1} |n+1\rangle + b_n |n-1\rangle , \tag{A.3}$$

where $|-1\rangle$ is assumed to be the null state. In order to guarantee the orthonormality of the states $\{|n\rangle\}$, the recursion coefficients $\{a_n\, b_n\}$ must be chosen according to the following rules:

$$\begin{aligned} a_n &= \langle n|\hat{H}|n\rangle \\ b_{n+1} &= \| (\hat{H}-a_n)|n\rangle - b_n|n-1\rangle \| , \end{aligned} \tag{A.4}$$

where $\| |u\rangle \|$ denotes for the norm of the state $|u\rangle$. The orthonormality property can be easily proved by induction: first, it is obviously satisfied by the state $|0\rangle$ alone; second, assuming the orthonormality of the states $|0\rangle, \cdots, |m\rangle$, the state $|m+1\rangle$ turns out to be (i) normalized and (ii) orthogonal to all the previous states. The recursion coefficients $\{a_n\, b_n\}$ are always real, as follows from Eq. (A.4); the recursion states $\{|n\rangle\}$ are also real, provided both the hamiltonian $\hat{H}$ and the initial state $|0\rangle$ are real.

In principle, the three-term recurrence relation (A.3) can be carried on until the state $|n_s\rangle$ is generated, n_s+1 being the dimension of the Hilbert subspace spanned by the vectors $\hat{H}^n|0\rangle$, $n=0,1,\cdots\infty$. Since the recursion states $|0\rangle, \cdots, |n_s\rangle$ are orthonormal, they form a complete basis set for this subspace; therefore, the state $\hat{H}|n_s\rangle$ is a linear combination of the states $|0\rangle, \cdots, |n_s\rangle$, and the coefficient b_{n_s+1} vanishes. For disordered systems, one usually has $n_s = M-1$, M being the dimension of the whole Hilbert space; only if symmetries are present it may happen that $n_s < M-1$. In the representation of the recursion states $\{|n\rangle, n=0,\cdots,n_s\}$ the hamiltonian turns out to be tridiagonal; as shown by Eq. (A.4), the diagonal elements are given by the coefficients $\{a_n, n=0,\cdots,n_s\}$, while the off-diagonal elements are given by the coefficients $\{b_n, n=1,\cdots,n_s\}$:

$$\mathbf{H} = \begin{pmatrix} a_0 & b_1 & 0 & \dots & 0 & 0 \\ b_1 & a_1 & b_2 & \dots & 0 & 0 \\ 0 & b_2 & a_2 & \dots & 0 & 0 \\ \vdots & \vdots & \vdots & \ddots & \vdots & \vdots \\ 0 & 0 & 0 & \dots & a_{n_s-1} & b_{n_s} \\ 0 & 0 & 0 & \dots & b_{n_s} & a_{n_s} \end{pmatrix} . \qquad (A.5)$$

This hamiltonian can be interpreted as the tight-binding hamiltonian of a linear chain of fictitious atoms: the recursion states $|0\rangle, \cdots, |n_s\rangle$ correspond to the "atomic orbitals", whereas the recursion coefficients a_n's and b_n's play the role of "on-site" and "hopping" terms, respectively. Therefore, any quantum-mechanical system can be transformed, by means of the three-term recurrence relation (A.3), into a simple one-dimensional model, the so-called *chain model*, which can be pictorially represented in the following way:

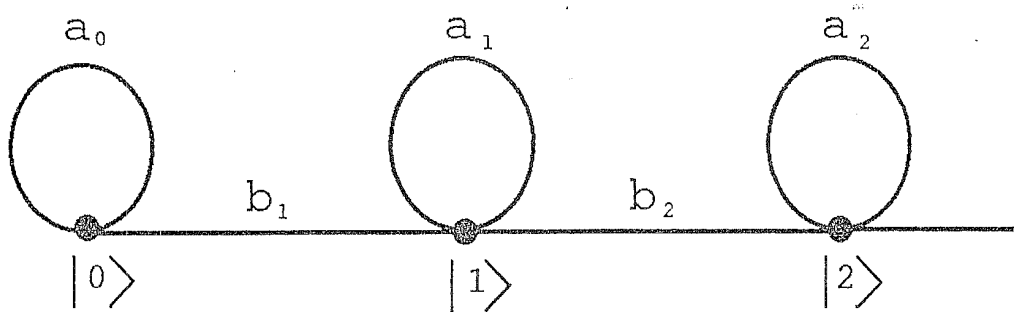

The chain model is exactly equivalent to the physical system, provided the recursion states span the entire Hilbert space.

A.2 Green's Function

Once the transformation to the chain model has been performed, the calculation of the Green's function diagonal element $G_0(z) = \langle\, 0 \,|\, \hat{G}(z) \,|\, 0 \,\rangle$ is straightforward. In the representation of the recursion states $|\, 0 \,\rangle, \cdots, |n_s\rangle$ the Green's function matrix reads:

$$\mathbf{G}(z) = \begin{pmatrix} z-a_0 & -b_1 & 0 & \dots & 0 & 0 \\ -b_1 & z-a_1 & -b_2 & \dots & 0 & 0 \\ 0 & -b_2 & z-a_2 & \dots & 0 & 0 \\ \vdots & \vdots & \vdots & \ddots & \vdots & \vdots \\ 0 & 0 & 0 & \dots & z-a_{n_s-1} & -b_{n_s} \\ 0 & 0 & 0 & \dots & -b_{n_s} & z-a_{n_s} \end{pmatrix}^{-1} . \qquad (A.6)$$

Let $\Delta_n(z)$ be the determinant of the matrix obtained from $(z-\mathbf{H})$ by deleting the first n rows and columns; the Green's function diagonal element reads:

$$G_0(z) = \left(z - \mathbf{H}\right)^{-1}_{0,0} = \frac{\Delta_1(z)}{\Delta_2(z)} . \qquad (A.7)$$

Since $\Delta_n(z) = (z-a_n)\,\Delta_{n+1}(z) - b^2_{n+1}\,\Delta_{n+2}(z)$, we obtain:

$$G_0(z) = \frac{1}{z - a_0 - b_1^2\,\Delta_2(z)/\Delta_1(z)} . \qquad (A.8)$$

Carrying on this procedure, the Green's function diagonal element $G_0(z)$ can be expanded as a continued fraction:

$$G_0(z) = K\left(\frac{b_n^2}{z-a_n}\right) = \cfrac{1}{z - a_0 - \cfrac{b_1^2}{z - a_1 - \cdots - \cfrac{b_{n_s}^2}{z - a_{n_s}}}} . \qquad (A.9)$$

An important feature of the continued-fraction expansion (A.9) is that it converges quickly to the required value $G_0(z)$, at least for complex values of z. From a physical point of view, this is a consequence of the fact that in the chain model the more distant "atomic orbitals" contribute less to the expectation value of the Green's function on the initial state $|0\rangle$. The convergence of the continued-fraction expansion (A.9) depends on the value of the complex energy z: the further is z from the real axis, the faster is the convergence.

The continued fraction (A.9) can be evaluated backwards, by repeated application of the fractional transformation

$$G_{n-1}(z) = \frac{1}{z - a_{n-1} - b_n^2\, G_n(z)} \qquad (A.10)$$

to the starting function $G_{n_s}(z) = 1/(z - a_{n_s})$. Any property of the function $G_{n_s}(z)$ which is conserved by the fractional transformation (A.10) is also shared by the Green's function $G_0(z)$. In particular, one can easily show that $G_0(z^*) = G_0^*(z)$, and that $G_0(z)$ satisfies the so-called Herglotz property: $\mathrm{sgn}\,\mathrm{Im}\,G_0(z) = -\mathrm{sgn}\,\mathrm{Im}\,z$.

The Green's function diagonal element $G_0(z)$ can also be expressed as the ratio of two polynomials. Let $Q_n(z)$ and $P_n(z)$ be the so-called "monic polynomials", recursively defined in the following way:

$$\begin{aligned} Q_0(z) &= 0 \\ Q_1(z) &= 1 \\ &\vdots \\ Q_{n+1}(z) &= (z - a_n)\, Q_n(z) - b_n^2\, Q_{n-1}(z) \end{aligned}$$

and

$$P_0(z) = 1$$

$$P_1(z) = z - a_0$$

$$\vdots$$

$$P_{n+1}(z) = (z - a_n)\, P_n(z) - b_n^2\, P_{n-1}(z)$$

The continued-fraction expansion (A.9) is mathematically equivalent to the polynomial ratio:

$$G_0(z) = \frac{Q_{n_s+1}(z)}{P_{n_s+1}(z)} \,. \qquad (A.11)$$

The polynomials $P_0, P_1 \cdots, P_{n_s+1}$ form a Sturm sequence; therefore, the $n_s + 1$ zeros of $P_{n_s+1}(z)$ are real and distinct. Since the polynomial P_{n_s+1} coincides with the characteristic polynomial of the hamiltonian matrix in the representation of the recursion states, its zeros are the eigenvalues of the hamiltonian restricted to the subspace spanned by the states $\hat{H}^n \,|\, 0 \,\rangle$. Let $\{\varepsilon_\alpha,\, \alpha = 0, \cdots, n_s\}$ be the $n_s + 1$ zeros of $P_{n_s+1}(z)$. Since the n_s zeros of $Q_{n_s+1}(z)$ separate the $n_s + 1$ zeros of $P_{n_s+1}(z)$, the Green's function $G_0(z)$ has $n_s + 1$ simple poles corresponding to the eigenvalues ε_α, and n_s simple zeros corresponding to the zeros of $Q_{n_s+1}(z)$. Therefore, it can be written as:

$$G_0(z) = \sum_{\alpha=0}^{n_s} \frac{\omega_\alpha}{z - \varepsilon_\alpha} \,, \qquad (A.12)$$

where ω_α is the residue at the pole ε_α. The residue ω_α can be easily calculated using the following trick:

$$\omega_\alpha = \lim_{z\to\varepsilon_\alpha} (z-\varepsilon_\alpha)\, G_0(z)$$

$$= \lim_{z\to\varepsilon_\alpha} \frac{(z-\varepsilon_\alpha)\, Q_{n_s+1}(z)}{P_{n_s+1}(z) - P_{n_s+1}(\varepsilon_\alpha)} \qquad (A.13)$$

$$= \frac{Q_{n_s+1}(\varepsilon_\alpha)}{P'_{n_s+1}(\varepsilon_\alpha)} \,.$$

The polynomials $P'_n(z)$ satisfy the following recurrence relation:

$$P'_{n+1}(z) = P_n(z) + (z-a_n)\, P'_n(z) - b_n^2\, P'_{n-1}(z)\,, \qquad (A.14)$$

with $P'_0(z) = 0$ and $P'_1(z) = 1$.

A.3 Terminator

Let us consider the first $n+1$ states of the chain model, and let $\hat{P}^{(n)}$ be the projector upon these states:

$$\hat{P}^{(n)} = \sum_{l=0}^{n} |\, l \,\rangle\langle\, l \,|\,. \qquad (A.15)$$

The Green's function operator projected upon the first $n+1$ states of the chain reads:

$$\hat{G}^{(n)}(z) = \hat{P}^{(n)}\, \hat{G}(z)\, \hat{P}^{(n)}\,, \qquad (A.16)$$

and the corresponding matrix is given by:

$$\mathbf{G}^{(n)}(z) = \begin{pmatrix} z-a_0 & -b_1 & \dots & 0 & 0 \\ -b_1 & z-a_1 & \dots & 0 & 0 \\ \vdots & \vdots & \ddots & \vdots & \vdots \\ 0 & 0 & \dots & z-a_{n-1} & -b_n \\ 0 & 0 & \dots & -b_n & z-a_n-t_n(z) \end{pmatrix}^{-1}, \qquad (A.17)$$

where $t_n(z)$ is the so-called *terminator*, which accounts for the remaining $n_s - n$ states of the chain model:

$$t_n(z) = \cfrac{b_{n+1}^2}{z - a_{n+1} - \cfrac{b_{n+2}^2}{z - a_{n+2} - \cdots - \cfrac{b_{n_s}^2}{z - a_{n_s}}}} . \qquad (A.18)$$

The inverse matrix occurring in Eq. (A.17) provides all of the matrix elements of the projected Green's function $\mathbf{G}^{(n)}(z)$; specifically, the diagonal element $G_0(z)$ can be expanded as a continued fraction terminated by $t_n(z)$:

$$G_0(z) = \cfrac{1}{z - a_0 - \cfrac{b_1^2}{z - a_1 - \cdots - t_n(z)}} . \qquad (A.19)$$

The convergence of the continued-fraction expansion of the Green's function means that the terminator can be neglected, provided n is large enough; however, it should be kept in mind that a continued-fraction expansion differs from a series expansion in that the convergence of the continued fraction does not require the terminator to vanish. In terms of the monic polynomials, the terminated Green's function reads:

$$G_0(z) = \frac{Q_{n+1}(z) - t_n(z)\, Q_n(z)}{P_{n+1}(z) - t_n(z)\, P_n(z)} . \qquad (A.20)$$

Clearly, the analytic properties of the terminator, as given by Eq. (A.18), are similar to those of the Green's function; in particular, $t_n(z)$ has $n_s - n$ distinct poles on the real axis. Furthermore, the terminator satisfies the identity $t_n(z^*) = t_n^*(z)$ and the Herglotz property $\operatorname{sgn} \operatorname{Im} t_n(z) = -\operatorname{sgn} \operatorname{Im} z$.

The terminator accounts for the more distant "atomic orbitals" of the chain model, which contribute less to the Green's function G_0; actually, only

the states of the chain further than n steps from the initial state are involved in the construction of the terminator t_n. Therefore, it is physically sensible to replace the exact terminator $t_n(z)$ with an approximate terminator $\tilde{t}_n(z)$; the corresponding approximate Green's function $\tilde{G}_0(z)$ is then recovered from Eqs. (A.19) or (A.20).

Of course, the most simple approximate terminator is the vanishing terminator $\tilde{t}_n(z) = 0$, which neglects all the states beyond n. The approximate Green's function $\tilde{G}_0(z)$ is then given by the truncated continued-fraction expansion:

$$\tilde{G}_0(z) = \cfrac{1}{z - a_0 - \cdots - \cfrac{b_1^2}{z - a_1 - \cdots - \cfrac{b_n^2}{z - a_n}}} , \qquad (A.21)$$

or, equivalently, by the polynomial ratio:

$$\tilde{G}_0(z) = \frac{Q_{n+1}(z)}{P_{n+1}(z)} . \qquad (A.22)$$

More sophisticated approximations for the terminator require a careful consideration of the problem at hand.

It might be useful to have an expression relating the exact terminator to the Green's function diagonal element

$$G_{n,n}(z) \equiv \langle n \,|\, \hat{G}(z) \,|\, n \rangle , \qquad (A.23)$$

which could be easier to approximate. Starting from Eq. (A.17), we obtain:

$$\begin{aligned} G_{n,n}(z) &= \frac{P_n(z)}{[z - a_n - t_n(z)]\, P_n(z) - b_n^2\, P_{n-1}(z)} \\ &= \frac{P_n(z)}{P_{n+1}(z) - t_n(z)\, P_n(z)} , \end{aligned} \qquad (A.24)$$

whence:

$$t_n(z) = \frac{P_{n+1}(z)}{P_n(z)} - \frac{1}{G_{n,n}(z)} \,. \qquad (A.25)$$

A.4 Density of States and Expectation Values

The local density of states projected upon the state $|\,0\,\rangle$, $n_0(\varepsilon)$, is related to the imaginary part of the Green's function diagonal element $G_0(z)$:

$$n_0(\varepsilon) = -\frac{1}{\pi} \lim_{\gamma \to 0+} \mathrm{Im}\, G_0(\varepsilon + i\gamma) \,. \qquad (A.26)$$

Therefore, the RM provides an efficient tool for the calculation of the local density of states. In finite systems, the local density of states is always given by a set of delta-functions, located at the poles of the Green's function and weighted by the corresponding residues. From the spectral decomposition of the Green's function, Eq. (A.12), we obtain:

$$n_0(\varepsilon) = \sum_{\alpha=0}^{n_s} \omega_\alpha \, \delta(\varepsilon - \varepsilon_\alpha) \,. \qquad (A.27)$$

A similar expression holds when the recursion chain is truncated after n steps, assuming a vanishing terminator:

$$n_0^{(n)}(\varepsilon) = \sum_{\alpha=0}^{n} \omega_\alpha \, \delta(\varepsilon - \varepsilon_\alpha) \,. \qquad (A.28)$$

In order to mimic the local density of states of an infinite system, the discrete density of states can be smoothed using a normalized broadening function $f_\sigma(\varepsilon - \varepsilon_\alpha)$:

$$n_0(\varepsilon) \simeq \sum\nolimits_\alpha \omega_\alpha \, f_\sigma(\varepsilon - \varepsilon_\alpha) \,, \qquad (A.29)$$

where:

$$f_\sigma(x) = \frac{1}{2\sqrt{\pi}\,\sigma}\, e^{-(x/2\sigma)^2} \qquad \text{(Gaussian broadening)}$$

or

$$f_\sigma(x) = \frac{\sigma}{\pi}\,\frac{1}{x^2+\sigma^2} \qquad \text{(Lorentzian broadening)}$$

The latter is equivalent to the use of a finite imaginary part of the Green's function argument in Eq. (A.27). The total density of states $n(\varepsilon)$ can be obtained tracing the Green's function:

$$n(\varepsilon) = -\frac{1}{\pi}\lim_{\gamma\to 0+} \mathrm{Im}\,\mathrm{tr}\,\hat{G}(\varepsilon+i\gamma)\,. \qquad (A.30)$$

For a system of non-interacting particles, the ground-state expectation value of a generic one-particle operator $\hat{A}$ reads:

$$\langle \hat{A} \rangle = \sum\nolimits_\alpha \langle \psi_\alpha |\, \hat{A}\, | \psi_\alpha \rangle\ \theta(\varepsilon_F - \varepsilon_\alpha)\,, \qquad (A.31)$$

where ψ_α denotes the α-th eigenstate of the single-particle hamiltonian $\hat{H}$, and ε_α is the corresponding eigenvalue. Here ε_F is the Fermi energy of the non-interacting system, and $\theta(x)$ is the step-like function:

$$\theta(x) = \begin{cases} 1 & \text{if } x \geq 0 \\ 0 & \text{if } x < 0 \end{cases} \qquad (A.32)$$

Introducing the one-particle density-matrix operator

$$\hat{\rho} = \sum\nolimits_\alpha |\psi_\alpha\rangle\langle\psi_\alpha|\ \theta(\varepsilon_F - \varepsilon_\alpha)\,, \qquad (A.33)$$

the expectation value of the operator $\hat{A}$ becomes:

$$\langle \hat{A} \rangle = \mathrm{tr}\,(\,\hat{\rho}\,\hat{A}\,)\,. \qquad (A.34)$$

The density matrix $\hat{\rho}$ is related to the one-particle Green's function operator $\hat{G}(z)$ by the following integral representation:

$$\hat{\rho} = \frac{1}{2\pi i} \oint_{C_F} \hat{G}(z)\, dz \,, \tag{A.35}$$

where C_F is an integration contour in the complex energy plane enclosing all and only the poles of the Green's function up to the Fermi energy ε_F. Eq. (A.35) can be easily proved starting from the spectral decomposition of the Green's function operator:

$$\hat{G}(z) = \sum\nolimits_{\alpha} \frac{|\psi_\alpha\rangle\langle\psi_\alpha|}{z - \varepsilon_\alpha} \,, \tag{A.36}$$

and using the residue theorem.

The ground-state expectation value of the operator $\hat{A}$ can now be written in terms of the Green's function $\hat{G}(z)$ as:

$$\langle \hat{A} \rangle = \frac{1}{2\pi i} \oint_{C_F} \mathrm{tr}\,[\,\hat{G}(z)\,\hat{A}\,]\, dz \,. \tag{A.37}$$

In general, the evaluation of this integral requires the calculation of the off-diagonal elements of the Green's function. Unfortunately, this is a rather demanding task within the recursion method; however, this bottleneck can be by-passed whenever (i) the operator $\hat{A}$ is an analytic function of the hamiltonian: $\hat{A} = f(\hat{H})$, or (ii) the operator $\hat{A}$ is diagonal in the representation chosen for the calculation of the trace. In the first case, it follows from Eq. (A.37) that:

$$\langle \hat{A} \rangle = \frac{1}{2\pi i} \oint_{C_F} f(z)\, \mathrm{tr}\, \hat{G}(z)\, dz \,. \tag{A.38}$$

Only the diagonal elements of the Green's function enter the calculation of the trace. Therefore, the RM provides an efficient algorithm for calculating

expectation values: given a complete set of orthonormal states $\{\phi_i\,, i = 1, \cdots, M\}$, Eq. (A.38) yields:

$$\langle \hat{A} \rangle = \frac{1}{2\pi i} \oint_{\mathcal{C}_F} f(z) \sum_{i=1}^{M} \langle \phi_i | \, \hat{G}(z) \, | \phi_i \rangle \, dz \; . \tag{A.39}$$

Since the singularities of the Green's function lie on the real axis, the integration contour can be deformed until it collapses on the real axis; in this case, we have:

$$\begin{aligned} \langle \hat{A} \rangle &= -\frac{1}{\pi} \lim_{\gamma \to 0+} \int_{-\infty}^{\varepsilon_F} f(\varepsilon) \, \mathrm{Im} \, \mathrm{tr} \, \hat{G}(\varepsilon + i\gamma) \, d\varepsilon \\ &= \int_{-\infty}^{\varepsilon_F} f(\varepsilon) \, n(\varepsilon) \, d\varepsilon \; . \end{aligned} \tag{A.40}$$

For a generic operator $\hat{A}$, the calculation of the off-diagonal elements of the Green's function can be by-passed using the following trick. Let $\hat{G}^{\lambda A}(z)$ be the perturbed Green's function:

$$\hat{G}^{\lambda A}(z) = (z - \hat{H} - \lambda \hat{A})^{-1} = \hat{G}^0(z) + \lambda \, \hat{G}^0(z) \, \hat{A} \, \hat{G}^0(z) + O(\lambda^2) \, , \tag{A.41}$$

where $\hat{G}^0(z) = (z - \hat{H})^{-1}$. Since

$$\frac{d}{d\lambda} \, \hat{G}^{\lambda A}(z) \Big|_{\lambda = 0} = \hat{G}^0(z) \; \hat{A} \; \hat{G}^0(z) \, , \tag{A.42}$$

we obtain from the residue theorem:

$$\langle \hat{A} \rangle = \frac{1}{2\pi i} \oint_{\mathcal{C}_F} z \, \frac{d}{d\lambda} \, \mathrm{tr} \, \hat{G}^{\lambda A}(z) \Big|_{\lambda = 0} dz \; . \tag{A.43}$$

The derivative of the trace can be calculated numerically to get the expectation value of the operator $\hat{A}$.

References

[1] W. Yang, Phys. Rev. Lett. **66**, 1438 (1991)

[2] W. Yang, Phys. Rev. A **44**, 7823 (1991)

[3] G. Galli and M. Parrinello, Phys. Rev. Lett. **69**, 3547 (1992)

[4] F. Mauri, G. Galli, and R. Car, Phys. Rev. B **47**, 9973 (1993)

[5] X.-P. Li, R.W. Nunes, and D. Vanderbilt, Phys. Rev. B **47**, 10891 (1993)

[6] M.S. Daw, Phys. Rev. B **47**, 10895 (1993)

[7] S. Baroni and P. Giannozzi, Europhys. Lett. **17** (6), 547 (1992)

[8] P. Hohenberg and W. Kohn, Phys. Rev. **136**, B864 (1964)

[9] M. Levy, Proc. Natl. Acad. Sci. **76**, 6062 (1979)

[10] W. Kohn and L.J. Sham, Phys. Rev. **140**, A1133 (1965)

[11] L.W. Wang and M.P. Teter, Phys. Rev. B **45**, 13196 (1992)

[12] L.H. Thomas, Proc. Cambridge Philos. Soc. **23**, 542 (1926); E. Fermi, Z. Phys. **48**, 73 (1928)

[13] R.O. Jones and O. Gunnarsson, Rev. Mod. Phys. **61**, 689 (1989)

[14] R. Car and M. Parrinello, Phys. Rev. Lett. **55**, 2471 (1985)

[15] M.C. Payne, J.D. Joannopoulos, D.C. Allan, M.P. Teter, and D. Vanderbilt, Phys. Rev. Lett. **56**, 2656 (1986)

[16] I. Stich, R. Car, M. Parrinello, and S. Baroni, Phys. Rev. B **39**, 4997 (1989)

[17] M.P. Teter, M.C. Payne, and D.C. Allan, Phys. Rev. B **40**, 12255 (1989)

[18] E.R. Davidson, in *Methods in Computational Molecular Physics*, edited by G.H.F. Diercksen and S. Wilson, Vol. 113 of *NATO Advanced Study Institute, Series C* (Plenum, New York, 1983), p.95

[19] V. Heine, in *Solid State Physics*, edited by H. Ehrenreich, F. Seitz, and D. Turnbull, (Academic, New York, 1980), Vol. 35, p.1

[20] W.H. Press, B.P. Flannery, S.A. Teukolsky, and W.T. Vetterling, *Numerical Recipes: The Art of Scientific Computing* (Cambridge Univ. Press, Cambridge, England, 1989), p.386

[21] J.A. Appelbaum and D.R. Hamann, Phys. Rev. B **8**, 1777 (1973)

[22] R. Haydock, in *Solid State Physics*, edited by H. Ehrenreich, F. Seitz, and D. Turnbull, (Academic, New York, 1980), Vol. 35, p.215

[23] K.E. Atkinson, *An Introduction to Numerical Analysis* (John Wiley & Sons, New York, 1978), p.231

[24] C.M.M Nex, J. Phys. A **11** (4), 653 (1978)

[25] W.H. Press, B.P. Flannery, S.A. Teukolsky, and W.T. Vetterling, *Numerical Recipes: The Art of Scientific Computing* (Cambridge Univ. Press, Cambridge, England, 1989), p.251

[26] W.L. Briggs, *A Multigrid Tutorial* (SIAM, Lancaster, 1987)

[27] J. Perdew and A. Zunger, Phys. Rev. B **23**, 5048 (1981)

[28] D.G. Anderson, J. Assoc. Comput. Mach. **12**, 547 (1964)

[29] M. Scheffler, J.P. Vigneron , and G.B. Bachelet, Phys. Rev. B **31**, 6541 (1985)

[30] P.J. Kelly and R. Car, Phys. Rev. B **45**, 6543 (1992)

[31] F. Alben, M. Blume, H. Krakauer and L. Schwartz, Phys. Rev. B **12**, 4090 (1975)

[32] A. MacKinnon, in *The Recursion Method and its Applications*, edited by D.G. Pettifor and D.L. Weaire (Springer-Verlag, New York, 1985), p.84

Ringraziamenti

Desidero ringraziare in primo luogo Stefano Baroni, per i continui incoraggiamenti e l'entusiasmo che ha dedicato a questo progetto. Vorrei poi ringraziare tutti i colleghi della SISSA, e in particolare Alberto Debernardi, Andrea Dal Corso e Santi Prestipino, per le frequenti e interessanti discussioni. Un grazie di cuore, infine, a tutti coloro che hanno contribuito a rendere piacevoli questi tre anni trascorsi a Trieste.